Basic micrometeorology

Nelson Luís Dias

April 17, 2020

Contents

List of Figures

List of Tables

Listings

Preface

Este texto começa com a introdução do conceito de *escala*, que é fundamental em tudo o que se segue. Vamos procurar entender a globalidade do problema descrevendo as várias camadas da atmosfera (troposfera, estratosfera, ...) e fazendo depois um "zoom" na Camada-Limite Atmosférica (CLA), que é a parte mais baixa da troposfera. Em seguida, reveremos as equações de Mecânica dos Fluidos aplicáveis à CLA , falaremos de turbulência e da sua abordagem clássica (decomposição de Reynolds e equações de transporte de covariâncias). Algumas soluções particulares simples destas equações proporcionam uma boa idéia da interação das camadas mais altas da atmosfera com a CLA. Estudaremos mais intensamente a parte mais baixa da CLA, chamada Camada Superficial (CS). Na CS, debaixo de algumas hipóteses simplificadoras, podemos utilizar a Teoria de Similaridade de Monin-Obukhov (SMO), que nos permite descrever uma série de grandezas relacionadas com a turbulência de forma extremamente simples. As equações básicas que descrevem a física da turbulência e as previsões da Teoria de Similaridade de Monin-Obukhov são utilizadas para prever o comportamento das grandezas médias $\overline{u}$, $\overline{\theta}$ e $\overline{q}$ na CS. Além do comportamento genérico previsto pela teoria SMO, dois casos-limite cujo significado físico é importante são abordados: a estratificação independente de z numa atmosfera muito *estável*, e a convecção livre local em uma atmosfera muito *instável*. Com as previsões da teoria sobre o comportamento das grandezas médias, é possível então utilizar medições delas para calcular os fluxos τ, H e E. Além de alguns métodos que utilizam exclusivamente a medição de grandezas médias, apresenta-se ao fim do relatório o método da variância, que é um híbrido que utiliza tanto grandezas médias como medições de turbulência.

1

Introduction

1.1 – The regions of the atmosphere

The atmosphere is a relatively thin layer of gas above the Earth's surface. Upwards of 100 km above the surface, the density of the atmosphere is very low. Meanwhile, since the Earth's great circle C is approximately 40 000 km, if we set the thickness of the atmosphere to $\mathcal{L} = 100\,\text{km}$, the ratio $\mathcal{L}/C = 0{,}0025$ shows how thin the atmosphere really is.

Figure 1.1 shows the main regions of the atmosphere in the first 100 km, for a standard atmosphere at 10° N in june (Houghton, 1986): in this case, the troposphere extends to 17 km; the stratosphere is a strongly stratified region ($\frac{dT}{dZ} > 0$) between 17 km and 50 km; the mesosphere displays a marked temperature fall between 50 km and 95 km; finally, from that point upwards the temperature rises again in the termosphere.

Existe uma enorme riqueza de fenômenos físicos, que ainda hoje estão sendo estudados, em toda a atmosfera terrestre. No entanto, a região mais importante para a vida na Terra, e a única que os seres vivos podem "experimentar" diretamente, é a troposfera: a montanha mais alta do mundo não chega a 9 km de altitude. A faixa mais diretamente relevante é a Camada-Limite Atmosférica (CLA), que se estende no máximo até cerca de 2 km de altura (e não altitude) sobre a superfície. Isto representa no máximo 2% da figura 1.1.

Da mesma maneira que utilizamos o perfil de temperatura termodinâmica para caracterizar praticamente toda a atmosfera, a CLA é caracterizada pelo perfil de temperatura potencial. Esta será definida na próxima seção; por enquanto, basta pensarmos na temperatura potencial como um indicador da densidade do ar: quanto maior a temperatura potencial, menor a densidade. A figura 1.2 mostra um perfil típico de temperatura potencial durante o dia. Os gradientes de temperatura são grandes até cerca de 100 m de altura, que configuram aproximadamente a camada superficial CS; a partir daí, o perfil é praticamente constante até cerca de 1100 m (esta é a camada convectiva CC); daí até 1300 m a temperatura eleva-se gentilmente: esta é a zona de arrasto ZA, onde a CLA interage com a "atmosfera livre" AL sobre ela, na qual a densidade do ar é fortemente estratificada, a intensidade da turbulência muito baixa e valem as aproximações invíscidas das equações de Navier-Stokes, que veremos na próxima seção sob o nome de "vento geostrófico".

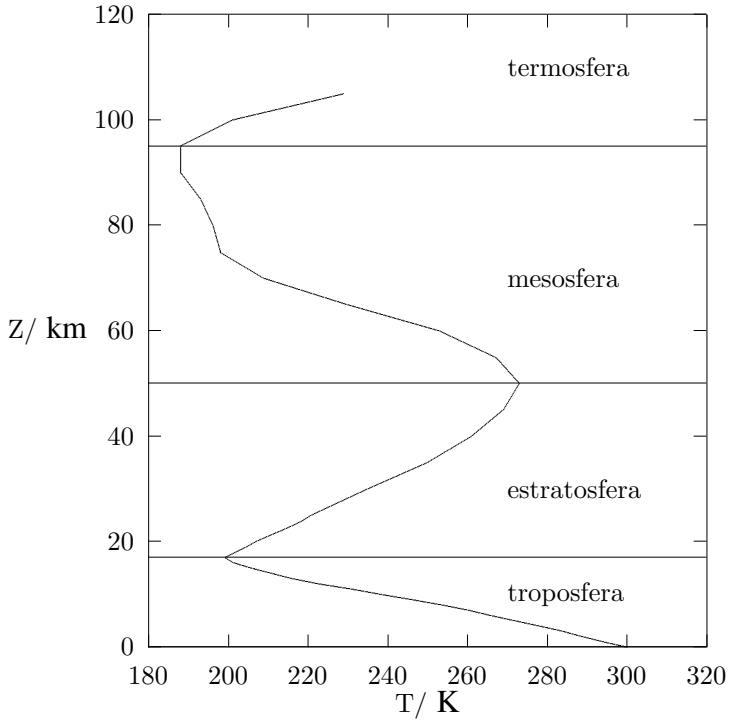

Figure 1.1: Perfil de temperatura numa atmosfera modelo, a 10 °N, em junho (Houghton, 1986)

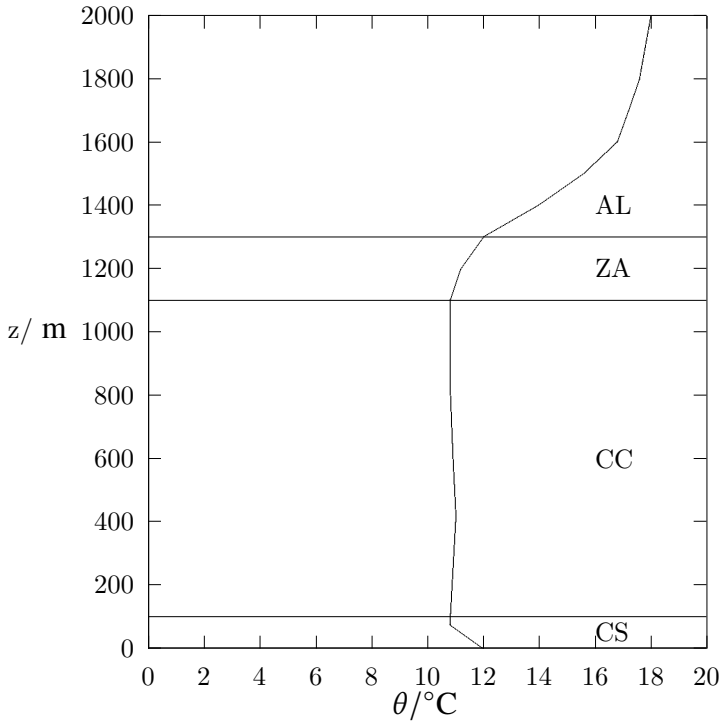

Figure 1.2: perfil de típico de temperatura potencial durante o dia na CLA (adaptado de (Stull, 1988))

Table 1.1: Classificação de escalas horizontais em meteorologia

Nome	Dimensão
macro β	10.000 km
meso α	2.000 km
meso β	200 km
meso γ	20 km
micro α	2 km
micro β	200 m
micro γ	20 m

Esta breve descrição da atmosfera mostra a grande riqueza de escalas verticais envolvidas. Neste texto, nós estaremos preocupados essencialmente com os primeiros 100 m da atmosfera, na camada superficial.

Como é de se esperar da discussão sobre a razão $\mathcal{L}/C$, as escalas *horizontais* sobre as quais se observam fenômenos físicos em meteorologia são consideravelmente maiores. A Tabela 1.1 dá uma descrição das escalas horizontais em meteorologia. Para tornar mais claro o significado da classificação da tabela 1.1, observe a seguinte lista de fenômenos e suas escalas horizontais correspondentes, dada por Holton 1992:

Table 1.2: Escalas de movimentos atmosféricos (Holton, 1992)

Tipo de movimento	Escala horizontal (m)
Caminho livre médio molecular	10^{-7}
Menores turbilhões turbulentos	10^{-2}–10^{-1}
Pequenos turbilhões turbulentos	10^{-1}–10^{0}
Vórtices não-turbulentos	10^{0}–10^{1}
Rajadas de vento	10^{1}–10^{2}
Tornados	10^{2}
Nuvens Cumulus Nimbus	10^{3}
Frentes	10^{4}
Furacões	10^{5}
Ciclones sinóticos	10^{6}
Ondas planetárias	10^{7}

No nosso caso, estaremos trabalhando dentro das fronteiras da micrometeorologia: nossas escalas horizontais são da ordem de 2 km ou menores (micro-α), e nossas escalas verticais da ordem da espessura da camada superficial, cerca de 100 m, ou menores. Este é o domínio por excelência da turbulência: movimentos turbulentos na atmosfera possuem escalas desde algumas centenas de metros (na horizontal) até poucos milímetros, que é a escala onde a turbulência é dissipada por efeitos viscosos. A modelação matemática da CLA é o assunto da próxima seção.

1.2 – The importance of the surface fluxes

A great deal of the physical evolution of the atmosphere is influenced by the exchange of mass, momentum and energy with the surface of the Earth. The surface of these quantities are the *surface fluxes*, and their knowledge is essential for applications in meteorology, hydrology and environmental sciences in general. In particular, the values of the *greenhouse gas* surface fluxes are needed to predict their impact on global warming and climate change.

A emissão de gases de efeito estufa (GEE) da superfície da Terra para a atmosfera é hoje, reconhecidamente, um dos grandes problemas ambientais que enfrentamos. O problema é global, tornando necessária a negociação internacional de limites para as emissões, bem como o desenvolvimento internacional de metodologias que sejam consensualmente aceitas para estimar estas emissões.

Uma das abordagens para a estimativa dos fluxos destes gases é a realização de medições micrometeorológicas. Ao evitar a complexidade dos processos que ocorrem na superfície ou abaixo dela (seja da água ou do solo/vegetação), e ao integrar as emissões e capturas de GEE tanto na vertical quanto sobre o comprimento de pista do vento, medições micrometeorológicas de GEE podem dar respostas importantes sobre o valor dos fluxos superficiais, seu padrão horário e sazonal, e sua relação com outras grandezas importantes tais como temperaturas do ar, água e solo, a qualidade da água, o tipo de vegetação, etc...

Medições micrometeorológicas de gases de efeito estufa em geral consistem em medições de grandezas atmosféricas relativamente próximo da superfície. Convencionalmente, as medições são divididas em "blocos", que podem ser tão curtos quanto 10 minutos, ou tão longos quanto 1 hora. Dentro de cada bloco, é usual supor a estacionariedade das séries temporais medidas. As medições podem ser realizadas por sensores relativamente lentos, quando então "médias" são obtidas, ou com sensores suficientemente rápidos para capturar uma parte signficativa das frequências associadas à turbulência atmosférica. Neste último caso, estatísticas da turbulência dentro do bloco, tais como desvios-padrão, covariâncias, funções de correlação cruzada e espectros podem ser medidos.

Medições de grandezas médias estão associadas ao método fluxo-gradiente (MFG) para a estimativa de fluxos. Medições de turbulência estão associadas ao método de medição de covariâncias turbulentas (MCT).

O MFG é mais antigo, e envolve mais hipóteses, do que as "medições diretas" realizadas pelo MCT. Na verdade, como veremos, estas medições não são tão diretas assim, e o MCT também envolve um grande número de hipóteses, embora talvez não tão restritivas quanto as do MFG. Devido a dificuldades tecnológicas e custo, o MFG ainda é amplamente utilizado para a estimativa de fluxos de gases tais como o CH_4 e o N_2O, para os quais medições (principalmente de longo prazo) de flutuações turbulentas ainda são problemáticas.

O método de medição de covariâncias turbulentas (MCT), originalmente desenvolvido para a medição dos fluxos de quantidade de movimento, calor sensível e massa de vapor d'água, possui uma série de características que o tornam uma opção interessante para a medição de fluxos de GEE: medições contínuas

de fluxos horários ou de 30 minutos são possíveis; as medições possuem uma representatividade espacial da ordem de centenas de metros corrente acima da torre de medição; e as tecnologias de medição envolvidas estão hoje (2011) razoavelmente bem desenvolvidas e possuem custos acessíveis.

2

A primer on the thermodynamics of the atmospheric boundary layer

2.1 – The ideal gas law for a pure substance

The ideal gas law applies well for typical conditions of the atmosphere close to the surface of the Earth. For a *pure substance*, it is

$$pV = nR^{\#}T, \tag{2.1}$$

where p is pressure, V is the volume occupied by the gas, n is the number of moles, $R^{\#} = 8{,}314\,462\,618\,15\,\mathrm{J\,mol^{-1}\,K^{-1}}$ (in the SI) is the universal gas constant, and T is thermodynamic temperature. Still for a pure substance, (2.1) can also be written as

$$\begin{aligned} p &= n\frac{R^{\#}}{V}T = \frac{m}{M}\frac{R^{\#}}{V}T = \frac{m}{V}\frac{R^{\#}}{M}T \;\Rightarrow \\ p &= \rho RT. \end{aligned} \tag{2.2}$$

Above, M is the molar mass; m is the mass of the gas, which is related to the number of moles by

$$m = nM; \tag{2.3}$$

the gas constant is

$$R = \frac{R^{\#}}{M}, \tag{2.4}$$

which depends on the specific gas through M in 2.4; and

$$\rho = \frac{m}{V} \tag{2.5}$$

is the density; its reciprocal

$$v = \frac{1}{\rho} \tag{2.6}$$

is the *specific volume* v. Note that (2.2) is more useful than (2.1) in practice: V does not appear in it, and it only involves intensive quantities (pressure, density and temperature), so it applies at every point in the atmosphere.

2.2 – The atmosphere as a mixture of ideal gases

The atmosphere however is not a pure substance, but a mixture of gases. The question then is how (2.1) can be reasonably extended to account for mixtures. In fact, from now on, often when we use one of (2.1)–(2.6), we will be referring to the total atmospheric pressure p (of a mixture of gases), the total density ρ, etc..

Therefore, we start by requiring that (2.1) *apply for the mixture*; then, the total number of moles, n, is the sum of the number of moles of each individual constituent. Let i be the index for each gas in a mixture; we have

$$n = \sum_i n_i, \tag{2.7}$$

where n_i is the number of moles of gas i.

We want the perfect gas law to apply for each constituent as well, and if we substitute (2.7) into (2.1), the question is what to do with the left-hand side of (2.1). There are two possibilities: the model of partial pressures, and the model of partial volumes. In the first case, we specify for each gas

$$p_i V = n_i R^{\#} T. \tag{2.8}$$

In this model all gases occupy a common volume V, each one exerting its own partial pressure p_i, such that the total pressure is

$$p = \sum_i p_i. \tag{2.9}$$

In the second case,

$$p V_i = n_i R^{\#} T, \tag{2.10}$$

and now all gases are subject to the same pressure p, each one occuping, nominally, a partial volume V_i, with

$$V = \sum_i V_i. \tag{2.11}$$

In both cases, summing the individual equations of state recovers the perfect gas law for the mixture. For example, starting from (2.8),

$$\begin{gathered} \sum_i (p_i V) = \sum_i \left(n_i R^{\#} T \right), \\ \left(\sum_i p_i \right) V = \left(\sum_i n_i \right) R^{\#} T, \\ p V = n R^{\#} T \end{gathered}$$

(recovering (2.1)), and similarly for (2.10).

From (2.1), (2.8) and (2.10), it follows that

$$x_i = \frac{p_i}{p} = \frac{V_i}{V} = \frac{n_i}{n} \tag{2.12}$$

defines a concentration (traditionally expressed in %, parts per million (ppm), parts per billion (ppb), etc.) either in partial pressure fraction, partial volume fraction, or *mole fraction*. The gas law for each constituent can also be written

$$p_i = n_i \frac{R^\#}{V} T = \frac{m_i}{M_i} \frac{R^\#}{V} T = \frac{m_i}{V} \frac{R^\#}{M_i} T \Rightarrow$$
$$p_i = \rho_i R_i T, \tag{2.13}$$

where (as before for a pure substance)

$$m_i = n_i M_i \tag{2.14}$$

and

$$\rho_i = m_i / V, \tag{2.15}$$
$$v_i = \frac{1}{\rho_i}, \tag{2.16}$$

are the density or the specific mass (with mass m_i occuping the volume V) and the specific volume respectively of the gas i, and M_i is the molar mass of gas i. In (2.13),

$$R_i = \frac{R^\#}{M_i} \tag{2.17}$$

is the gas constant for gas i.

Once more, (2.2) holds for the mixture. To see how, note that the total mass of the mixture is

$$m = \sum_i m_i; \tag{2.18}$$

and similarly for the total density:

$$\rho = \frac{m}{V} = \frac{\sum_i m_i}{V} = \sum_i \frac{m_i}{V} = \sum_i \rho_i. \tag{2.19}$$

We will also need to define the *mass concentration*, or *mass fraction* of each constituent,

$$c_i \equiv \frac{m_i}{m} = \frac{\rho_i}{\rho}. \tag{2.20}$$

With (2.18)–(2.19) in hand, we sum (2.13) to obtain

$$\sum_i p_i = \sum_i \rho_i R_i T,$$
$$p = \left(\sum_i \rho_i R_i \right) T \equiv \rho R T.$$

This *defines* the gas constant R of the mixture; now

$$R = \frac{\sum_i \rho_i R_i}{\rho}$$
$$= \frac{\sum_i \frac{m_i}{V} R_i}{\frac{m}{V}}$$
$$= \sum_i \frac{m_i}{m} R_i = \sum_i c_i R_i. \tag{2.21}$$

Thus, given the mass concentrations, we can calculate the equivalent gas constant.

The *mean molar mass* of the mixture is

$$M = \sum_i x_i M_i = \frac{\sum_i n_i M_i}{n} = \frac{m}{n}, \tag{2.22}$$

which recovers (2.3). This finally allows us to close the circuit to recover (2.4) for the mixture. From (2.21),

$$\begin{aligned} R &= \frac{1}{m}\left(\sum_i m_i R_i\right) \\ &= \frac{1}{m}\left(\sum_i n_i M_i R_i\right) \\ &= \frac{1}{m}\left(\sum_i n_i R^\#\right) = \frac{1}{m}\left(\sum_i n_i\right) R^\# \\ &= \frac{n}{m} R^\# = \frac{R^\#}{M}, \end{aligned} \tag{2.23}$$

by virtue of (2.22), which recovers (2.4).

2.3 – Concentrations

A relationship between x_i and c_i can now be readily obtained:

$$x_i = \frac{n_i}{n} = \frac{\frac{m_i}{M_i}}{\frac{m}{M}} = \frac{m_i}{m}\frac{M}{M_i},$$

or

$$x_i M_i = c_i M. \tag{2.24}$$

Other concentration measures are also in use in meteorology, and need to be defined. The *mixing ratio* can be expressed either as a *mole ratio*,

$$\eta_i = \frac{n_i}{n - n_i}, \tag{2.25}$$

or as a *mass ratio*

$$r_i = \frac{m_i}{m - m_i}. \tag{2.26}$$

The mixing ratio, therefore, is the ratio of the amount (either in moles or in mass) of substance i to the amount of all *other* substances. It follows that for any substance *other than* water vapor, the denominator includes the amount of water vapor present in the air at the time of measurement. For this reason, when i is not water vapor, (2.27)–(2.28) are often called *wet mixing ratios*. The water vapor content of the air, however, is highly variable in the atmosphere; also, in scalar turbulent flux measurements it is often better to employ concentrations measured in (an equivalent) dry air. This leads to the definition of *dry* mixing ratios (see, for example, Butenhoff and Khalil, 2002),

$$\eta_{di} = \frac{n_i}{n_d - n_i}, \tag{2.27}$$

Table 2.1: Constitution of a "dry" atmosphere (not including water vapor). The values are approximate, and adjusted to garantee that the molar fractions sum up to 1.

Gas	M_i ($\mathrm{g\,mol^{-1}}$)	x_{di}
N_2	28.0134	0.78078700
O_2	31.9988	0.20943200
Ar	39.948	0.00934000
CO_2	44.0095	0.00041390
Ne	20.1797	0.00001818
He	4.002602	0.00000524
CH_4	16.0425	0.00000170
Kr	83.798	0.00000110
H_2	2.01588	0.00000055
N_2O	44.0128	0.00000033
sum		1.00000000

and

$$r_{di} = \frac{m_i}{m_d - m_i}. \tag{2.28}$$

Above, n_d is the number of moles and m_d is the mass of *dry air* present in the atmosphere. The foregoing concepts are only useful if we can obtain n_d or ρ_d operationally. For that, we need to look at the composition of the atmosphere, and define a few more concepts.

For a temperature $T = 288.15\,\mathrm{K}$ (15 °C) and atmospheric pressure $p = 101\,325\,\mathrm{Pa}$ for a standard atmosphere (COESA, 1976), we list on table 2.1 the molar fractions densities of several atmospheric gases in $\mathrm{g\,m^{-3}}$ in a *dry* atmosphere. The M_i values were obtained from NIST (2020). The x_i values are given in Dias (2020), and they are *approximations*, based on several existing references Iribarne and Godson (1981); COESA (1976); Wallace and Hobbs (2006); Wikipedia (2020); the values of x_i, particularly for CO_2, are updated to the most recent (as of 2020) available data. Morever, the values have been manually adjusted to ensure that

$$\sum_i x_i = 1. \tag{2.29}$$

The densities are readily calculated in the last column as $\rho_i = p_i/(R_i T) = x_i p/(R_i T)$. Note that the table is not exhaustive, and that CH_4 is not the most abundant element after CO_2! Also note that the values of x_i are updated to some of the most recent (2020) values, and are not those from COESA (1976). All gases in table 2.1 after Argon, *and not including water vapor*, are called *trace gases*. Their mole fractions and mass fractions are very small, and sometimes this allows some simplifications in the calculation of their concentrations.

We are now in a position to calculate the gas constant for *dry air*, R_d. For simplicity, we lump all the trace gases into an equivalent CO_2 entry, and produce a smaller table 2.2. The result using (2.21) is

$$R_d = 287.0359\,\mathrm{J\,kg^{-1}\,K^{-1}}. \tag{2.30}$$

Table 2.2: Calculation of the gas constant for dry air. The values are approximate.

Gas	$i =$	M_χ(g mol^{-1})	x_{di} (%)	ρ_χ (g m^{-3})
N_2	n	28.014	78.080	925.0778
O_2	o	31.999	20.945	283.4515
Ar	a	39.948	0.934	15.7799
CO_2	c	44.009	0.041	0.7631
sum			100.000	1225.0723

This value is slightly less than the one adopted for the standard 1976 atmosphere $R_d = 287.05283$, which is compatible with Iribarne and Godson (1981)'s table I-4, whose equivalent here is table 2.2. Note however that there has been a steady increase in atmospheric CO_2 since the publication of the 1976 U. S. Standard Atmosphere, so besides not being too different from the COESA (1976) figure, the value adopted here is probably closer to the current (2020) state of the atmosphere.

Let us now calculate wet and dry mixing ratios. Because the water vapor content in the atmosphere is variable, we will adopt a reasonable value $x_v = 2.5\%$, and reapportion the gases in table 2.1 among the remaining 97.5%.

Note the drastic progressive density reduction of the greenhouse gases H_2O, CO_2, CH_4 and N_2O, in the last 4 lines of the table.

What table 2.1 reveals is that the measurement of CO_2 is much more difficult than the measurement of H_2O; similarly, CH_4 measurement is harder than CO_2's, and so on, by the simple fact that it is necessary to measure increasingly smaller concentrations. Although this is possible in controlled laboratory conditions with various types of chemical analyzers, *in situ* measurements, necessary to obtain continuous data series, are substantially more difficult.

Thus, the task of measuring fluxes and performing greenhouse gas material balances is also extraordinarily hard, and one of its greatest scientific challenges is still the obtention of accurate error estimates. It is noticeable that even the H_2O balance in a watershed (or a reservoir) is still very hard, and many of the terms of the "water balance" of a reservoir remain highly uncertain.

2.4 – Thermodynamics of a pure substance

The perfect gas law in the form (2.1) or (2.2) is an example of a state equation in thermodynamics. It is convenient to introduce the *specific volume* v and the density ρ,

$$v = \frac{1}{\rho} = \frac{V}{m}, \tag{2.31}$$

where m is the total mass occupying volume V. For a *pure substance*, then, the state equation takes one of the forms

$$p = p(v, T) \qquad \text{or} \qquad v = v(p, T) \qquad \text{or} \qquad T = T(p, v).$$

For atmospheric gases, the lower case letters indicate specific quantities (per unit mass or unit volume), and are more convenient since we will not usually treat individual "systems" or "lumps" of air.

Two important thermodynamical functions are the specific internal energy u and the specific enthalpy h defined by

$$h = u + pv. \tag{2.32}$$

For a pure substance, they are functions of two variables, chosen between p, v and T. We usually write

$$u = u(v, T), \tag{2.33}$$
$$h = h(p, T), \tag{2.34}$$

since these pairs lead to useful definitions of measurable quantities such as specific heats. Equations (2.33) and (2.34) lead to perfect differentials

$$\mathrm{d}u = \left(\frac{\partial u}{\partial v}\right)_T \mathrm{d}v + \left(\frac{\partial u}{\partial T}\right)_v \mathrm{d}T, \tag{2.35}$$
$$\mathrm{d}h = \left(\frac{\partial h}{\partial p}\right)_T \mathrm{d}p + \left(\frac{\partial h}{\partial T}\right)_p \mathrm{d}T. \tag{2.36}$$

The specific heats at constant volume and constant temperature are defined by

$$c_v = \left(\frac{\partial u}{\partial T}\right)_v, \tag{2.37}$$

$$c_p = \left(\frac{\partial h}{\partial T}\right)_p. \tag{2.38}$$

The subscripts v and p on the right-hand side of the equations above are used in thermodynamics as reminders that u is being taken as a function of v, T, and that h is being taken as a function of p, T.

For a perfect gas, the equation of state takes the form

$$pv = RT, \tag{2.39}$$

where R is a gas constant specific for the pure substance (or the equivalent mixture of gases, as is the case of dry air) and it is possible to show that in this case u and h are functions of T only (Adkins, 1983). Then, (2.37)–(2.38) become ordinary derivatives. Also,

$$\begin{aligned}\left(\frac{\partial h}{\partial T}\right)_p &= \left(\frac{\partial}{\partial T}[u + pv]\right)_p \\ &= \left(\frac{\partial u}{\partial T}\right)_p + p\left(\frac{\partial v}{\partial T}\right)_p \\ &= \frac{\mathrm{d}u}{\mathrm{d}T} + p\frac{R}{p} \Rightarrow \\ c_p &= c_v + R. \end{aligned} \tag{2.40}$$

Physically, $c_p > c_v$ due to the extra energy necessary for the expansion of the air against the constant pressure p.

2.5 – Moist air

Note that the equations of section 2.4 are not strictly valid for atmospheric air, which is not a *pure* substance; rather, it is a mixture of many gases. Each new constituent makes the thermodynamical equations more complex; in particular, functions of state such as u and h then become also functions of the concentrations of each new constituent.

We will not follow the rigorous path of treating the atmosphere as a mixture of several gases and writing down the full thermodynamical equations for that mixture; instead, we will consider "dry air" (a mixture of nitrogen and oxygen in essentially constant proportions) as the main constituent, and will introduce various indices for the concentration of water vapor (the most important varying component). Later, the concentrations of other gases and their relevant effects will also be introduced as needed. However, the rigorous modifications in the thermodynamical functions of state will not be discussed.

Consider now a certain volume V of air with total mass m, composed of dry air with mass m_d and water vapor with mass m_v. We have:

$$\begin{aligned} m &= m_d + m_v, \\ \frac{m}{V} &= \frac{m_d}{V} + \frac{m_v}{V}, \\ \rho &= \rho_d + \rho_v. \end{aligned} \tag{2.41}$$

This defines the air density ρ; the density of dry air ρ_d and the water vapor density ρ_v. In itself, ρ_v is an index of water vapor concentration; in meteorology, it is often called absolute humidity. Note that the atmosphere, obviously, contains many more *trace gases* such as CO_2, CH_4, etc.. However, because $\rho_\chi \ll \rho_v$ for $\chi = c, m, n$, etc., (2.41) is still a good approximation for the total density of the atmosphere at any point and instant.

The partial pressure model introduced already in section **??** and Equation (2.2) for the two components of moist air leads to the pair of equations

$$p_d = p - e = \rho_d R_d T, \tag{2.42}$$

$$e = \rho_v R_v T, \tag{2.43}$$

where p_d is the partial pressure of dry air; p is total atmospheric pressure, and e is the partial pressure of water vapor. Note that following the general notation introduced in section **??**, $e = p_v$. In meteorology, it is customary to use e, and we will follow this tradition.

$R_d = 287.05\,\mathrm{J\,kg^{-1}\,K^{-1}}$ and $R_v = 461.51\,\mathrm{J\,kg^{-1}\,K^{-1}}$, which can be calculated per (2.17), are the gas constants for dry air and water vapor, respectively.

The *specific humidity* q is defined as

$$q = \frac{\rho_v}{\rho}. \tag{2.44}$$

Summing (2.42) and (2.43), one obtains

$$\begin{aligned} p &= (\rho_d R_d + \rho_v R_v)\, T \\ &= \rho \left(\frac{\rho_d}{\rho} R_d + \frac{\rho_v}{\rho} R_v \right) T \\ &= \rho R_d \left(\frac{\rho_d}{\rho} + \frac{\rho_v}{\rho} \frac{R_v}{R_d} \right) T \\ &= \rho R_d \left((1 - q) + \frac{R_v}{R_d} q \right) T. \end{aligned} \tag{2.45}$$

Replacing

$$\begin{aligned} \frac{R_v}{R_d} = 1.608 \approx 1.61 \qquad &\Rightarrow \\ p = \rho R_d \underbrace{(1 + 0.61q)T}_{T_v} \end{aligned} \tag{2.46}$$

The *virtual temperature* T_v defined above is the temperature of a dry atmosphere with the same density ρ. A further index atmospheric moisture is the mixing ratio

$$r = \frac{\rho_v}{\rho_d}. \tag{2.47}$$

Useful relations among the humidity indices can be derived as follows:

$$\begin{aligned} r &= \frac{\rho_v}{\rho} = \frac{\frac{e}{R_v T}}{\frac{(p-e)}{R_d T}} \\ &= \frac{R_d}{R_v}\frac{e}{p-e} = 0.622\,\frac{e}{p-e}; \end{aligned} \tag{2.48}$$

$$\begin{aligned} q &= \frac{\rho_v}{\rho} = \frac{\frac{e}{R_v T}}{\rho_d + \rho_v} \\ &= \frac{\frac{e}{R_v T}}{\frac{p-e}{R_d T} + \frac{e}{R_v T}} \\ &= \frac{R_d}{R_v}\frac{e}{p + \left(\frac{R_d}{R_v} - 1\right)e} \\ &= 0.622\frac{e}{p - 0.378e} \approx 0.622\frac{e}{p}. \end{aligned} \tag{2.49}$$

2.6 – Atmospheric humidity

The latent heat of water, L_w, is the amount of energy used to change the phase of a unit of mass from liquid to vapor, in a pure mixture of the two phases. A good approximation for L_w is the assumption that the heat capacities of the two phases are equal. This leads to (Adkins, 1983, Chap. 10, Eq. 10.16)

$$\mathrm{d}L_w = [c_{pv} - c_{p\ell}]\mathrm{d}T \tag{2.50}$$

where c_{pv} and $c_{p\ell}$ are the specific heats at constant pressure of water vapor and liquid water, respectively. If the specific heats, in turn, are assumed to be constant, we obtain

$$L_w = L_a + L_b T. \tag{2.51}$$

In the SI, with T in Kelvins, Linsley et al. (1975) give

$$L_w = 3.1458 \times 10^6 - 2.3613 \times 10^3 T \tag{2.52}$$

in $\mathrm{J\,kg^{-1}}$. A reasonable alternative is to use a constant value, given the very small variation of L_w with T. At $T = 295\,\mathrm{K}$, $L_w = 2.462 \times 10^6\,\mathrm{J\,kg^{-1}}$.

For a system composed of water vapor and liquid water in equilibrium, an equation can be derived relating the derivative with respect to temperature of the *saturation vapor pressure* e^* (the vapor pressure of the gas in equilibrium with the liquid water), the change in specific volume v between the two phases and the latent heat, *viz.*

$$\frac{\mathrm{d}e^*}{\mathrm{d}T} = \frac{L_w}{T\Delta v}; \tag{2.53}$$

it is the *Clausius-Clapeyron* equation (Adkins, 1983, Chap. 10, Eq. (10.11)). Assuming the validity of the perfect-gas law, and that the specific volume of the liquid phase is negligible in comparison with that of the vapor phase, the Clausius-Clapeyron equation takes the form (Adkins, 1983, Chap. 10, Eq. (10.12))

$$\frac{\mathrm{d}e^*}{\mathrm{d}T} = \frac{L_w e^*}{R_v T^2} \tag{2.54}$$

Note that Eqs. (2.51)– (2.52) can be used to integrate (2.54), yielding

$$e^*(T) = \left(\frac{T}{T_0}\right)^{\frac{L_b}{R_v}} e^*(T_0) \exp\left[\frac{L_a}{R_v}\left(\frac{1}{T_0} - \frac{1}{T}\right)\right], \tag{2.55}$$

where T_0 is a reference temperature. With $L_b = 0$, (2.55) bears a strong resemblance to (but is not the same as) Teten's empirical formula (Murray, 1966; Dilley, 1968; Stull, 1995; Alduchov and Eskridge, 1996):

$$e^*(T) = e^*(T_0) \exp\left[\frac{b(T - T_1)}{T - T_2}\right], \tag{2.56}$$

with $T_0 = 273.16$, $b = 17.2694\,\mathrm{K}^{-1}$, $T_1 = 273.16\,\mathrm{K}$ and $T_2 = 25.86\,\mathrm{K}$.

For most meteorological applications, Teten's formula is more than enough. Note however that the constants change for saturation vapor pressure over *ice*; also, note that the presence of salts in the water alters e^* significantly. Finally, Richards' equation (Brutsaert, 1982) is

$$e^*(T) = 101\,325 \exp\left[13.3185 t_r - 1.9760 t_r^2 - 0.6445 t_r^3 - 0.1299 t_r^4\right] \tag{2.57}$$

$$\frac{\mathrm{d}e^*}{\mathrm{d}T} = \frac{373.15}{T^2} e^*(T)\left[13.3185 - 3.9520 t_r - 1.9335 t_r^2 - 0.5996 t_r^3\right], \tag{2.58}$$

$$t_r = 1 - \frac{373.15}{T}. \tag{2.59}$$

The concept of saturation now allows for the definition of several humidity indices based on it. The *relative humidity* y is the ratio of the actual mixing ratio and the mixing ratio in water vapor saturated air at the same temperature and pressure:

$$y = \frac{r}{r^*}. \tag{2.60}$$

Note that, because it is at the same temperature and pressure, the density of dry air in the saturated atmosphere (ρ_{d*}) is actually smaller than the density of dry air in the non-saturated atmosphere (ρ_d). The gas law equations are

$$p - e = \rho_d R_d T, \qquad e = \rho_v R_v T, \tag{2.61}$$

$$p - e^* = \rho_{d*} R_d T, \qquad e^* = \rho_v^* R_v T. \tag{2.62}$$

Therefore,

$$\begin{aligned} y &= \frac{r}{r^*} \\ &= \frac{\frac{\rho_v}{\rho_d}}{\frac{\rho_v^*}{\rho_{d*}}} \\ &= \frac{\rho_{d*}}{\rho_d} \times \frac{\rho_v}{\rho_v^*} \\ &= \frac{\frac{p-e^*}{R_d T}}{\frac{p-e}{R_d T}} \times \frac{\frac{e}{R_v T}}{\frac{e^*}{R_v T}} \\ &= \frac{p-e^*}{p-e} \times \frac{e}{e^*} \\ &= \frac{p(1-e^*/p)}{p(1-e/p)} \times \frac{e}{e^*} \\ &\approx (1-e^*/p)(1+e/p)\frac{e}{e^*} \\ &\approx \frac{e}{e^*}. \end{aligned} \tag{2.63}$$

The last form, (2.63), is the one commonly used in calculations.

The *dewpoint temperature* T_d is the temperature at which the water vapor pressure becomes the saturated vapor pressure:

$$e^*(T_d) = e. \tag{2.64}$$

Usually, temperature varies with height in the surface layer. A subscript like T_x or e_x will often be used to specify temperature, water vapor pressure, etc., at some specified level. Also, we will often use the simplified notation

$$e_x^* = e^*(T_x), \tag{2.65}$$

$$d_x = \frac{\mathrm{d}e^*(T_x)}{\mathrm{d}T}, \tag{2.66}$$

$$\rho_{vx}^* = \rho_v^*(T_x). \tag{2.67}$$

In figure 2.1, we show in frame A the prevailing conditions in the atmosphere. In frame B, saturation is reached, from A, through an increase in water vapor content. In frame C, saturation conditions are also reached, but this time through a continuous drop in temperature down to the dew point temperature T_d.

2.7 – Potential temperature

Consider the adiabatic expansion of a parcel of air, from a level (higher up) where the ambient pressure is p down to a level where the ambient pressure is p_0. The first law of thermodynamics is (q is heat per unit mass added to the system; w is work per unit mass performed on the system)

$$\mathrm{d}u = đq + đw;$$

For an adiabatic ($đq = 0$) and reversible process,

$$\mathrm{d}u = -p\mathrm{d}v \tag{2.68}$$

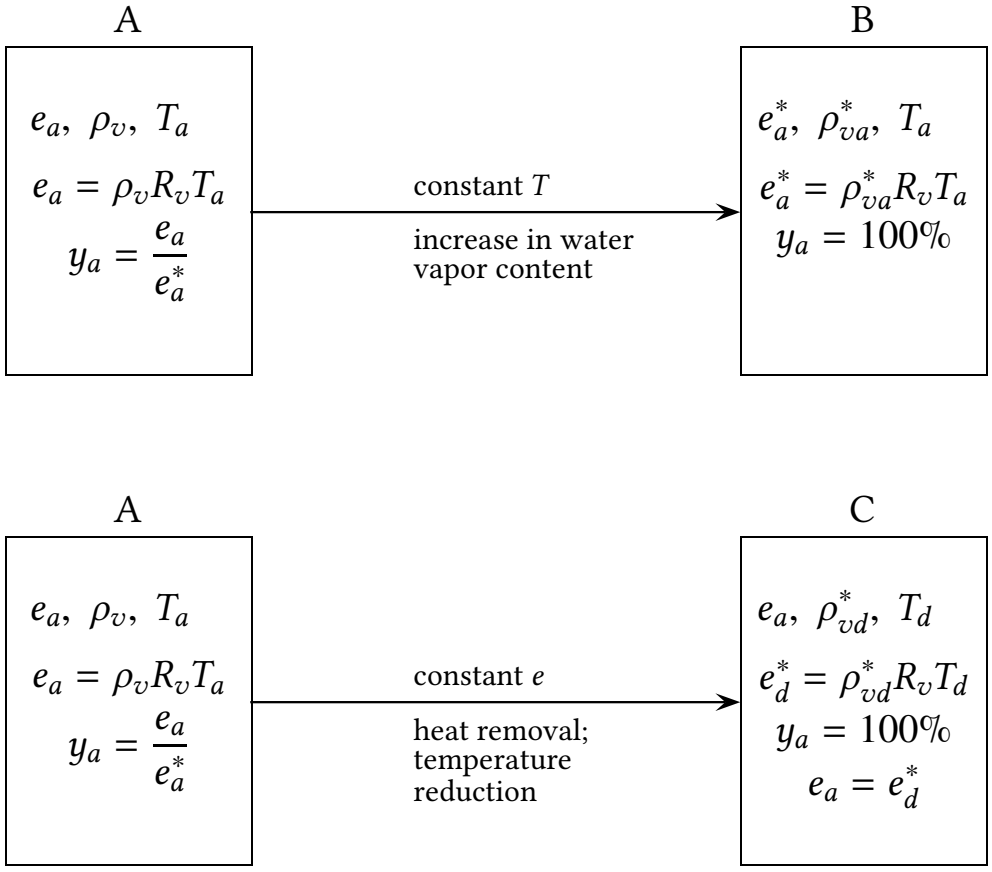

Figure 2.1: The concepts of atmospheric saturation, relative humidity and dew-point.

Differentiation of (2.39) and use of (2.37) (keeping in mind that $u = u(T)$ for a perfect gas) produce

$$\begin{aligned} p\mathrm{d}v + v\mathrm{d}p &= R\mathrm{d}T \\ c_v\mathrm{d}T &= v\mathrm{d}p - R\mathrm{d}T \\ (c_v + R)\mathrm{d}T &= v\mathrm{d}p = \frac{RT}{p}\mathrm{d}p \\ c_p\mathrm{d}T &= v\mathrm{d}p = \frac{RT}{p}\mathrm{d}p \qquad (2.69) \\ \frac{\mathrm{d}T}{T} &= \frac{R}{c_p}\frac{\mathrm{d}p}{p}. \qquad (2.70) \end{aligned}$$

We now integrate between the temperature-pressure pairs (T, p) and (θ, p_0):

$$\theta = T\left(\frac{p_0}{p}\right)^{\frac{R}{c_p}}. \qquad (2.71)$$

The potential temperature θ, defined above, is therefore the temperature of a parcel of air brought adiabatically and reversibly from state p, T to a reference pressure p_0.

Equation (2.71) needs to be used with the correct value of R/c_p in the case of moist air. This is because the effective gas constant and the effective specific heat at constant pressure for moist air depend on the specific humidity q.

To see this, suppose that the total enthalpy (not the *specific enthalpy*) for a parcel of air with total mass m can be calculated by adding the enthalpies of dry and moist air:

$$mh = m_d h_d + m_v h_v.$$

This produces

$$\begin{aligned} h &= \frac{\rho_d}{\rho}h_d + \frac{\rho_v}{\rho}h_v, \\ h &= (1-q)h_d + qh_v, \\ c_p &= \left(\frac{\partial h}{\partial T}\right)_p = (1-q)c_{pd} + qc_{pv} = (1 + 0.84q)c_{pd} \qquad (2.72) \end{aligned}$$

(using tabulated values for c_{pd} and c_{pv}).

On the basis of (2.46), the effective gas constant for moist air can be written as

$$R = R_d(1 + 0.61q) \qquad (2.73)$$

(note that this is an alternative interpretation to (2.46): we are now changing the gas constant R, and keeping the absolute temperature T, so that 2.39 still applies.) Therefore,

$$\frac{R}{c_p} = \frac{R_d}{c_{pd}}\frac{1 + 0.61q}{1 + 0.84q}. \qquad (2.74)$$

Using the identity

$$\frac{1 + ax}{1 + bx} \equiv 1 - (b - a)x + \frac{(b - a)bx^2}{1 + bx} \approx 1 - (b - a)x, \qquad (2.75)$$

we find (for small x)

$$\frac{R}{c_p} \approx (1 - 0.23q)\frac{R_d}{c_{pd}} \tag{2.76}$$

for moist air. Therefore,

$$\theta = T\left(\frac{p_0}{p}\right)^{(1-0.23q)\frac{R_d}{c_{pd}}} \tag{2.77}$$

It is also straightforward to obtain the specific heat at constant volume for moist air:

$$c_v = \left(\frac{\partial u}{\partial T}\right)_v = (1 - q)c_{vd} + qc_{vv} \tag{2.78}$$

Finally, these definitions extend to virtual temperature, but not uniquely, as discussed by (Brutsaert, 1982, section 3.2b). The *virtual potential temperature* is the virtual temperature that a parcel of moist air would have if changed adiabatically from its actual state to the standard pressure p_0:

$$\theta_{vp} = T_v\left(\frac{p_0}{p}\right)^{(1-0.23q)\frac{R_d}{c_{pd}}}. \tag{2.79}$$

This is slightly different from *potential virtual temperature*, which is the potential temperature of dry air at the same initial pressure and density, and which is given by

$$\theta_{pv} = T_v\left(\frac{p_0}{p}\right)^{\frac{R_d}{c_{pd}}}. \tag{2.80}$$

The two quantities defined by (2.79) and (2.80) are, evidently, numerically very similar. From here on, we will always use the virtual potential temperature (2.79). Also, for simplicity, we will refer to it simply as θ_v.

3

The measurement of surface fluxes

3.1 – Introduction

The emission of greenhouse gases from the surface of the Earth to its atmosphere is nowadays one of the largest environmental problems faced by humanity. It is a global problem, requiring the international negotiation of limits for the GEE emissions, as well as the development of internationally-accepted methodologies for their estimation.

One of the approaches to estimate these gases' fluxes is to perform micrometeorological measurements. Avoiding the complexity of the processes that occur at the surface or below it (be it water or soil/vegetation) and integrating greenhouse gas emissions vertically and over the wind fetch, micrometeorological measurements of greenhouse gases can give important answers about the value of surface fluxes, their seasonal and hourly pattern, and their relation with other important variables such as air, water, and soil temperatures, water quality, vegetation type, etc..

Micrometeorological measurements of greenhouse gases usually consist in measuring atmospheric variables close to the surface of the Earth. Conventionally, the measurements are split into "runs" that can be as short as 10 minutes, or as long as 1 hour. Within each run, it is common to assume stationarity of the measured time series. Measurements can be done by relatively slow sensors, when "averages" are obtained, or with sufficiently fast sensors to capture a significant part of the frequencies associated with atmospheric turbulence. In the latter case, turbulence statistics such as standard deviations, covariances, cross-correlation functions and spectra can be measured.

Measurements of average quantities are associated with the gradient flux method (GFM) for flux estimation. Measurements of turbulence quantities are associated with the eddy covariance method (ECM).

The GFM is older and involves more assumptions than the "direct measurements" performed by the ECM. In fact, as we will see, ECM measurements are not as direct as sometimes assumed. Due to the technological difficulties and cost, the GFM is still widely used to estimate gas fluxes such as CH_4 and N_2O, for which the measurement of turbulent fluctuations (especially in long-term studies) is still problematic.

The eddy covariance method (ECM), originally developed with momentum, sensible heat and water vapor mass fluxes in mind, has several desirable characteristics that make it appealing for GHG flux measurements: continuous measurements at the 30-minute or the hourly time scales can be made; spatial coverage is good, being of the order of hundreds of meters upwind of the measuring tower; and sensor technology is currently well developed and has a reasonable cost.

3.2 – Theorical foundation

This section has the objective of showing the bases of the GFM and especially of the ECM. In it, we review basic concepts about atmospheric gases and their concentrations; the *Reynolds decomposition* of a turbulent flow in average and fluctuation; and different kinds of averages — and consequently turbulent fluctuations — which are found in practice.

3.2.1 – The Reynolds and Boussinesq decompositions for turbulent flows

The Reynolds decomposition is the formal proceedure by which we decompose any variable a measured in the atmosphere into its average $\overline{a}$ and its turbulent fluctuation a'. The Reynolds decomposition consists of writing

$$a = \overline{a} + a', \tag{3.1}$$

but the subsequent manipulation of $\overline{a}$ and a' in the Navier-Stokes equation and the transport equation for a gas χ depends on the precise definition of the average. In this text, we will consider only 3 kinds of averages: block averages, running averages, and ensemble averages.

The Boussinesq decomposition is different. It separates the variable into its value in a reference hydrostatic state a_r and a fluctuation around it δa, as

$$a = a_r + \delta a. \tag{3.2}$$

3.2.2 – Ensemble averages

We will adopt here a variation of Kundu (1990)'s approach to calculate ensemble averages. In this approach, the realizations k of a random variable a, $a^{(k)}(x, y, z, t)$, are seen as a four-dimensional stochastic process. The realizations are considered in a countable, possibly infinite, sample space. The probability of realization k is p_k (in this context, we see no danger of confusing p_k with "pressure"). The ensemble average of $a(x, y, z, t)$ is defined as

$$\overline{a}(x, y, z, t) \equiv \sum_{k=1}^{\infty} a^{(k)}(x, y, z, t) p_k. \tag{3.3}$$

The fluctuation a' (that is also an stochastic process) is thence defined by (3.1). In turbulence, *we do not adopt the usual notation of writing uppercase letters for random variables*: the nature of the variables must be understood from the context or made explicit by the author.

When the stochastic process is stationary, the left side of (3.3) is reduced to $\overline{a}(x, y, z)$; if moreover the process is horizontally homogeneous, the dependence is reduced yet to $\overline{a}(z)$.

Having (3.3), it is possible now to prove the so-called Reynolds' postulates (that in this context should be properly called Reynolds' Theorems or, even better, Reynolds' Lemmas). They are:

$$\begin{aligned}
\overline{\overline{a}(x,y,z,t)} &= \sum_{k=1}^{\infty} \overline{a}(x,y,z,t)p_k \\
&= \overline{a}(x,y,z,t) \underbrace{\left[\sum_{k=1}^{\infty} p_k\right]}_{=1} \\
&= \overline{a}(x,y,z,t); \qquad (3.4)\\
\overline{a'(x,y,z,t)} &= \sum_{k=1}^{\infty} \left[a^{(k)}(x,y,z,t) - \overline{a}(x,y,z,t)\right] p_k \\
&= \sum_{k=1}^{\infty} a^{(k)}(x,y,z,t)p_k - \overline{a}(x,y,z,t) \sum_{k=1}^{\infty} p_k \\
&= \overline{a}(x,y,z,t) - \overline{a}(x,y,z,t) = 0; \qquad (3.5)
\end{aligned}$$

$$\begin{aligned}
\overline{\overline{a}(x,y,z,t)b'(x,y,z,t)} &= \sum_{k=1}^{\infty} \overline{a}(x,y,z,t) \left[b^{(k)}(x,y,z,t) - \overline{b}(x,y,z,t)\right] p_k \\
&= \overline{a}(x,y,z,t) \sum_{k=1}^{\infty} b^{(k)}(x,y,z,t)p_k \\
&\quad - [\overline{a}(x,y,z,t)] \left[\overline{b}(x,y,z,t)\right] \sum_{k=1}^{\infty} p_k \\
&= [\overline{a}(x,y,z,t)] \left[\overline{b}(x,y,z,t)\right] \\
&\quad - [\overline{a}(x,y,z,t)] \left[\overline{b}(x,y,z,t)\right] = 0; \qquad (3.6)\\
\overline{\frac{\partial a}{\partial x}} &= \sum_{k=1}^{\infty} \frac{\partial a^{(k)}}{\partial x} p_k \\
&= \frac{\partial}{\partial x} \sum_{k=1}^{\infty} a^{(k)}(x,y,z,t)p_k \\
&= \frac{\partial \overline{a}}{\partial x}. \qquad (3.7)
\end{aligned}$$

The last equation, (3.7), tells us that the partial derivatives commute with the ensemble average. Identical results hold, obviously, for any other independent variable than x.

3.2.3 – Block averages

The block average is maybe the simplest one that can be imagined; for a block of length T (we see no danger of confusing T with thermodynamic temperature T), it is defined by

$$n_t \equiv \lfloor t/T \rfloor; \qquad t_n \equiv n_t T; \tag{3.8}$$

$$\overline{a}(x,y,z,t) \equiv \frac{1}{T}\int_{t_n-T/2}^{t_n+T/2} a(x,y,z,\tau)\,d\tau, \qquad t_n - T/2 < t < t_n + T/2. \tag{3.9}$$

In (3.8), $\lfloor\cdot\rfloor$ is the "floor" function, which gives the integer part of the number. By definition, $\overline{a}(x,y,z,t)$ is a "step" function, that is not continuous at t_n. In the standard interpretation, the derivative of $\overline{a}(x,y,z,t)$ is either null or it does not exist; in the sense of distributions, the derivative is a series of *** Dirac's deltas each one over a t_n. Neither sense works for Renolds' lemma (3.7); notice, however, that (3.4)–(3.6) are all true:

$$\begin{aligned}
\overline{\overline{a}(x,y,z,t)} &= \frac{1}{T}\int_{t_n-T/2}^{t_n+T/2} \overline{a}(x,y,z,t)\,dt = \overline{a}(x,y,z,t);\\
\overline{a'(x,y,z,t)} &= \frac{1}{T}\int_{t_n-T/2}^{t_n+T/2} \left[a(x,y,z,t) - \overline{a}(x,y,z,t)\right]\,dt\\
&= \overline{a}(x,y,z,t) - \overline{a}(x,y,z,t) = 0;\\
\overline{\overline{a}(x,y,z,t)b'(x,y,z,t)} &= \frac{1}{T}\int_{t_n-T/2}^{t_n+T/2} \overline{a}(x,y,z,t)b'(x,y,z,t)\,dt\\
&= \overline{a}(x,y,z,t)\int_{t_n-T/2}^{t_n+T/2} b'(x,y,z,t)\,dt = 0.
\end{aligned}$$

The "problem" is with the last of the lemmas; it is trivial to verify that

$$\overline{\frac{da}{dt}} = \frac{1}{T}\int_{t_n-T/2}^{t_n+T/2} \frac{da}{d\tau}(x,y,z,\tau)\,d\tau = \frac{a(x,y,z,t_n+T/2) - a(x,y,z,t_n-T/2)}{T}, \tag{3.10}$$

but how to define in a decent way $d\overline{a}/dt$, if $\overline{a}$ is constant for $t_n - T/2 < t < t_n + T/2$? Some thought will bring us to the conclusion that there are not many choices, and a choice as good as any, and certainly one of the simplest, is to *define*

$$\frac{d\overline{a}}{dt} \equiv \frac{\overline{a}(t_{n+1}) - \overline{a}(t_{n-1})}{2T} = \frac{\frac{\overline{a}(t_{n+1})+\overline{a}(t_n)}{2} - \frac{\overline{a}(t_n)+\overline{a}(t_{n-1})}{2}}{T}. \tag{3.11}$$

Lemma (3.7) is therefore valid *approximately* for block averages as long as

$$a(t_n + T/2) \approx \frac{\overline{a}(t_{n+1}) + \overline{a}(t_n)}{2}, \tag{3.12}$$

$$a(t_n - T/2) \approx \frac{\overline{a}(t_n) + \overline{a}(t_{n-1})}{2}; \tag{3.13}$$

in this case, we have, *approximately* for block averages,

$$\overline{\frac{\mathrm{d}a}{\mathrm{d}t}} \approx \frac{\mathrm{d}\overline{a}}{\mathrm{d}t}. \tag{3.14}$$

Considering that $t_n - T/2$ and $t_n + T/2$ are exactly at the discontinuity points of $\overline{a}$, the approximations above — the arithmetic average of the block averages left and right of the discontinuity point — are reasonable and certainly the simplest ones we can imagine. This is the maximum we can obtain regarding the Reynolds postulates.

3.2.4 – Running averages

The running average of a quantity $a(x, y, z, t)$ is defined as

$$\overline{a}(x, y, z, t) \equiv \frac{1}{P} \int_{t-P/2}^{t+P/2} a(x, y, z, \tau)\, d\tau. \tag{3.15}$$

The window of the running average, P, is not to be confused with the length of the micrometeorological run, T, in (3.9); in micrometeorology, it is common to choose P in such a way that

$$\Delta t \ll P \ll T, \tag{3.16}$$

where Δt is the interval of data acquisition. More about this in ???

The main advantage of (3.15) is that a similar property to (3.7) continues to be valid for all independent variables, *including* t. In fact, from its definition we have

$$\overline{\frac{\partial a}{\partial t}} = \frac{1}{P} \int_{t-P/2}^{t+P/2} \frac{\partial a(\tau)}{\partial \tau}\, d\tau = \frac{1}{P} \left[a(t + P/2) - a(t - P/2) \right] \tag{3.17}$$

(where the dependence with (x, y, z) was omitted for simplicity), while

$$\begin{aligned} \frac{\partial \overline{a}}{\partial t} &= \frac{\partial}{\partial t} \left[\frac{1}{P} \int_{t-P/2}^{t+P/2} a(\tau)\, d\tau \right] \\ &= \frac{1}{P} \left[a(t + P/2) - a(t - P/2) + \int_{t-P/2}^{t+P/2} \frac{\partial a(\tau)}{\partial t}\, d\tau \right] \\ &= \frac{1}{P} \left[a(t + P/2) - a(t - P/2) \right]. \end{aligned} \tag{3.18}$$

(the second line of (3.18) is an application of Leibnitz's rule: note that $\partial a(\tau)/\partial t = 0$). The other results (3.4)–(3.6), however, do not hold:

$$\overline{\overline{a}}(t) = \frac{1}{P} \int_{t-P/2}^{t+P/2} \left[\frac{1}{P} \int_{\tau-P/2}^{\tau+P/2} a(\xi)\, d\xi \right] d\tau \neq \overline{a}(t); \tag{3.19}$$

$$\begin{aligned} \overline{a'}(t) &= \frac{1}{P} \int_{t-P/2}^{t+P/2} \left[a(\tau) - \frac{1}{P} \int_{\tau-P/2}^{\tau+P/2} a(\xi)\, d\xi \right] d\tau \\ &= \overline{a}(t) - \overline{\overline{a}}(t) \neq 0; \end{aligned} \tag{3.20}$$

$$\begin{aligned} \overline{\overline{a}b'}(t) &= \frac{1}{P} \int_{t-P/2}^{t+P/2} \left\{ \overline{a}(\tau) \left[b(\tau) - \overline{b}(\tau) \right] \right\} d\tau, \\ &= \frac{1}{P} \int_{t-P/2}^{t+P/2} \overline{a}(\tau) b(\tau)\, d\tau - \frac{1}{P} \int_{t-P/2}^{t+P/2} \overline{a}(\tau) \overline{b}(\tau)\, d\tau \\ &= \overline{\overline{a}b}(t) - \overline{\overline{a}\overline{b}}(t) \neq 0. \end{aligned} \tag{3.21}$$

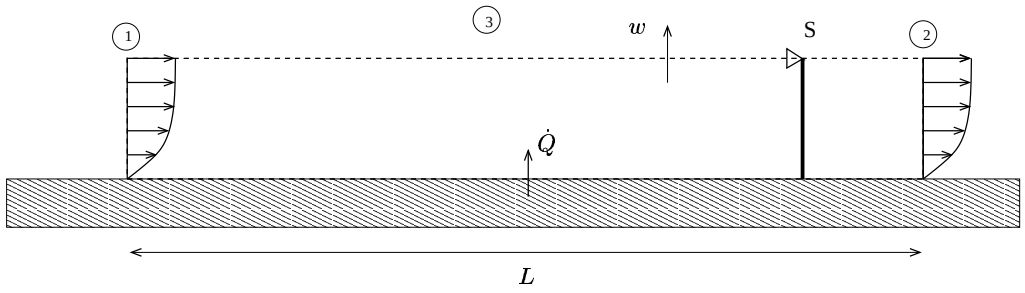

Figure 3.1: Mass balance to a virtual "box" (a control volume) of a height z_a over a homogeneous surface of length L throughout in the wind direction.

Results (3.19)–(3.21) mean that *a priori* it is considerably more complex to manipulate averages of the Navier-Stokes equations with running averages (3.15) than with ensemble averages (3.3) or with block averages (3.9).

One "practical" alternative in micrometeorology is to use the greater generality of (3.4)–(3.6) in the theoretical derivations, and then use the ergodic hypothesis and substitute all of the ensemble averages by running averages (that is: sample averages) in the analysis of results of micrometeorological experiments.

The use of block averages or the running averages carries with itself the necessity to estimate sample errors systematically when interpreting the experimental results. This analysis is not absolutely trivial, because these errors depend on the integral scales of the associated process (Lumley and Panofksy, 1964). There exists a considerable difficulty, and actually very few systematic research, to estimate integral scales. In the first place, integral scales need themselves to be estimated from the measured data. In principle, this is not possible: the integral scale implies an infinite averaging time to be calculated (Yaglom, 1987), which is not possible even asymptotically in the surface layer of the atmosphere, due to its non-stationarity at the hourly scale. (Stull, 1988). Moreover, in spite of what many researchers do when adopting a single value for the integral scale, each turbulence quantity has its own integral scale, and they should be calculated separately (Dias et al., 2004).

Alternatives to the *a priori* calculation of integral scales, however, do exist. They are: bootstrapping methods (Gluhovsky and Agee, 1994; Garcia et al., 2006), the filtering method (Salesky et al., 2012; Salesky and Chamecki, 2012) and the relaxed filtering method (Dias et al., 2018).

3.3 – The eddy covariance method (ECM)

3.3.1 – The integral balances for control volume

Figure 3.1 shows the essence of the eddy covariance method. We will illustrate it for several pairs of intensive quantity ↔ extensive quantity (Fox and McDonald, 1981) (indentified by the extensive quatities in the following list): the mass of dry air, the mass of water vapor, and the mass of CO_2.

For the control volume $\mathscr{V}$, limited by the closed surface $\mathscr{S}$, the mass balance equation of an atmospheric gas χ is

$$\int_{\mathscr{V}} s_\chi \, dV - \oint_{\mathscr{S}} (\boldsymbol{n} \cdot \boldsymbol{j}_\chi) \, dS = \frac{\partial}{\partial t} \int_{\mathscr{V}} \rho_\chi \, dV + \oint_{\mathscr{S}} \rho_\chi (\boldsymbol{n} \cdot \boldsymbol{u}) \, dS. \tag{3.22}$$

In (3.22), $\boldsymbol{j}_\chi$ is the diffusive mass flux of the gas χ on the surface of $\mathscr{V}$ and s_χ are the production sources of the gas χ inside $\mathscr{V}$ (for example, the production of CO_2 by the respiration of plants). These terms form the *total flux* of the gas χ into the control volume $\mathscr{V}$:

$$\mathscr{F}_\chi \equiv \int_{\mathscr{V}} s_\chi \, dV - \oint_{\mathscr{S}} (\boldsymbol{n} \cdot \boldsymbol{j}_\chi) \, dS. \tag{3.23}$$

To proceed, it is necessary to take into consideration the gaseous composition of the atmosphere, and the importance of the contributions to the sources and the diffusive fluxes at the boundaries of $\mathscr{V}$. Consider the atmosphere constituted essentially by 3 components. The "dry" part consists mainly of O_2 e N_2, taken together as a simple gas with constant $R_s = 287{,}05 \ \mathrm{J\,kg^{-1}\,K^{-1}}$ (the gas constant for dry air; see (2.17)). The wet component is the water vapor H_2O, whose gas constant is $R_v = 461{,}52\,\mathrm{J\,kg^{-1}\,K^{-1}}$. Now, consider a third component formed by a greenhouse gas. To fix the ideas, suppose it is CO_2, whose gas constant is $R_c = 188{,}92\,\mathrm{J\,kg^{-1}\,K^{-1}}$. The air density is the sum of each component:

$$\rho = \rho_s + \rho_v + \rho_c, \tag{3.24}$$

where ρ_s is the density of dry air, ρ_v is the density of water vapor, and ρ_c is the density of CO_2. Similarly, the diffusive fluxes and the sources add up:

$$s = s_s + s_v + s_c, \tag{3.25}$$

$$\boldsymbol{j} = \boldsymbol{j}_s + \boldsymbol{j}_v + \boldsymbol{j}_c. \tag{3.26}$$

For dry air, $s_s = 0$, and $\boldsymbol{j}_s = 0$ at the surface-atmosphere interface (Finnigan, 2009). According to Lee and Massman (2011), this hypotheses is a fundamental novelty of the theory proposed by Webb et al. (1980).

Expanding the derivative with respect to time in (3.22),

$$\mathscr{F}_\chi = \int_V \frac{\partial \rho_\chi}{\partial t} \, dV + \oint_S \rho_\chi (\boldsymbol{n} \cdot \boldsymbol{u}) \, dS. \tag{3.27}$$

The term involving the mass advection through the control surface needs to be evaluated for each of the surfaces ①, ② and ③:

$$\int_{①} \rho_\chi (\boldsymbol{n} \cdot \boldsymbol{u}) \, dS = - \int_{y=0}^{b} \int_{z=0}^{z_a} \rho_\chi u(x = 0, y, z, t) \, dz \, dy, \tag{3.28}$$

$$\int_{②} \rho_\chi (\boldsymbol{n} \cdot \boldsymbol{u}) \, dS = + \int_{y=0}^{b} \int_{z=0}^{z_a} \rho_\chi u(x = L, y, z, t) \, dz \, dy, \tag{3.29}$$

$$\int_{③} \rho_\chi (\boldsymbol{n} \cdot \boldsymbol{u}) \, dS = + \int_{x=0}^{L} \int_{y=0}^{b} \rho_\chi w(x, y, z = z_a, t) \, dy \, dx. \tag{3.30}$$

Consider now the average of (3.27), denoted by a bar. Using the commutation properties of the average with the derivative, expressed by (3.7), (3.14) and (3.17)–(3.18) respectively for the ensemble average, the block average and the running average,

$$\overline{\mathscr{F}_\chi} = \int_V \frac{\partial \overline{\rho}}{\partial t}\, dV + \oint_S \overline{\rho(\boldsymbol{n}\cdot\boldsymbol{u})}\, dS. \tag{3.31}$$

Note that $\overline{\mathscr{F}_\chi}$ is a mass transfer rate into $\mathscr{V}$, in $\mathrm{kg}_\chi\,\mathrm{s}^{-1}$ in the SI.

If the flow is *homogeneous* in x and y, then, for the ensemble average,

$$\overline{[\rho_\chi u]}(x=0,y,z) = \overline{[\rho_\chi u]}(x=L,y,z),\ \forall y,z \tag{3.32}$$

note that this *is valid only on average*; proceeding,

$$\int_{①} \overline{\rho_\chi(\boldsymbol{n}\cdot\boldsymbol{u})}\, dS + \int_{②} \overline{\rho_\chi(\boldsymbol{n}\cdot\boldsymbol{u})}\, dS = 0. \tag{3.33}$$

Also note that in the case of block and running averages, (3.32) and (3.33) are valid only approximately.

Horizontal homogeneity also implies that $\overline{[\rho_\chi w]}(x,y,z=z_a)$ is independent of both x and y, whence

$$\int_{x=0}^{L}\int_{y=0}^{b} \overline{[\rho_\chi w]}(x,y,z=z_a)\, dy\, dx = \overline{[\rho_\chi w]}(z=z_a)bL. \tag{3.34}$$

For the average density $\overline{\rho_\chi}$ the hypothesis of horizontal homogeneity produces

$$\overline{\rho_\chi} = \overline{\rho_\chi}(z,t), \tag{3.35}$$

where (3.27), using (3.33) and (3.34), reduces to

$$\begin{aligned} \overline{\mathscr{F}_\chi} &= bL\int_0^{z_a} \frac{\partial \overline{\rho_\chi}}{\partial t}\, dz + bL\overline{[\rho_\chi w]}(z=z_a), \\ \frac{\overline{\mathscr{F}_\chi}}{bL} \equiv F_\chi &= \int_0^{z_a} \frac{\partial \overline{\rho_\chi}}{\partial t}\, dz + \overline{[\rho_\chi w]}(z=z_a), \end{aligned} \tag{3.36}$$

where F_χ is the specific mass flux (flux per unit of surface area) of the gas. The transient term is kept in (3.36) to allow an analysis of its importance, which now follows.

By the mean value theorem of differential and integral calculus, if $0 \le z^* \le z_a$:

$$F_\chi = \frac{\partial}{\partial t}\left\{z_a \overline{\rho_\chi}(z^*)\right\} + \overline{[\rho_\chi w]}(z=z_a). \tag{3.37}$$

The transient term can be neglected if

$$z_a \frac{\partial}{\partial t}\left\{\overline{\rho_\chi}(z^*)\right\} \ll \overline{[\rho_\chi w]}(z=z_a); \tag{3.38}$$

in this case, we get the standard equation of the eddy covariance method for the surface flux of gas χ:

$$F_\chi = \overline{[\rho_\chi w]}(z=z_a). \tag{3.39}$$

Note that the choice of z_a is crucial: the bigger the value, the more important becomes the effect of $\partial\overline{\rho_\chi}/\partial t$; as one would expect the value of $\overline{\rho_\chi}$ to evolve over over time as a funcion of the flux F_χ, it is not realistic to assume that the transient term is identically null in a real atmosphere; strictly speaking, it is a combination of a small value of the time derivative with a "low" height of measurement (besides of course the horizontal homogeneity hypothesis) that assures that (3.39) gives us an accurate value of F_χ in the surface.

As we saw above, for dry air $\mathscr{F}_s \equiv 0$, where (3.39) with $\chi = s$, gives

$$\frac{\overline{\mathscr{F}_s}}{bL} = 0 = \overline{[\rho_s w]}(z = z_a). \tag{3.40}$$

This is a fundamental hypothesis in the deduction of the WPL correction (Webb et al., 1980), that however is only briefly mentioned in that paper. In this text, (3.40) is rigorously derived from the horizontal homogeneity hypothesis and from the stationarity and dry air budget for a control volume, in essentially the same way as in Finnigan (2009), and Lee and Massman (2011).

Under the same hypothesis of homogeneity and stationarity, and taking respectively $\chi = v$ e $\chi = c$, the specific fluxes (*i.e.*, per unit of area) of water vapor mass and CO_2 mass are

$$E \equiv \frac{\overline{\mathscr{F}_v}}{bL} = \overline{[\rho_v w]}(z = z_a), \tag{3.41}$$

$$F \equiv \frac{\overline{\mathscr{F}_c}}{bL} = \overline{[\rho_c w]}(z = z_a). \tag{3.42}$$

Besides the mass fluxes described above, also indispensable in micrometeorological measurements are the momentum flux,

$$\tau \equiv \frac{\overline{\mathscr{F}_u}}{bL} = \overline{[\rho u w]}(z = z_a), \tag{3.43}$$

and the sensible heat flux,

$$H \equiv \frac{\overline{\mathscr{F}_\theta}}{bL} = \overline{[\rho c_p w \theta]}(z = z_a), \tag{3.44}$$

where θ is potential temperature.

In the name of simplicity, from now on we will omit the measurement level; in this way, for example, we write $\overline{\rho_v w}$ instead of $\overline{[\rho_v w]}(z = z_a)$.

3.3.2 – Non-ideal conditions

Nocturnal turbulence tends to be intermittent. In strongly stable conditions with Richardson number $\mathrm{Ri} \lesssim 0{,}2$, turbulence is strongly damped or even suppressed (Kondo et al., 1978; Cheng et al., 2005). This value, however, is debatable; see Zilitinkevich et al. (2007) and Galperin et al. (2007).

Two important problems of the nocturnal measurement of CO_2 fluxes with the eddy covariance method are (Aubinet, 2008):

1. The turbulence intermittency that produces non-stationarity conditions during which the method's hypothesis can fail; and

2. The occurrence of breezes and katabatic flows, during which the effects of horizontal advection, that also invalidate (in principle) the method can become very important.

The observation that the measurements with the eddy covariance method could be systematically underestimating the CO_2 fluxes appears to have been done for the first time by Goulden et al. (2006). Once this is realized, it is possible to correct the error ("correction approach") or eliminate the suspect measurements ("filtering approach") (Aubinet, 2008). The most usual approach is to eliminate the measurements associated to a friction velocity below a certain level.

Once the problems posed by the relatively simplistic measurement of the CO_2 flux with only one tower, and in only only level, were identified, explanations started to be searched. Among them, we found the analysis of Lee (1998), and the subsequent, and very important, comments of Finnigan (1999).

In real conditions, the perfect horizontal homogeneity and stationarity assumed in MOS theory, and used in the derivation of the equation of the eddy covariance method presented in the text, obviously fail. The degree to which this affects the surface flux measurements, however, is extremely hard to be established. Attempts to calculate, in particular, the advective terms neglected in the theory (the calculation of local advection effects) are very hard, because they involve the need to measure horizontal and vertical gradients of gas concentration. For this it is necessary that sensors placed at different points be carefully calibrated to eliminate the systematic errors, since the advective terms always involve the measurement of concentration *differences* between two points. In this sense the study of Heinesch et al. (2007) suggests that it is possible to estimate CO_2 horizontal gradients, and therefore its local horizontal advection, but that the vertical advection term estimate, that involves the vertical velocity $\overline{w}$ measurement, is considerably harder.

Similar conclusions, although more detailed, were obtained in the careful study of Leuning et al. (2008), in which all of the terms of the mass integral balance of CO_2 in a control volume of $50 \times 50 \times 6\,m^3$ were measured or very well estimated: in this work, the vertical and horizontal advection terms were shown to be important in nocturnal measurements, with smaller errors occurring in diurnal conditions.

As we shall see next, an estimate of the mean vertical velocity is at the core of the WPL correction, and more studies (and possibly technological progress) are probably necessary for the improvement of the flux measurements in non-ideal conditions, such as with undulating topography and in the presence of advective and non-stationarity effects.

4

The dynamical equations for the ABL

The transport equations express the principles of conservation of total mass, momentum, energy and mass of a mixed substance (for instance water vapor) at a point in space and instant in time. In principle, any fluid mechanics problem can be solved if we know the constitutive equation (the rate of strain – stress relation) and the boundary conditions.

In practice, the problem is much more complicated. The momentum equations are non-linear, making the solution (either analytical or numerical) much more difficult. Morever, they display chaotic behavior, which causes very small differences in the boundary conditions to amplify very fast (Ruelle, 1994). Finally, their full solution requires the resolution of extremely small scales (the Kolmogorov microscales), rendering the problem impossible to solve on the basis of the fundamental equations alone, and requiring additional hypothesis regarding their closure at some level: this is the well known turbulence closure problem (Wyngaard, 1981).

4.1 – Differential operators

It is convenient to adopt a double notation for the position and velocity vectors, and the basis for $\mathbb{R}^3$, *viz.*

$$\boldsymbol{x} = (x, y, z) \equiv (x_1, x_2, x_3), \tag{4.1}$$

$$\boldsymbol{u} = (u, v, w) \equiv (u_1, u_2, u_3), \tag{4.2}$$

$$(\boldsymbol{i}, \boldsymbol{j}, \boldsymbol{k}) \equiv (\boldsymbol{e}_1, \boldsymbol{e}_2, \boldsymbol{e}_3). \tag{4.3}$$

The equations of fluid mechanics involve four differential operators: the divergence, the curl, the laplacian, and the operator for the material derivative. They are:

$$\begin{aligned} \boldsymbol{\nabla} \cdot \boldsymbol{u} &= \frac{\partial u}{\partial x} + \frac{\partial v}{\partial y} + \frac{\partial w}{\partial z} \\ &= \sum_{k=1}^{3} \frac{\partial u_k}{\partial x_k}; \end{aligned} \tag{4.4}$$

$$\begin{aligned}\boldsymbol{\nabla}\times\boldsymbol{u} &= \left(\frac{\partial w}{\partial y}-\frac{\partial v}{\partial z}\right)\boldsymbol{i}+\left(\frac{\partial u}{\partial z}-\frac{\partial w}{\partial x}\right)\boldsymbol{j}+\left(\frac{\partial v}{\partial x}-\frac{\partial u}{\partial y}\right)\boldsymbol{k}\\ &= \sum_{k=1}^{3}\sum_{i=1}^{3}\sum_{j=1}^{3}\epsilon_{ijk}\frac{\partial u_j}{\partial x_i}\boldsymbol{e}_k;\end{aligned} \tag{4.5}$$

$$\begin{aligned}\nabla^2 a &= \frac{\partial^2 a}{\partial x\partial x}+\frac{\partial^2 a}{\partial y\partial y}+\frac{\partial^2 a}{\partial z\partial z}\\ &= \sum_{k=1}^{3}\frac{\partial^2 a}{\partial x_k\partial x_k};\end{aligned} \tag{4.6}$$

$$\begin{aligned}\frac{Da}{Dt} &= \frac{\partial a}{\partial t}+u\frac{\partial a}{\partial x}+v\frac{\partial a}{\partial y}+w\frac{\partial a}{\partial z}\\ &= \frac{\partial a}{\partial t}+\sum_{k=1}^{3}u_k\frac{\partial a}{\partial x_k},\end{aligned} \tag{4.7}$$

where a represents any scalar field and $\boldsymbol{\nabla}$ is the "symbolic" vector $(\frac{\partial}{\partial x},\frac{\partial}{\partial y},\frac{\partial}{\partial z})$. The first line in each of the equations above gives the formula for each operator in x, y, and z notation. The second line shows that all operators can be written in a compact form as sums. For the curl, the permutation symbol $\epsilon_{ijk}=+1$ for cyclic permutations (1,2,3), (2,3,1), (3,1,2); $\epsilon_{ijk}=-1$ for anti-cyclic permutations (1,3,2), (2,1,3), (3,1,2); and $\epsilon_{ijk}=0$ if $i=j$, $j=k$, $k=i$ or $i=j=k$.

In the equations that follow, we will adopt most of the time the compact sum notation. In particular cases, it will be more frutiful to shift back to the notation involving (x,y,z) and (u,v,w).

4.2 – The hydrostatic reference state

Consider again the first law for an adiabatic atmosphere, as in 2.69, repeated here,

$$c_p\mathrm{d}T_r = v_r\mathrm{d}p_r, \tag{4.8}$$

together with the hydrostatic equation

$$\frac{\mathrm{d}p_r}{\mathrm{d}z} = -\rho_r g. \tag{4.9}$$

Above, the subscript r means the reference state for a hydrostatic equation. Together with the state equation (2.39), equations (4.8)–(4.9) form a system from which we can eliminate either T_r, p_r or $v_r=1/\rho_r$. Three equations result for the reference pressure, temperature or density as a function of z (bear in mind that in a moist atmosphere c_p, c_v and R are given by 2.72, (2.78) and 2.73 respectively):

$$T_r(z) = T_0-\frac{g}{c_p}z, \tag{4.10}$$

$$p_r(z) = p_0\left(\frac{T_0-\frac{g}{c_p}z}{T_0}\right)^{c_p/R}, \tag{4.11}$$

$$\rho_r(z) = \rho_0\left(\frac{T_0-\frac{g}{c_p}z}{T_0}\right)^{c_v/R}. \tag{4.12}$$

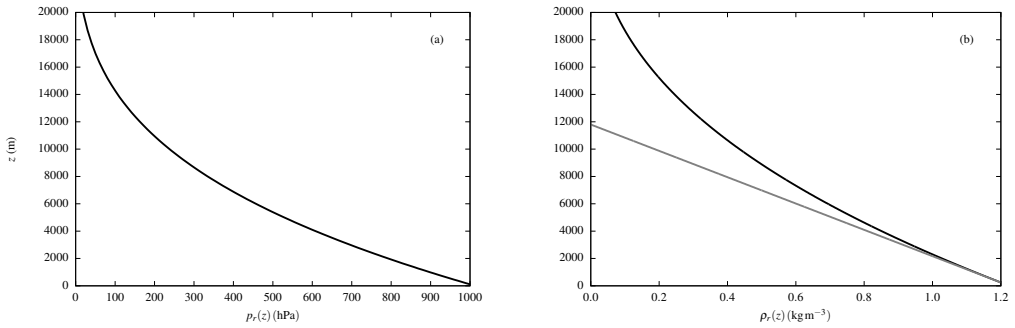

Figure 4.1: Reference pressure p_r and density ρ_r in a hydrostatic and adiabatic equation.

Figure 4.1 shows the pressure and density reference states in the atmosphere as functions of z, for $T_0 = 15\,^\circ$C and $p_0 = 101\,325$ Pa. The *scale height* is defined as

$$D = \left| \frac{1}{\rho_0} \frac{\mathrm{d}\rho_r(0)}{\mathrm{d}z} \right|^{-1}; \tag{4.13}$$

it is obtained by extrapolating the straight line with the same slope as the reference density profile at the surface up to $\rho_r = 0$, as seen in figure 4.1-b.

4.3 – Mass conservation and the Boussinesq approximation

The derivation of the transport equations for u, v, w, θ, q, θ_v, ... is a long process involving a fair amount of physics and mathematics. It can be found in various texts, such as Batchelor (1967), Bird et al. (1960) and Landau and Lifshitz (1959). An excellent itroduction to the equations in a form often used in the ABL is Stull (1988)'s book.

We will briefly analyze the dynamical equations in light of the *Boussinesq approximation*. First we define a thickness ℓ such that the reference density changes little between $z = 0$ and $z = \ell$. From figure 4.1-b, it can be seen that

$$\frac{\Delta\rho_r}{\rho_0} \leq \frac{\ell}{D} \equiv \epsilon_b \ll 1, \tag{4.14}$$

where $\rho_0 = \rho_r(0)$. In (4.14), we use any appropriately small value of ϵ_b (say $\epsilon_b = 0.01$), to define ℓ rigorously.

Next we define the *Boussinesq decompositions*

$$u_i = 0 + u_{\delta i}, \tag{4.15}$$
$$\rho = \rho_r + \rho_\delta, \tag{4.16}$$
$$p = p_r + p_\delta, \tag{4.17}$$
$$T = T_r + T_\delta. \tag{4.18}$$

Above, u_δ, ρ_δ, p_δ and T_δ are the fluctuations of velocity, density, pressure, and temperature of an actual ("dynamic") atmosphere with respect to the reference hydrostatic state.

Of course, (4.15)–(4.18) can be further expanded by means of a Reynolds' decomposition, yielding

$$\overline{u_i} + u_i' = \overline{u_{\delta i}} + u_{\delta i}', \tag{4.19}$$
$$\overline{\rho} + \rho' = \rho_r + \overline{\rho_\delta} + \rho_\delta', \tag{4.20}$$
$$\overline{p} + p' = p_r + \overline{p_\delta} + p_\delta', \tag{4.21}$$
$$\overline{T} + T' = T_r + \overline{T_\delta} + T_\delta'. \tag{4.22}$$

Then, the following relations hold (trivially) between the Reynolds decomposition and the Boussinesq decomposition:

$$\overline{u_i} = \overline{u_{\delta i}} \qquad u_i' = u_{\delta i}', \tag{4.23}$$
$$\overline{\rho} = \rho_r + \overline{\rho_\delta} \qquad \rho' = \rho_\delta', \tag{4.24}$$
$$\overline{p} = p_r + \overline{p_\delta} \qquad p' = p_\delta', \tag{4.25}$$
$$\overline{T} = T_r + \overline{T_\delta} \qquad T' = T_\delta', \tag{4.26}$$

whence

$$u_i = 0 + \overline{u_{\delta i}} + u', \tag{4.27}$$
$$\rho = \rho_r + \overline{\rho_\delta} + \rho', \tag{4.28}$$
$$p = p_r + \overline{p_\delta} + p', \tag{4.29}$$
$$T = T_r + \overline{T_\delta} + T'. \tag{4.30}$$

Clearly, the notations $\overline{u_{\delta i}}$ and $u_{\delta i}'$, ρ_δ', p_δ' and T_δ' in (4.23)–(4.26) are excessive, and will not be used any further.

Only now we introduce the Boussinesq approximation proper: it is the assumption that the dynamic density fluctuations ρ_δ are of the same order of magnitude of the variation of the reference density ρ_r within the layer of thickness ℓ. In view of the definition of D in (4.13) and (4.14), it is

$$\rho_\delta \sim \rho_0 \frac{\ell}{D} \ll \rho_r, \qquad 0 \le z \le \ell. \tag{4.31}$$

Now consider the full form for the equation for (total) mass conservation, which reads

$$\frac{\partial \rho}{\partial t} + \sum_{k=1}^{3} \frac{\partial (\rho u_k)}{\partial x_k} = 0. \tag{4.32}$$

Its ensemble average is

$$\frac{\partial \overline{\rho}}{\partial t} + \sum_{k=1}^{3} \frac{\partial \overline{\rho u_k}}{\partial x_k} = 0. \tag{4.33}$$

Expanding all terms with the help of (4.27)–(4.30) and Reynolds' postulates (3.4)–(3.7),

$$\underbrace{\frac{\partial \overline{\rho_\delta}}{\partial t}}_{\text{I}} + \sum_{k=1}^{3} \underbrace{\overline{u_k} \frac{\partial \rho_r}{\partial x_k}}_{\text{II}} + \sum_{k=1}^{3} \underbrace{\overline{u_k} \frac{\partial \overline{\rho_\delta}}{\partial x_k}}_{\text{III}} + \sum_{k=1}^{3} \underbrace{\rho_r \frac{\partial \overline{u_k}}{\partial x_k}}_{\text{IV}} + \sum_{k=1}^{3} \underbrace{\overline{\rho_\delta} \frac{\partial \overline{u_k}}{\partial x_k}}_{\text{V}} + \sum_{k=1}^{3} \underbrace{\frac{\partial \overline{\rho' u_k'}}{\partial x_k}}_{\text{VI}} = 0. \tag{4.34}$$

The order of magnitude of each individual term in the sums above can be established relatively easily. For that, we need to define in some useful way a density scale $\tilde{\rho}$ and a velocity scale $\tilde{u}$. Due to (4.28) and (4.31), we will define

$$\tilde{\rho} \sim \overline{\rho_\delta} \sim \rho', \tag{4.35}$$

and

$$\tilde{u} \sim \overline{u_k}; \qquad \tilde{\rho}\tilde{u} \sim \overline{\rho' u_k'}. \tag{4.36}$$

With that, one finds

$$\begin{aligned}
\mathrm{I} &\sim \frac{\tilde{\rho}\tilde{u}}{\ell};\\
\mathrm{II} &\sim \frac{\wp_0 \tilde{u}}{D} \sim \frac{\tilde{\rho}\tilde{u}}{\ell};\\
\mathrm{III} &\sim \frac{\tilde{\rho}\tilde{u}}{\ell};\\
\mathrm{IV} &\sim \frac{\rho_0 \tilde{u}}{\ell};\\
\mathrm{V} &\sim \frac{\tilde{\rho}\tilde{u}}{\ell};\\
\mathrm{VI} &\sim \frac{\tilde{\rho}\tilde{u}}{\ell}.
\end{aligned}$$

The upshot is that all individual terms in I–III, and V–VI, are much smaller than the individual terms in IV. The *sum* of all three terms in IV must be of the same order of the other terms, whence

$$\sum_{k=1}^{3} \frac{\partial \overline{u_k}}{\partial x_k} \sim \frac{\tilde{\rho}}{\rho_0}\frac{\tilde{u}}{\ell} \ll \frac{\tilde{u}}{\ell} \Rightarrow \sum_{k=1}^{3} \frac{\partial \overline{u_k}}{\partial x_k} \approx 0. \tag{4.37}$$

Equation (4.37) is often first found in fluid mechanics in the context of mass conservation in an incompressible flow. Here, it is only *approximately valid* (we are in the context of the Boussinesq *approximation*); it is valid (at this point) for the mean velocity field $\overline{\boldsymbol{u}}$ only; and *it does not mean that there are no density fluctuations*.

The same approach can be taken for the full momentum equation, which is (for a Newtonian fluid)

$$\begin{aligned}
\left[\frac{\partial(\rho u_i)}{\partial t} + \sum_{k=1}^{3}\frac{\partial(\rho u_i u_k)}{\partial x_k} + \sum_{k=1}^{3}\sum_{j=1}^{3} 2\epsilon_{ijk}\Omega_j u_k\right] &= \rho g_i - \frac{\partial p}{\partial x_i} + \\
\frac{\partial}{\partial x_i}\left(\lambda \sum_{k=1}^{3}\frac{\partial u_k}{\partial x_k}\right) + \nu\rho \sum_{k=1}^{3}\frac{\partial s_{ik}}{\partial x_k}, &\qquad i = 1,\ldots,3,
\end{aligned} \tag{4.38}$$

where Ω is the angular velocity of the Earth; $\sum_{k=1}^{3}\sum_{j=1}^{3} 2\epsilon_{ijk}\Omega_j u_k$ is the Corilis acceleration along x_i; $\boldsymbol{g} = (0, 0, -g)$ is the accelration of gravity, and ν is the kinematic viscosity. Expanding and estimating orders of magnitude for (4.38) however, is now a lengthy and somewhat tedious procedure. Perhaps the most

revealing part is the effect that the Boussinesq decomposition has on the gravity and pressure terms:

$$\begin{aligned}\rho g_i - \frac{\partial p}{\partial x_i} &= (\rho_r + \rho_\delta) g_i - \frac{\partial (p_r + p_\delta)}{\partial x_i} \\ &= \rho_\delta g_i - \frac{\partial p_\delta}{\partial x_i},\end{aligned} \tag{4.39}$$

in view of the hydrostatic equation (4.9). Equation (4.39) shows very clearly that an important part of the acceleration in the fluid is caused by the differences in bouyancy caused *Boussinesq fluctuations* in density, ρ_δ.

If one now proceeds with the Boussinesq and Reynolds decomposition, followed by averaging and simplification with (4.33) (which we omit, but encourage the reader to undertake!), the final result is

$$\rho_r \left[\frac{\partial \overline{u_i}}{\partial t} + \overline{u_k} \frac{\partial \overline{u_i}}{\partial x_k} + \frac{\partial \overline{u_i u_k}}{\partial x_k} \right] - \left[\overline{\rho_\delta} g_i - \frac{\partial \overline{p_\delta}}{\partial x_i} \right] \sim \frac{\tilde{\rho} \tilde{u}^2}{\ell}. \tag{4.40}$$

Each of the individual terms above can be shown to be $\sim \rho_0 \tilde{u}^2/\ell$. The Coriolis terms, which do not appear above, are of the order of $\rho_0 \tilde{u}^2/(\mathrm{Ro}\ell)$ (where $\mathrm{Ro} = \tilde{u}/(f\ell)$ is the Rossby number, and $f = 2\Omega \sin(\phi)$ is the Coriolis parameter). At the scale of the flow, ℓ, the Rossby number is very large and consequently Coriolis effects are negligible. For the left-hand side of (4.40), therefore, one has

$$g\tilde{\rho} \sim \rho_0 \frac{\tilde{u}^2}{\ell}, \tag{4.41}$$

$$\frac{\tilde{p}}{\ell} \sim \rho_0 \frac{\tilde{u}^2}{\ell} \quad \Rightarrow \tag{4.42}$$

$$\tilde{p} \sim \tilde{\rho} g \ell. \tag{4.43}$$

Pressure fluctuations are extremely difficult to measure in the atmosphere. Wyngaard (2010) gives the estimate $p' \sim \rho_0 \tilde{u}^2$; this is the same as (4.42). Hauf et al. (1996) observed values of p' of the order of 2.5 Pa, which again is the same order as given by Wyngaard. The main consequence of (4.43) is that the effects of the pressure fluctuations p_δ and p' can often be neglected in the atmosphere.

The order of magnitude of the Boussinesq pressure fluctuations now leads to the following approximation in the state equation:

$$\begin{aligned} p &= \rho R_d T_v, \\ [p_r + p_\delta] &= [\rho_r + \rho_\delta] R_d [T_{vr} + T_{v\delta}], \\ p_r + p_\delta &\approx \rho_r R_d T_{vr} + \rho_r R_d T_{v\delta} + \rho_\delta R_d T_{vr}, \end{aligned}$$

where the product $\rho_\delta R_d T_{v\delta}$ has been neglected. By definition, the equation of state, $p_r = \rho_r R_d T_{vr}$ holds for the hydrostatic reference state; therefore,

$$\begin{aligned} p_\delta &\approx \rho_r R_d T_{v\delta} + \rho_\delta R_d T_{vr}, \\ \underbrace{\frac{p_\delta}{p_r}}_{\sim \frac{\tilde{p}}{p_0}} &\approx \underbrace{\frac{T_{v\delta}}{T_{vr}}}_{\sim \frac{\tilde{T}}{T_0}} + \underbrace{\frac{\rho_\delta}{\rho_r}}_{\sim \frac{\tilde{\rho}}{\rho_0}} \end{aligned}$$

But

$$\frac{\tilde{\rho}}{\rho_0} \sim \epsilon_b = 0.01 \qquad \text{by definition,}$$
$$\frac{\tilde{p}}{p_0} \sim \frac{2.5}{101\,325} = 2.47 \times 10^{-5} \ll 0.01.$$

Therefore, the Boussinesq pressure fluctuations can be safely dismissed. This leads to a much simpler linear equation of state that does not include pressure, namely

$$\frac{\rho_\delta}{\rho_r} = -\frac{T_{v\delta}}{T_r}. \tag{4.44}$$

Exercise

4.1 Using Reynolds' decomposition (3.1) and Reynolds' postulates (3.4)–(3.7), show that

$$\frac{\overline{\rho_\delta}}{\rho_r} = -\frac{\overline{T_{v\delta}}}{T_r},$$
$$\frac{\rho'}{\rho_r} = -\frac{T'_v}{T_r}.$$

4.4 – The Reynolds-averaged Navier-Stokes equations

Under the validity of the Boussinesq approximation (4.31), the mass and momentum conservation equations (4.37) and (4.40) are correct to order ϵ_b. We are unaware of works that deal with the extension of the Boussinesq approximation to the higher-order, second-moment equations that are essential to understand the mechanics of turbulent flow, and which were introduced by O. Reynolds in 1895 (Reynolds, 1895). We will however *assume* that the equations for the turbulent fluctuations of velocity and other quantities are analogous to (4.37) and (4.40) for the means.

Under these further assumptions, application of Reynolds' decomposition (3.1) to the mass and momentum equations (4.33) and (4.38), and subtraction of the equations for means,(4.37) and (4.40), eventually results in

$$\sum_{k=1}^{3} \frac{\partial u'_k}{\partial x_k} = 0 \tag{4.45}$$

$$\frac{\partial u'_i}{\partial t} + \sum_{k=1}^{3} \overline{u_k} \frac{\partial u'_i}{\partial x_k} = \sum_{k=1}^{3} \left[-u'_k \frac{\partial \overline{u_i}}{\partial x_k} - \frac{\partial u'_i u'_k}{\partial x_k} \right] - \sum_{j=1}^{3} \sum_{k=1}^{3} 2\epsilon_{ijk} \Omega_j u'_k$$
$$- \frac{1}{\overline{\rho}} \frac{\partial p'}{\partial x_i} - \frac{g_i}{\overline{\theta}_v} \theta'_v + 2\nu \sum_{k=1}^{3} \frac{\partial s'_{ik}}{\partial x_k}, \tag{4.46}$$

where $\boldsymbol{g} = (0, 0, -g)$ with $g = 9.81\,\mathrm{m\,s^{-2}}$. Note that the average of (4.45) and (4.46) above is zero. Multiplication of (4.46) by u_j', exchange of the indices i and j and summation of the two resulting equations, followed by averaging, leads the the second-order equations

$$\begin{aligned}
&\underbrace{\frac{\partial \overline{u_i' u_j'}}{\partial t}}_{\mathrm{I}} + \sum_{k=1}^{3} \underbrace{\overline{u_k} \frac{\partial \overline{u_i' u_j'}}{\partial x_k}}_{\mathrm{II}} = \sum_{k=1}^{3} \underbrace{-\overline{u_i' u_k'} \frac{\partial \overline{u_j}}{\partial x_k} - \overline{u_j' u_k'} \frac{\partial \overline{u_i}}{\partial x_k}}_{\mathrm{III}} - \sum_{k=1}^{3} \underbrace{\frac{\partial\, \overline{u_i' u_j' u_k'}}{\partial x_k}}_{\mathrm{IV}} \\
&\qquad \underbrace{-\frac{1}{\theta_{vr}} \left[g_i \overline{u_j' \theta_v'} + g_j \overline{u_i' \theta_v'} \right]}_{\mathrm{V}} \\
&\qquad \underbrace{-2 \sum_{k=1}^{3} \sum_{l=1}^{3} \Omega_l \left(\epsilon_{ilk} \overline{u_j' u_k'} + \epsilon_{jlk} \overline{u_i' u_k'} \right)}_{\mathrm{VI}} \\
&\qquad \underbrace{-\frac{1}{\rho_r} \left(\frac{\partial\, \overline{u_i' p'}}{\partial x_j} + \frac{\partial\, \overline{u_j' p'}}{\partial x_i} \right)}_{\mathrm{VII}} \underbrace{- \overline{\frac{p'}{\rho_r} \left(\frac{\partial u_i'}{\partial x_j} + \frac{\partial u_j'}{\partial x_i} \right)}}_{\mathrm{VIII}} \\
&\qquad + 2\nu \sum_{k=1}^{3} \underbrace{\frac{\partial}{\partial x_k} \left[\overline{u_j' s_{ik}'} + \overline{u_j' s_{jk}'} \right]}_{\mathrm{IX}} \\
&\qquad - 2\nu \sum_{k=1}^{3} \underbrace{\left[\overline{s_{ik}' \frac{\partial u_j'}{\partial x_k}} + \overline{s_{jk}' \frac{\partial u_i'}{\partial x_k}} \right]}_{\mathrm{X}}
\end{aligned} \tag{4.47}$$

In (4.47),

$$s_{ik}' = \frac{1}{2} \left(\frac{\partial u_i'}{\partial x_k} + \frac{\partial u_k'}{\partial x_i} \right) \tag{4.48}$$

is the fluctuation rate of deformation.

The set (4.47) is essential to understand the physics of turbulence. We borrow from (Stull, 1988) their meanings:

I. Is the local rate of change of the covariance $\overline{u_i' u_j'}$.

II. Is the advection of $\overline{u_i' u_j'}$ by the mean wind $\overline{u_k}$.

III. Is the *gradient production/destruction term*. A loose interpretation is that the average profiles are subject to perturbations that generate large-scale structures that progressively break into smaller structures, and so on. The larger structures are anisotropic, an evidence of this fact being the very existence of the mean gradients $\partial \overline{u_j} / \partial x_k$, but the smaller structures ("eddies") become more and more isotropic, and their statistics more homogeneous and stationary.

IV. This is the *transport term*: it reflects turbulence's *closure problem*: note that in equation (4.40) for the mean $\overline{u_i}$ there are 2$^{\underline{\text{nd}}}$-order moments $\overline{u_i'u_k'}$; here, in the equation for the second-order moments $\overline{u_i'u_j'}$ the *3$^{\underline{rd}}$-order moments* $\overline{u_i'u_j'u_k'}$ appear, and so on *ad infinitum*. Indeed, Reynold's decomposition always leads to more equations than unknowns to any order. In the atmospheric boundary layer, the divergence of 3$^{\underline{\text{rd}}}$-order moments is often important and reflects *non-local* redistribution of covariances: it adds considerable difficulty in modeling and understanding its physics.

V. This is the buoyancy term: the buoyancy flux $\overline{\rho' u_j'}$ has a counterpart in the virtual sensible heat flux $\overline{u_j'\theta_v'}$, via the simplified equation of state (4.44) that emerges from the Boussinesq approximation. Depending on the sign of $\overline{u_j'\theta_v'}$, it can either produce or destroy the covariance $\overline{u_i'u_j'}$. Production of turbulence by buoyancy makes the atmosphere more *unstable*, and destrution makes it more *stable*.

VI. This is the Coriolis term: it is negligible in the atmospheric boundary layer (Stull, 1988).

VII. Like III, this is a divergence term: it is called the *pressure redistribution* term, and also like III it redistributes $\overline{u_i'u_j'}$ without creating nor destroying covariances in the overall flow domain Tennekes and Lumley (1972).

VIII. This is the *return to isotropy* term (Rotta, 1951a,b; Hinze, 1975; Lumley and Newman, 1977; CHOI and LUMLEY, 2001). Its sum for the 3 components $\overline{u_1'u_1'}$, $\overline{u_2'u_2'}$ and $\overline{u_3'u_3'}$ is zero, showing that it acts to reduce the anisotropy of turbulence, and to nudge the Reynolds stress tensor $\overline{u_i'u_j'}$ to become isotropic.

IX. This term accounts for the molecular diffusion of $\overline{u_i'u_j'}$: it is very small and can be neglected.

X. This is the viscous dissipation term. It can be shown to be small for the case $i \neq j$ Wyngaard (1981), but is very important and always when $i = j$; then, it accounts for the dissipation of turbulence kinetic energy, and is of the same order of the other important terms in (4.47), such as gradient production and buoyancy.

An equation that has a central role in the understanding of the physics (or, at least, the phenomenology) of turbulence is the turbulence kinetic energy (TKE) equation. It is obtained by setting $i = j$ in (4.47), summing from 1 to 3, and dividing by two. The quantity

$$\overline{e} = \frac{1}{2}\sum_{i=1}^{3}\overline{u_i'u_i'} \tag{4.49}$$

is the kinetic energy of the flow that is due to the turbulent velocity fluctuations. The TKE equation is

$$\underbrace{\frac{\partial \overline{e}}{\partial t}}_{\text{I}} + \sum_{k=1}^{3} \underbrace{\overline{u_k} \frac{\partial \overline{e}}{\partial x_k}}_{\text{II}} = - \sum_{k=1}^{3} \underbrace{\overline{u_i' u_k'} \frac{\partial \overline{u_i}}{\partial x_k}}_{\text{III}} - \sum_{k=1}^{3} \underbrace{\frac{\partial \overline{e' u_k'}}{\partial x_k}}_{\text{IV}}$$
$$+ \underbrace{\frac{g}{\theta_r} \overline{w' \theta_v'}}_{\text{V}} \underbrace{- 2 \sum_{i=1}^{3} \sum_{k=1}^{3} \sum_{l=1}^{3} \epsilon_{ilk} \Omega_l \overline{u_i' u_k'}}_{\text{VI}} \underbrace{- \frac{1}{\rho_r} \sum_{i=1}^{3} \left[\frac{\partial \overline{u_i' p'}}{\partial x_i} \right]}_{\text{VII}}$$
$$\underbrace{+ 2\nu \sum_{i=1}^{3} \sum_{k=1}^{3} \frac{\partial \overline{u_i' s_{ik}'}}{\partial x_k}}_{\text{VIII}} \underbrace{- 2\nu \sum_{i=1}^{3} \sum_{k=1}^{3} \overline{s_{ik}' s_{ik}'}}_{\text{IX}} . \quad (4.50)$$

In (4.50),

I is the time rate of change of $\overline{e}$;

II is the advection of $\overline{e}$ (the advective derivative of $\overline{e}$);

III is the gradient production term;

IV is the transport term;

V is the buoyancy production of $\overline{e}$;

VI is the (negligible) Coriolis term;

VII is the pressure redistribution term;

VIII is the (negligible) diffusive transport of $\overline{e}$;

IX is the dissipation of TKE.

Note that, on account of the mass conservation equation for the fluctuations, (4.45), the return to isotropy term in (4.47) now sums to zero:

$$\sum_{i=1}^{3} \overline{\frac{p'}{\rho_r} \frac{\partial u_i'}{\partial x_i}} = \overline{\frac{p'}{\rho_r} \left[\sum_{i=1}^{3} \frac{\partial u_i'}{\partial x_i} \right]} = 0. \quad (4.51)$$

Further simplification can be achieved if we assume the conditions under which the Monin-Obukhov Similarity Theory is valid: horizontal homogeneity, stationarity, mean flow along the x direction only. Then one has

$$0 = -\overline{u'w'} \frac{\partial \overline{u}}{\partial z} - \frac{\partial \overline{e'w'}}{\partial z} + \frac{g}{\theta_r} \overline{w' \theta_v'} - \frac{1}{\rho_r} \frac{\partial \overline{w'p'}}{\partial z} - 2\nu \sum_{i=1}^{3} \sum_{k=1}^{3} \overline{s_{ik}' s_{ik}'}$$
$$0 = -\overline{u'w'} \frac{\partial \overline{u}}{\partial z} - \frac{\partial \overline{e'w'}}{\partial z} + \frac{g}{\theta_r} \overline{w' \theta_v'} - \frac{1}{\rho_r} \frac{\partial \overline{w'p'}}{\partial z} - \epsilon_e \quad (4.52)$$

5

Monin-Obukhov Similarity Theory (MOST)

The Monin-Obukhov Similarity Theory (Obukhov, 1971) — MOST for short — appeared in the Soviet Union during the Second World War. It became known in the west in the 1950's and since the 1960's it has become a standard tool for micrometeorological analysis.

5.1 – Physical justification

The fundamental hypotheses of the MOS theory are the following:

- The flow is near stationary on average:

$$\frac{\partial \overline{(\cdot)}}{\partial t} = 0. \tag{5.1}$$

- The flow is unidirectional:

$$\overline{\boldsymbol{u}} = (\overline{u}, 0, 0), \quad \overline{v} = \overline{w} = 0. \tag{5.2}$$

- The flow is homogeneous in x and y, on average:

$$\frac{\partial \overline{(\cdot)}}{\partial x} = \frac{\partial \overline{(\cdot)}}{\partial y} = 0. \tag{5.3}$$

In these conditions, the *local advection* of any quantity in the x direction is null:

$$\overline{u}\frac{\partial \overline{(\cdot)}}{\partial x} = 0. \tag{5.4}$$

In particular, the vertical fluxes of momentum τ, sensible heat H, mass of water vapor E and greenhouse gas mass F are constant along x. These surface fluxes are the desired quantities, for example: by hydrologists interested in evaporation (or evapotranspiration) and meteorologists interested in using them as boundary conditions for their weather forecast models, atmospheric dispersion models, etc..

As seen in section 3.3.1, from the turbulence theory point of view, the surface fluxes are turbulence statistics, next to the surface, in which one of the variables is the vertical velocity w:

$$\tau = \overline{\rho} u_*^2 = -\overline{\rho w u} \tag{5.5}$$

$$H = \overline{\rho} c_p u_* \theta_* = \overline{\rho c_p w \theta} \tag{5.6}$$

$$E = \overline{\rho} u_* q_* = \overline{\rho_v w} \tag{5.7}$$

$$H_v = \overline{\rho} c_p u_* \theta_{v*} = \overline{\rho c_p w \theta_v} \tag{5.8}$$

$$F = \overline{\rho} u_* c_* = \overline{\rho_c w} \tag{5.9}$$

These equations define new types of *scales*: the velocity scale u_*, the temperature scale θ_* the specific humidity scale q_*, the greenhouse gas scale q_* and the virtual temperature scale θ_{v*}. The latter is associated to the virtual heat flux H_v. According to what we discussed in the previous section, it is necessary to measure the turbulent statistics close to the surface.

A standard justification (but not derivation!) for Monin-Obukhov Similarity Theory can be obtained from the TKE equation with *further simplifications*. Note that in a moist atmosphere we should use the virtual temperature θ_v for the buyoancy term. Also, assuming that all fluxes are constant with height, and that the TKE transport term and pressure terms can both be neglected, (4.52) simplifies to

$$\begin{aligned} -u_*^2 \frac{\mathrm{d}\overline{u}}{\mathrm{d}z} + \frac{g}{\theta_{vr}} u_* \theta_* - \epsilon_e = 0, \\ \frac{\kappa(z-d)}{u_*} \frac{\mathrm{d}\overline{u}}{\mathrm{d}z} + \frac{\kappa g (z-d) \theta_{v*}}{\theta_{vr} u_*^2} - \frac{\kappa (z-d) \epsilon_e}{u_*^3} = 0. \end{aligned} \tag{5.10}$$

In applications, one typically replaces θ_{vr} by $\overline{\theta_v}$, a mean virtual temperature measured close to the surface.

The Obukhov stability variable is now defined by

$$\zeta = \frac{z-d}{L_O} = -\frac{\kappa g (z-d) \theta_{v*}}{\overline{\theta_v} {u_*}^2} \tag{5.11}$$

and indicates the relative magnitude of the turbulent kinetic energy production by buoyancy (θ_{v*} appears in the numerator) and by friction (u_* appears in the denominator). In (5.11), d is the "zero plane" displacement. It takes into consideration the height of the vegetation, and establishes a level d above the ground from which the effects of the surface turbulent fluxes on the atmosphere above the vegetation are felt.

The other two terms in () can now be defined as

$$\phi_\tau \equiv \frac{\kappa(z-d)}{u_*} \frac{\mathrm{d}\overline{u}}{\mathrm{d}z}, \tag{5.12}$$

$$\phi_{\epsilon_e} \equiv \frac{\kappa(z-d)\epsilon_e}{u_*^3}. \tag{5.13}$$

The surface layer (SL) is the region inside the atmospheric boundary layer where, roughly, the surface fluxes τ, H, H_v, etc., are approximately constant with z. In other words, in principle, turbulence measurements inside the SL produce the surface fluxes. The SL has many sub-layers: the interfacial sublayer, the

roughness sublayer, the dynamic sublayer, the dynamic-convective sublayer and the local free convection sublayer. The latter, depending on the author, may or may not be considered a part of the SL. The nomenclature also varies according to the author. The three first classifications are reasonably universal (Brutsaert, 1982; Garratt, 1994); the term dynamic-convective sublayer is due to Kader and Yaglom (1990); the term free convection sublayer (or layer, depending on it being considered or not a part of the SL) is due to Wyngaard et al. (1971). We refer the reader to these references for details on the many sublayers of the SL.

The SL is unstable when $\zeta < 0$, and the buoyancy term in the turbulence kinetic energy equation contributes to produce turbulence. The SL is stable when $\zeta > 0$, and that term helps to destroy the turbulence. The SL is neutral when $\zeta = 0$.

MOST predicts that all the turbulent fluctuation moments, non-dimensionalized correctly by the proper combination of z, u_*, θ_*, q_*, θ_{v*} and c_*, are functions of the independent variable ζ. For the gradients of mean quantities, (moments of order 1) these functions are

$$\frac{\kappa z}{u_*}\frac{\mathrm{d}\overline{u}}{\mathrm{d}z} = \phi_\tau(\zeta), \qquad \frac{\kappa z}{\theta_*}\frac{\mathrm{d}\overline{\theta}}{\mathrm{d}z} = \phi_H(\zeta), \qquad \frac{\kappa z}{q_*}\frac{\mathrm{d}\overline{q}}{\mathrm{d}z} = \phi_E(\zeta), \qquad \frac{\kappa z}{q_*}\frac{\mathrm{d}\overline{c}}{\mathrm{d}z} = \phi_F(\zeta). \tag{5.14}$$

The use of the ordinary derivative $\mathrm{d}/\mathrm{d}z$ in the above equations, instead of the partial derivative, simply indicates that we consider that the flow is stationary and horizontally homogeneous, so that the only independent variable (from the statistical point of view of turbulence) is z.

5.2 – Integration of the dimensionless gradient

Equation (5.14), which defines the dimensionless gradients of Monin-Obukhov, is equivalent to postulate turbulent diffusivities. For example, consider a turbulent flow in a boundary layer with density stratification. The turbulent diffusivity of momentum, K_τ, is defined by analogy with the molecular diffusivity as

$$\tau \equiv \overline{\rho} K_\tau \frac{d\overline{u}}{dz}. \tag{5.15}$$

From (5.5) and (5.14), the turbulent diffusivity is

$$K_\tau = \kappa z u_* / \phi_\tau(\zeta) \tag{5.16}$$

Now, consider (5.14) for the profile of horizontal mean velocity $\overline{u}$ and $\zeta = 0$ ($L_O = +\infty$):

$$\frac{\kappa z}{u_*}\frac{d\overline{u}}{dz} = \phi_\tau(0) = 1 \tag{5.17}$$

where the value $\phi_\tau(0) = 1$ is classically obtained in non-stratified flows (Brutsaert, 1982). Integrating,

$$\begin{aligned} \frac{dz}{z-d} &= \kappa \frac{d\overline{u}}{u_*} \\ \int_{x=d+z_{0\tau}}^{z-d} \frac{dx}{x-d} &= \kappa \frac{\overline{u}}{u_*} \\ \frac{\overline{u}}{u_*} &= \frac{1}{\kappa} \ln \frac{z-d}{z_{0\tau}} \end{aligned} \tag{5.18}$$

Note that the integral over z has lower limit $d + z_{0\tau}$, and not d, because (5.18) is valid only in the fully turbulent region of the SL, but is no longer valid at the thin interfacial sublayer IL immediately above the surface where the transport by molecular diffusion is significant. The integration constant $z_{0\tau}$ is called the roughness length for momentum.

Equation (5.18) is the logarithmic profile of velocity that appears in turbulent boundary layers without density stratification. Clearly, $\phi_\tau(\zeta)$ "corrects" this profile for non-null stratification ($\zeta \neq 0$).

The general integration procedure for the case $\zeta \neq 0$ is the following:

$$\begin{aligned}
\frac{\kappa z}{u_*}\frac{d\overline{u}}{dz} &= \phi_\tau(\zeta), \\
\frac{\kappa \zeta}{u_*}\frac{d\overline{u}}{d\zeta} &= \phi_\tau(\zeta), \\
\phi_\tau(\zeta)\frac{d\zeta}{\zeta} &= \kappa\frac{d\overline{u}}{u_*}, \\
\int_{\zeta_1}^{\zeta_2}\frac{\phi_\tau(x)\,dx}{x} &= \kappa\frac{\overline{u}_2 - \overline{u}_1}{u_*},
\end{aligned} \tag{5.19}$$

for $\zeta_1 < \zeta_2$. If

$$\Phi_\tau(\zeta) \equiv \int \frac{\phi_\tau(x)\,dx}{x} \tag{5.20}$$

then

$$u_* = \kappa\frac{\overline{u}_2 - \overline{u}_1}{\Phi_\tau(\zeta_2) - \Phi_\tau(\zeta_1)} \tag{5.21}$$

Similarly, integrating the dimensionless gradients of temperature, specific humidity and greenhouse effect gas concentration,

$$\theta_* = \kappa\frac{\overline{\theta}_1 - \overline{\theta}_2}{\Phi_H(\zeta_2) - \Phi_H(\zeta_1)}, \tag{5.22}$$

$$q_* = \kappa\frac{\overline{q}_1 - \overline{q}_2}{\Phi_E(\zeta_2) - \Phi_E(\zeta_1)}, \tag{5.23}$$

$$c_* = \kappa\frac{\overline{c}_1 - \overline{c}_2}{\Phi_F(\zeta_2) - \Phi_F(\zeta_1)}. \tag{5.24}$$

In the same way of the case of a neutral atmosphere ($\zeta = 0$), the relations (5.14) (the first of which was used in the obtaining of (5.19)) are not valid down to $z - d = 0$. That way, when level "1" is the surface, we use $z_1 - d = z_{0\tau}$ in (5.21), $z_1 - d = z_{0H}$ in (5.22), $z_1 - d = z_{0E}$ in (5.23) and $z_1 - d = z_{0F}$ in (5.24).

It is common to assume $\phi_H = \phi_E = \phi_F$ in the SL. The equality of the turbulent diffusivities of heat and water vapor was supposed explicitly in the first time in the micrometeological context by Bowen in 1926 (Brutsaert, 1982), and constantly used ever since, but this hypothesis was only proved by Hill (1989) by means of dimensional analysis, and Dias (1994) and Dias and Brutsaert (1996) from the Reynolds equations for the case of homogeneous turbulence in the vertical axis. In the following events, we will assume that the similarity functions ϕ for heat and water vapor are always identical, *i.e.*: $\phi_H = \phi_E = \phi_F$. Strictly speaking, z_{0H}, z_{0E} and z_{0F} are not equal (Brutsaert, 1982); however, we'll assume in this text that they are sufficiently close ($z_{0H} \approx z_{0E} \approx z_{0F}$) for practical purposes.

5.3 – Classical formulas of the MOS theory

The classical profiles for the velocity $\overline{u}$ and scalars $(\overline{\theta}, \overline{q}, \overline{c})$ most used probably are the Businger-Dyer functions (Brutsaert, 1982). For unstable conditions ($\zeta < 0$):

$$\phi_\tau^2 = \phi_H = \phi_E = \phi_F(1 - 16\zeta)^{-1/2} \tag{5.25}$$

and for stable conditions ($\zeta > 0$):

$$\phi_\tau = \phi_H = \phi_E = \phi_F = 1 + 5\zeta. \tag{5.26}$$

Although there is still some discussion about the constants's values and even the form of these functions, they still represent a reasonable consent; a recent revision on the ϕ profiles that are similar to the ones in this text can be found in (Högström, 1988). Stimulated by the findings of Kader and Yaglom (1990), Brutsaert (1992) suggested, for example, new formulations for unstable conditions. In stable conditions, Cheng and Brutsaert (2005) also re-evaluated the similarity functions using data from the CASES-99 experiment.

Note that in a neutral atmosphere $\zeta = 0$, where $\Phi_\tau(0) = \Phi_H(0) = \Phi_E(0) = \Phi_F(0) = -\infty$. This makes it difficult to use equations (5.21)–(5.23), because of the singularity in the denominator. Therefore, it is preferable to work with functions Ψ that define the *deviation* of $\overline{u}$, $\overline{\theta}$ and $\overline{q}$ in relation of the logarithmic profiles due to the stability $\zeta \neq 0$:

$$\Psi(\zeta) \equiv \int \frac{1 - \phi}{\zeta}\, d\zeta = \ln|\zeta| - \Phi(\zeta). \tag{5.27}$$

Starting with Psi_τ,

$$\begin{aligned} \Psi_\tau(\zeta) &= \int_{\zeta_{0\tau}}^{\zeta} \frac{1 - (1 - 16u)^{-1/4}}{u}\, du \\ &= \int_{\zeta_{0\tau}}^{\zeta} \left[\frac{1}{u} - \frac{1}{u(1 - 16u)^{1/4}}\right] du \end{aligned} \tag{5.28}$$

To calculate the integral, do

$$x = (1 - 16u)^{1/4}; \qquad x^4 = (1 - 16u); \qquad \frac{1 - x^4}{16} = u; \qquad du = -\frac{u^3}{4}\, dx; \tag{5.29}$$

$$a = (1 - 16\zeta_{0\tau})^{1/4}; \qquad b = (1 - 16\zeta)^{1/4}. \tag{5.30}$$

Then,

$$\begin{aligned}\Psi_\tau(\zeta) &= \int_a^b \left[\frac{16}{1-x^4} - \frac{16}{x(1-x^4)}\right]\left(-\frac{x^3}{4}\right) dx \\ &= 4\int_a^b \left[\frac{x}{x(x^4-1)} - \frac{1}{x(x^4-1)}\right] x^3\, dx \\ &= \int_a^b \frac{4(x-1)x^2}{x^4-1}\, dx \\ &= \int_a^b \left[\frac{2x}{x^2+1} - \frac{2}{x^2+1} + \frac{2}{x+1}\right] dx \\ &= \ln(x^2+1) + 2\ln(x+1) - 2\operatorname{arctg} x\Big|_a^b. \end{aligned} \tag{5.31}$$

Making $a \approx 1$:

$$\begin{aligned}\Psi_\tau(b(\zeta)) &= \ln(b^2+1) + 2\ln(b+1) - 2\operatorname{arctg} b - [\ln(2) + 2\ln(2) - 2\operatorname{arctg}(1)] \\ &= \ln\frac{b^2+1}{2} + 2\ln\frac{b+1}{2} - 2\operatorname{arctg} b + \frac{\pi}{2}. \end{aligned} \tag{5.32}$$

Note that $\Psi_\tau(b=1) \equiv 0$.
For Ψ_H:

$$\begin{aligned}\Psi_H(\zeta) &= \int_{\zeta_{0\tau}}^{\zeta} \frac{1-(1-16u)^{-1/2}}{u}\, du \\ &= \int_{\zeta_{0\tau}}^{\zeta} \left[\frac{1}{u} - \frac{1}{u(1-16u)^{1/2}}\right] du \end{aligned} \tag{5.33}$$

Using the same change of variables (5.29)–(5.30),

$$\begin{aligned}\Psi_H(\zeta) &= \int_a^b \left[\frac{16}{1-x^4} - \frac{16}{x^2(1-x^4)}\right]\left(-\frac{x^3}{4}\right) dx \\ &= 4\int_a^b \left[\frac{x^2}{x^2(x^4-1)} - \frac{1}{x^2(x^4-1)}\right] x^3\, dx \\ &= \int_a^b \frac{4(x^2-1)x}{x^4-1}\, dx \\ &= 2\ln(x^2+1)\Big|_a^b. \end{aligned} \tag{5.34}$$

Making $a \approx 1$:

$$\Psi_H(b(\zeta)) = 2\ln\frac{b^2+1}{2}. \tag{5.35}$$

Note that, again, we have $\Psi_H(b=1) \equiv 0$. Finally, in stable conditions, using (5.26):

$$\begin{aligned}\Psi_{\tau,H,E,F} &= \int_{\zeta_0}^{\zeta} \frac{1-(1+5\zeta)}{\zeta}\, d\zeta \\ &= -5(\zeta - \zeta_{0\tau,0H,0E,0F}) \approx -5\zeta. \end{aligned} \tag{5.36}$$

Thus, equations (5.21)–(5.23) are now written as

$$u_* = \kappa \frac{\overline{u}_2 - \overline{u}_1}{\ln \frac{\zeta_2}{\zeta_1} - [\Psi_\tau(\zeta_2) - \Psi_\tau(\zeta_1)]}, \tag{5.37}$$

$$\theta_* = \kappa \frac{\overline{\theta}_1 - \overline{\theta}_2}{\ln \frac{\zeta_2}{\zeta_1} - [\Psi_H(\zeta_2) - \Psi_H(\zeta_1)]}, \tag{5.38}$$

$$q_* = \kappa \frac{\overline{q}_1 - \overline{q}_2}{\ln \frac{\zeta_2}{\zeta_1} - [\Psi_E(\zeta_2) - \Psi_E(\zeta_1)]}, \tag{5.39}$$

$$c_* = \kappa \frac{\overline{c}_1 - \overline{c}_2}{\ln \frac{\zeta_2}{\zeta_1} - [\Psi_F(\zeta_2) - \Psi_F(\zeta_1)]}. \tag{5.40}$$

Along with (5.11), which defines L_O in terms of u_*, θ_*, q_* e c_*, this provides a non-linear system in the variables u_*, θ_*, q_*, c_* and L_O, that can be iteratively solved from the measurement of the mean profiles $\overline{u}(z)$, $\overline{\theta}(z)$, $\overline{q}(z)$ and $\overline{c}(z)$. In general, this is done postulating $|L_O| = +\infty$ initially, where $\Psi_{\tau,H,E,F} = 0$; with the values of u_*, θ_* and q_* obtained from the initial logarithmic profiles, we re-calculate L_0 e then ζ_1, ζ_2, that can be used in a new estimate of the turbulent scales, and so on until the process converges.

5.4 – The flux-gradient method (FGM)

The transfer equations quantify the surface fluxes as a function of the differences in wind velocity, temperature, humidity and greenhouse gas between the surface and one or more measurement levels. We will assume that temperature $\overline{\theta}_a$, specific humidity $\overline{q}_a$, and mass concentration $\overline{c}_a$ are measured at height z_a, while the wind velocity $\overline{u}_b$ is measured at height z_b. The sub-index 0 indicates the surface. In his case, the transfer equations are

$$\tau = \overline{\rho} C_\tau \, \overline{u}_b^2, \tag{5.41}$$

$$H = \overline{\rho} c_p C_H \, \overline{u}_b \left(\overline{\theta}_0 - \overline{\theta}_a \right), \tag{5.42}$$

$$E = \overline{\rho} C_E \, \overline{u}_b \left(\overline{q}_0 - \overline{q}_a \right), \tag{5.43}$$

$$F = \overline{\rho} C_F \, \overline{u}_b \left(\overline{c}_0 - \overline{c}_a \right), \tag{5.44}$$

where C_τ, C_H, C_E and C_F are *dimensionless transfer coefficients* (respectively for momentum, heat, H_2O mass and (an unspecified?) gas mass). The use of the transfer equations for the estimation of surface fluxes is often called the *flux-gradient method*.

To derive (5.41)–(5.43), we start from (5.37)–(5.39). They aren't directly applicable in $z = 0$, for $\ln 0 = -\infty$; hence, we need to assume that the values $\overline{u}_0 = 0$, $\overline{\theta}_0$, $\overline{q}_0$ and $\overline{c}_0$ in the surface occur at the corresponding roughness lengths $z_{0\tau}$, z_{0H}, z_{0E} and z_{0F}. For each quantity, we then take level 1 as being equal to its roughness length, and level 2 as being equal to its measurement level. At level 1, the roughness lengths are very small, so that it is reasonable to write

$$\frac{z_{0\tau}}{L_O} \approx 0, \qquad \frac{z_{0H}}{L_O} \approx 0, \qquad \frac{z_{0E}}{L_O} \approx 0, \qquad \frac{z_{0F}}{L_O} \approx 0, \tag{5.45}$$

whence

$$\Psi\left(\frac{z_{0\tau}}{L_O}\right) \approx 0, \quad \Psi\left(\frac{z_{0H}}{L_O}\right) \approx 0, \quad \Psi\left(\frac{z_{0E}}{L_O}\right) \approx 0, \quad \Psi\left(\frac{z_{0F}}{L_O}\right) \approx 0. \tag{5.46}$$

Using (5.5)–(5.7) and (5.37)–(5.40):

$$\tau = \overline{\rho}\frac{\kappa^2}{\left[\ln\frac{z_b-d}{z_{0\tau}} - \Psi_\tau\left(\frac{z_b-d}{L_O}\right)\right]^2}\,\overline{u}_b^2, \tag{5.47}$$

$$H = \overline{\rho}c_p\frac{\kappa^2}{\left[\ln\frac{z_b-d}{z_{0\tau}} - \Psi_\tau\left(\frac{z_b-d}{L_O}\right)\right]\left[\ln\frac{z_a-d}{z_{0H}} - \Psi_H\left(\frac{z_a-d}{L_O}\right)\right]}\,\overline{u}_b\left(\overline{\theta}_0 - \overline{\theta}_a\right), \tag{5.48}$$

$$E = \overline{\rho}\frac{\kappa^2}{\left[\ln\frac{z_b-d}{z_{0\tau}} - \Psi_\tau\left(\frac{z_b-d}{L_O}\right)\right]\left[\ln\frac{z_a-d}{z_{0E}} - \Psi_E\left(\frac{z_a-d}{L_O}\right)\right]}\overline{u}_b\left(\overline{q}_0 - \overline{q}_a\right), \tag{5.49}$$

$$F = \overline{\rho}\frac{\kappa^2}{\left[\ln\frac{z_b-d}{z_{0\tau}} - \Psi_\tau\left(\frac{z_b-d}{L_O}\right)\right]\left[\ln\frac{z_a-d}{z_{0F}} - \Psi_E\left(\frac{z_a-d}{L_O}\right)\right]}\overline{u}_b\left(\overline{c}_0 - \overline{c}_a\right). \tag{5.50}$$

The penultimate equation above is, naturally, "Dalton's Law". In the same way that occurs in the energy balance method, it is more commonly written with vapor pressure e instead of the specific humidity q,

$$E = \frac{0{,}622\overline{\rho}}{\overline{p}}\frac{\kappa^2}{\left[\ln\frac{z_b-d}{z_{0\tau}} - \Psi_\tau\left(\frac{z_b-d}{L_O}\right)\right]\left[\ln\frac{z_a-d}{z_{0E}} - \Psi_E\left(\frac{z_a-d}{L_O}\right)\right]}\overline{u}_b\left(\overline{e}_0 - \overline{e}_a\right). \tag{5.51}$$

This equation should be compared with many empirical formulas of evaporation of the nineteenth century and the first half of the twentieth century, of the kind

$$E = (a + b\overline{u})(\overline{e}_0 - \overline{e}_a). \tag{5.52}$$

From the micrometeorological point of view, a does not have physical meaning (*i.e.*: shouldn't be in the equation) if (5.52) is used over time scales that are not compatible with atmospheric turbulence, between 30 minutes and one hour. Historically, however, we find that equations like (5.52) are widely used at the daily and monthly scales. Finally notice that, strictly speaking, b is not constant; for fixed measurement heights z_a and z_b and roughness lengths (note that the surface roughness can vary over an agricultural area, or with wind direction), b still depends on the MO stability length, which varies in a (semi-)hourly scale along the day.

Os momentos de ordem 2 mais relevantes são

$$\frac{\overline{w'w'}}{u_*^2} = \phi_{ww}(\zeta) \quad \frac{\overline{\theta'\theta'}}{\theta_*^2} = \phi_{\theta\theta}(\zeta) \quad \frac{\overline{q'q'}}{q_*^2} = \phi_{qq}(\zeta) \tag{5.53}$$

e

$$\frac{\overline{w'p'}}{\overline{\rho}u_*^3} = \phi_{wp}(\zeta), \qquad \frac{\kappa z\epsilon_e}{u_*^3} = \phi_{\epsilon_e}(\zeta) \tag{5.54}$$

e alguns momentos de ordem 3 importantes são

$$\frac{\overline{w'e'}}{u_*^3} = \phi_{we}(\zeta) \quad \frac{\overline{w'\theta'\theta'}}{u_*\theta_*^2} = \phi_{w\theta\theta}(\zeta) \quad \frac{\overline{w'q'q'}}{u_*q_*^2} = \phi_{wqq}(\zeta) \tag{5.55}$$

Voltando agora à equação (**??**) vemos que ela pode ser totalmente escrita em termos dos ϕ's de Monin-Obukhov:

$$0 = \phi_\tau - \frac{1}{2}\kappa\zeta\frac{\partial\phi_{we}}{\partial\zeta} - \zeta - \kappa\zeta\frac{\partial\phi_{wp}}{\partial\zeta} - \phi_{\epsilon_e} \tag{5.56}$$

Outro processo totalmente análogo é a produção/dissipação de variância de um escalar — por exemplo, a temperatura.

Fazendo-se $i = j = 4$ em (4.47), *sem que isto implique em somatório*, obtém-se

$$0 = -2\,\overline{w'\theta'}\,\frac{\partial\overline{\theta}}{\partial z} - \frac{\partial\,\overline{w'\theta'\theta'}}{\partial z} - 2\epsilon_{\theta\theta} \tag{5.57}$$

(observe a analogia com a equação de balanço de energia cinética turbulenta), a qual pode ser adimensionalizada pelo produto com $(\kappa z)/(u_*^2\theta_*)$, do que resulta

$$0 = 2\phi_H - \kappa\zeta\frac{\partial\phi_{w\theta\theta}}{\partial\zeta} - 2\phi_{\epsilon_{\theta\theta}} \tag{5.58}$$

Novamente, o mesmo quadro de produção por gradientes versus destruição por viscosidade molecular pode ser imaginado.

Como toda teoria baseada em Análise Dimensional, a teoria SMO é incapaz, em princípio, de nos fornecer a forma analítica das funções ϕ. Estas entretanto podem ser mais ou menos bem determinadas experimentalmente. Uma vez conhecidas, as funções ϕ abrem caminho para um grande número de técnicas com as quais é possível "inverter o jogo", e determinar u_*, θ_* e q_* e portanto calcular os fluxos superficiais τ, H e E que são os objetos últimos de interesse no caso de modelos de previsão atmosférica e em Hidrologia. Este é o conteúdo da próxima seção.

5.5 – Aplicações clássicas

5.5.1 – O método do balanço de energia-razão de Bowen

Considere uma superfície sobre a qual incide uma irradiância líquida R_l [$\mathrm{W\,m^{-2}}$]. Na literatura micrometeorológica, o termo "radiação líquida" é mais comum. O conceito de radiação líquida já envolve as complexidades da incidência, reflexão e emissão da radiação em diversos comprimentos de onda. Esta energia disponível na superfície é utilizada de três maneiras:

- para aquecer/resfriar o ar, sob a forma do fluxo de calor sensível H;
- para evaporar/condensar a umidade da superfície; se o calor latente de evaporação é L, o fluxo de calor latente associado é LE; e
- para aquecer/resfriar as camadas sub-superficiais, por meio do fluxo de calor sub-superficial G.

A equação de balanço de energia da superfície é

$$R_l = H + LE + G \tag{5.59}$$

Das equações definidoras dos fluxos superficiais (5.5)–(5.7), e das equações para os perfis médios (5.22) e (5.23), segue-se que, debaixo da hipótese $\phi_H = \phi_E$ mencionada na seção anterior, a *razão de Bowen* B_o é dada por

$$B_o = \frac{H}{LE} = \frac{c_p}{L}\frac{\overline{\theta}_1 - \overline{\theta}_2}{\overline{q}_1 - \overline{q}_2} \tag{5.60}$$

Das equações de estado para ar seco e vapor de água, (**??**), (**??**) e (**??**), obtém-se a fórmula bem conhecida

$$q \approx 0,622\frac{e}{p} \tag{5.61}$$

donde

$$B_o = \underbrace{\frac{c_p p}{0{,}622L}}_{\gamma}\frac{\overline{\theta}_1 - \overline{\theta}_2}{\overline{e}_1 - \overline{e}_2} \tag{5.62}$$

em termos das pressões parciais de vapor de água $\overline{e}$; γ é a "constante psicrométrica". Segue-se que é possível calcular LE como

$$LE = \frac{R_l - G}{1 + \gamma\frac{\overline{\theta}_1 - \overline{\theta}_2}{\overline{e}_1 - \overline{e}_2}} \tag{5.63}$$

que é a equação do método do balanço de energia-razão de Bowen para o cálculo de E.

5.5.2 – Medição de umidade do ar

Um segundo exemplo, mais corriqueiro, é a medição de umidade do ar por psicrômetros aspirados. Se calcularmos o balanço de energia para o bulbo úmido de um termômetro à temperatura $\overline{\theta}_h$ sobre o qual sopra ar à temperatura $\overline{\theta}_a$ do bulbo seco, $R_l - G = 0 \Rightarrow B_o = -1$; a umidade do ar em contato com o bulbo úmido é dada pela pressão de saturação de vapor de água à temperatura do bulbo úmido, $e^*(\overline{\theta}_h)$, e a umidade do ar que se deseja medir é $\overline{e}_a$. De (5.60), então,

$$\begin{aligned} -1 &= \gamma\frac{\overline{\theta}_h - \overline{\theta}_a}{e^*(\overline{\theta}_h) - \overline{e}_a} \\ \overline{e}_a - e^*(\overline{\theta}_h) &= -\gamma\left(\overline{\theta}_a - \overline{\theta}_h\right) \\ \overline{e}_a &= e^*(\overline{\theta}_h) - \gamma\left(\overline{\theta}_a - \overline{\theta}_h\right) \end{aligned} \tag{5.64}$$

que é a equação de um psicrômetro aspirado.

5.5.3 – Momentos de 2 [a]ordem

Para os momentos de 2[a]ordem na CS, valem as seguintes formulações (Tillman, 1972; Hicks, 1981; Wesely, 1988):

$$\phi_{ww}^{1/2} = \begin{cases} 1.3(1 - 2\zeta)^{1/3} & \zeta > 0 \\ 1.3 & \zeta \leq 0 \end{cases} \tag{5.65}$$

$$\phi_{\theta\theta}^{1/2} = \phi_{qq}^{1/2} = \begin{cases} (2 - \zeta)^{-1/3} & \zeta > 0 \\ 2 & \zeta \leq 0 \end{cases} \tag{5.66}$$

O leitor deve notar que as constantes que aparecem nessas equações, bem como sua própria forma, são ajustadas empiricamente e podem variar consideravelmente de autor para autor. Os valores, assim como as formas funcionais, apresentados acima tentam ser um consenso entre diversos resultados.

5.6 – Atmosferas muito estáveis e muito instáveis

5.6.1 – Estratificação independente de z

O efeito da estabilidade atmosférica é criar uma força restauradora de empuxo que tende a retornar parcelas de ar deslocadas verticalmente às suas posições de equilíbrio. Isto significa que numa atmosfera fortemente estratificada a turbulência é *destruída* pelas forças de empuxo. Quanto mais estável a atmosfera, menores são as excursões verticais permitidas às parcelas de ar, com a consequência de que z deixa de ser uma escala relevante do problema. Outra maneira de ver isto é assumir que as estatísticas da turbulência são independentes de z, ou seja: a turbulência é *homogênea* na vertical. A consequência desta situação na equação de balanço de energia cinética turbulenta, (**??**), é imediata: as derivadas em relação a z das momentos $\overline{w'e'}$ e $\wp$ são nulas, enquanto que $\overline{w'w'}$, $\overline{w'\theta'_v}$ e ϵ_e que também são momentos turbulentos, devem ser independentes de z. Logo, a derivada de $\overline{u}$ em relação a z também não pode ser função de z, donde $\partial\overline{u}/\partial z$ = constante, e o perfil de velocidade média é linear. Naturalmente, tem que haver uma transição do perfil logaritmico em condições neutras para o perfil linear em condições fortemente estáveis: isto é o que expressam as fórmulas (5.36) do perfil log-linear. O mesmo raciocínio pode ser aplicado para as equações de balanço de $\overline{\theta'\theta'}$ e $\overline{q'q'}$, com o resultado de que $\partial\overline{\theta}/\partial z$ e $\partial\overline{q}/\partial z$ também são constantes em condições de estratificação independente de z. No que concerne aos momentos de ordem 2 em condições estáveis, a previsão teórica passa a ser

$$\phi_{ww} = \text{cte} \quad \phi_{\theta\theta} = \text{cte} \quad \phi_{qq} = \text{cte} \tag{5.67}$$

Isto está de acordo com as formas de (5.65) e (5.66) na região estável. Entretanto, evidências muito recentes (Pahlow et al., 2001) sugerem que estas funções de similaridade de Monin-Obukhov voltam a crescer para valores de ζ muito grandes.

5.6.2 – Convecção livre local

No topo da CS, a influência da produção de energia cinética turbulenta por gradiente tende a se reduzir, porque $\partial\overline{u}/\partial z \downarrow 0$, já que o perfil de velocidade tende a ser muito mais uniforme na camada convectiva CC sobrejacente; o mesmo acontece com a produção de variância $\overline{\theta'\theta'}$ e com o perfil de temperatura média $\overline{\theta}$. A importância da velocidade de atrito u_* nestas condições desaparece, e se torna necessário encontrar uma outra escala de velocidade representativa destas condições locais. Considere portanto um balanço de energia cinética turbulenta altamente simplificado e irrealista, no qual se retém entretanto uma característica física fundamental do topo da CS: a produção por empuxo e a dissipação molecular devem ser da mesma ordem de grandeza:

$$\frac{g}{\overline{\theta}_v}\,\overline{w'\theta'_v} \sim \epsilon_e \tag{5.68}$$

Ao multiplicarmos ambos os lados pela escala de comprimento z "natural" do problema, obtemos

$$1 \sim \frac{z\epsilon_e}{\left[\frac{zg\overline{w'\theta'_v}}{\overline{\theta}_v}\right]} \tag{5.69}$$

e agora, por analogia com $\phi_{\epsilon_e} = \kappa z \epsilon_e / u_*^3$ fica fácil identificar a escala convectiva de velocidade

$$w_f = \left[\frac{zg\,\overline{w'\theta'_v}}{\overline{\theta}_v}\right]^{1/3} \tag{5.70}$$

É preciso compreender que o conceito de convecção livre local não implica que $u_* = 0$, mas sim que a importância relativa do termo de produção de turbulência por gradiente é assintoticamente decrescente. De fato, $u_* \neq 0$ na CS sempre, e é possível formar o grupo adimensional

$$\frac{w_*}{u_*} = \frac{1}{\sqrt[3]{\kappa}}\left[\frac{\kappa z g u_* \theta_{v*}}{\overline{\theta}_v u_*^3}\right]^{1/3} = \frac{1}{\sqrt[3]{\kappa}}\left(\frac{-z}{L_O}\right)^{1/3} \tag{5.71}$$

Da mesma maneira que z, g, $\overline{w'\theta'_v}$ e $\overline{\theta}_v$ formam uma escala de velocidade convectiva w_*, z, g, $\overline{w'\theta'}$ e $\overline{\theta}$ são capazes de formar uma escala de temperatura convectiva, que nós chamaremos de ϑ_*. Para vermos isso, lançamos mão do balanço de variância de temperatura turbulento sem o termo de produção por gradiente,

$$-\frac{\partial\,\overline{w'\theta'\theta'}}{\partial z} - 2\epsilon_{\theta\theta} = 0 \tag{5.72}$$

Ambos os termos têm que ser estimados. Uma análise clássica de ordem de grandeza dos momentos turbulentos envolvidos (Tennekes and Lumley, 1972) fornece:

$$-\frac{\partial\,\overline{w'\theta'\theta'}}{\partial z} \sim \frac{\overline{w'\theta'}\,\vartheta_*}{z} \tag{5.73}$$

$$\epsilon_{\theta\theta} \sim \frac{w_*\vartheta_*^2}{z} \tag{5.74}$$

substituindo estas estimativas em (5.72) obtém-se

$$\vartheta_* = \left[\frac{(\overline{w'\theta'})^2\overline{\theta}}{zg}\right]^{1/3} \tag{5.75}$$

Novamente, é possível relacionar a "nova" escala ϑ_* com a "velha" escala θ_*,

$$\frac{\vartheta_*}{\theta_*} = \kappa^{1/3}\left(\frac{-z}{L_O}\right)^{-1/3} \tag{5.76}$$

Vale a pena analisar o que acontece com diversas funções de similaridade neste limite; por exemplo,

$$\begin{aligned}\phi_\tau &= \frac{\kappa z}{u_*}\frac{\partial\overline{u}}{\partial z} \\ &= \frac{\kappa z}{u_*}\frac{w_*}{w_*}\frac{\partial\overline{u}}{\partial z} \\ &= \frac{\kappa z}{w_*}\frac{\partial\overline{u}}{\partial z}\frac{1}{\sqrt[3]{\kappa}}(-\zeta)^{1/3}\,.\end{aligned} \tag{5.77}$$

Se nós supusermos que w_* é uma grandeza natural para definir a escala do gradiente de velocidade média nesta região (Garratt (1994) faz o mesmo),

$$\frac{\partial \overline{u}}{\partial z} \sim \frac{w_*}{z} \tag{5.78}$$

e, no limite de convecção livre,

$$\phi_\tau(\zeta) = \text{cte}(-\zeta)^{1/3}. \tag{5.79}$$

No caso de ϕ_{H_v},

$$\begin{aligned} \phi_{H_v} &= -\frac{\kappa z}{\theta_{v*}} \frac{\theta_{v*}}{\theta_{v*}} \frac{\partial \overline{\theta}_v}{\partial z} \\ &= -\frac{\kappa z}{\vartheta_*} \frac{\partial \overline{\theta}_v}{\partial z} (-\zeta)^{-1/3}. \end{aligned} \tag{5.80}$$

Supondo, de forma análoga ao que fizemos com w_*, que ϑ_* é uma escala válida para o gradiente de temperatura potencial virtual nesta região,

$$\frac{\partial \overline{\theta}_v}{\partial z} \sim \frac{\vartheta_*}{z}, \tag{5.81}$$

donde

$$\phi_{H_v} = \text{cte}(-\zeta)^{-1/3}. \tag{5.82}$$

Da mesma forma, os momentos de 2ªordem de w e θ_v produzem

$$\phi_{ww} = \frac{\overline{w'w'}}{w_*^2} \left(\frac{w_*}{u_*}\right)^2 = \text{cte} \left(\frac{-z}{L_O}\right)^{2/3} \tag{5.83}$$

$$\phi_{\theta\theta} = \frac{\overline{\theta'\theta'}}{\vartheta_*^2} \left(\frac{\vartheta_*}{\theta_*}\right)^2 = C_{\theta\theta}^2 \left(\frac{-z}{L_O}\right)^{-2/3} \tag{5.84}$$

Novamente, note que a forma de (5.65) e (5.66) é assintoticamente correta e corresponde às equações (5.65) e (5.66) acima.

Note também que w_* já tem a altura z "embutida" em sua definição; assim, enquanto que a Teoria de Similaridade de Monin-Obukhov trabalha com quatro escalas,

$$u_*, \quad \theta_{v*}, \quad g/\overline{\theta}_v \quad \text{e} \quad z,$$

em condições de convecção livre nós "perdemos" u_*, ficando com

$$g/\overline{\theta}_v, \quad z \quad \text{e} \quad \overline{w'\theta'_v}|_0.$$

Em particular, isto significa que

$$\frac{\overline{w'w'}}{w_*^2} = \text{cte} \quad \text{(e independente de } u_*\text{)}. \tag{5.85}$$

Consequentemente, não se pode mais usar $\overline{w'w'}$ para estimar u_* em condições de convecção livre.

5.7 – O método da variância

Existem muitas maneiras de calcular os fluxos τ, H e E a partir de medições micrometeorológicas. Nós já vimos duas delas: o método do balanço de energia – razão de Bowen, e o método de medição de perfis médios. Ambos utilizam apenas grandezas médias. A medição "direta" de fluxos consiste em medir as flutuações turbulentas w', u', θ' e q' com instrumentos de resposta rápida (frequências de medição típicas situam-se entre 10 e 100 Hz). Estas entretanto são medidas caras e difíceis, que ainda não podem ser feitas rotineiramente. Por outro lado, os métodos baseados em medição de perfis médios sofrem do fato de que as diferenças de temperatura $\overline{\theta}_1 - \overline{\theta}_2$ na CS podem ser de apenas alguns décimos, ou mesmo centésimos, de Kelvin. "Um híbrido" muito interessante é a estimativa de u_* e θ_* por meios diferentes. Por exemplo, pode-se estimar u_* a partir de medidas de velocidade média do vento $\overline{u}$ em dois níveis, com 2 anemômetros, por meio de (5.37), e medir apenas as flutuações de temperatura θ', obtendo

$$\theta_* = \sqrt{\frac{\overline{\theta'\theta'}}{\phi_{\theta\theta}}} \tag{5.86}$$

e então calcular H por meio de (5.6). Este método, que é uma das variantes do método da variância (Tillman, 1972; Hicks, 1981; Wesely, 1988) obviamente envolve algumas iterações partindo do perfil logaritmico, da mesma forma que no caso de medição de perfis médios. Ele apresenta uma considerável economia em relação a medições turbulentas de fluxo, e é um candidato a um sistema contínuo de monitoramento de fluxos superficiais Kustas et al. (1994).

O método original de Tillman (1972) envolvia também o conhecimento da assimetria da temperatura:

$$\gamma_\theta \equiv \frac{\overline{\theta^3}}{\sigma_\theta^3}. \tag{5.87}$$

Tillman (1972) constatou que γ_θ depende de ζ. Supondo-se a validade da Teoria de Similaridade de Monin-Obukhov, isto pde ser previsto:

$$\begin{aligned} \gamma_\theta &= \frac{\overline{\theta^3}}{\sigma_\theta^3} \\ &= \frac{\overline{\theta^3}}{\theta_*^3}\frac{\theta_*^3}{\sigma_\theta^3} \\ &= \phi_{\theta\theta\theta}\left[\phi_{\theta\theta}\right]^{-3/2}. \end{aligned} \tag{5.88}$$

A relação obtida por Tillman é

$$\zeta = -A\exp(B\gamma_\theta), \tag{5.89}$$

com $A = 0{,}0137$, $B = 4{,}39$. Seja agora uma relação de variância para a temperatura na forma (Dias et al., 2009)

$$\frac{\sigma_\theta}{\theta_*} = A(1 + B|\zeta|)^{-1/3}; \tag{5.90}$$

rearranjando a equação:

$$\frac{\sigma_\theta}{H}\wp c_p u_* = A(1+B|\zeta|)^{-1/3}$$
$$\sigma_\theta(1+B|\zeta|)^{1/3} = A\frac{H}{\wp c_p u_*} \tag{5.91}$$

Mas

$$\frac{1}{L} = -\frac{\kappa g H}{\wp c_p \overline{\Theta} u_*^3} \Rightarrow$$
$$u_*^3 = -\frac{\kappa g}{\overline{\Theta}}\frac{H}{\wp c_p} L \Rightarrow$$
$$u_* = \left[\frac{\kappa g}{\overline{\Theta}}\right]^{1/3}\left[\frac{H}{\wp c_p}\right]^{1/3}(-L)^{1/3}. \tag{5.92}$$

Substituindo-se (5.92) em (5.91):

$$\sigma_\theta(1+B|\zeta|)^{1/3} = A\frac{H}{\wp c_p}\left[\frac{\overline{\Theta}}{\kappa g}\right]^{1/3}\left[\frac{\wp c_p}{H}\right]^{1/3}\left[\frac{-1}{L}\right]^{1/3}$$
$$= A\left[\frac{H}{\wp c_p}\right]^{2/3}\left[\frac{\overline{\Theta}}{\kappa g z}\right]^{1/3}\left[\frac{-z}{L}\right]^{1/3} \Rightarrow$$
$$\left[\frac{H}{\wp c_p}\right]^{2/3} = \frac{\sigma_\theta}{A}(1+B|\zeta|)^{1/3}\left[\frac{\kappa g z}{\overline{\Theta}}\right]^{1/3}\left[\frac{1}{|\zeta|}\right]^{1/3} \Rightarrow$$
$$\frac{H}{\wp c_p} = \left[\left(\frac{\sigma_\theta}{A}\right)^3\left(\frac{\kappa g z}{\overline{\theta}}\right)\left(\frac{1+B|\zeta|}{|\zeta|}\right)\right]^{1/2}. \tag{5.93}$$

Esta é uma equação quase milagrosa, pois ela mostra que é possível calcular H desde que se conheça σ_θ e $|\zeta|$, em condições instáveis. O método é interessante e promissor, e a questão é estendê-lo para outros escalares, e verificar qual é a melhor forma de se estimar ζ: se com a assimetria da própria medição de temperatura, ou se com dados da velocidade média $\overline{U}$ (ver esta última alternativa em Dias et al. (2009)).

5.8 – Número de Richardson

Considere a razão dos termos de produção de energia cinética turbulenta por empuxo e por gradiente:

$$R_f \equiv \frac{\frac{g}{\overline{\theta}_v}\overline{w'\theta'_v}}{\overline{u'_i u'_k}\frac{\partial \overline{u}_i}{\partial x_k}}; \tag{5.94}$$

Se a turbulência é homogênea na horizontal e não há efeitos verticais significativos,

$$R_f = \frac{\frac{g}{\overline{\theta}_v}\overline{w'\theta'_v}}{\overline{w'u'}\frac{\partial \overline{u}}{\partial z} + \overline{w'v'}\frac{\partial \overline{v}}{\partial z}}. \tag{5.95}$$

Esta é a forma usual do *Número de Richardson para fluxos*. Agora, se supusermos que todos os fluxos turbulentos cinemáticos podem ser escritos em termos de uma difusividade turbulenta comum K,

$$\overline{w'\theta'_v} = K\frac{\partial\overline{\theta}_v}{\partial z}, \tag{5.96}$$

$$\overline{w'u'} = K\frac{\partial\overline{u}}{\partial z}, \tag{5.97}$$

$$\overline{w'v'} = K\frac{\partial\overline{v}}{\partial z}, \tag{5.98}$$

o número de Richardson se "transforma" em

$$R_g \equiv \frac{\frac{g}{\overline{\theta}_v}\frac{\partial\overline{\theta}_v}{\partial z}}{\left(\frac{\partial\overline{u}}{\partial z}\right)^2 + \left(\frac{\partial\overline{v}}{\partial z}\right)^2}. \tag{5.99}$$

Esta é a forma usual do *Número de Richardson para gradientes*.

5.9 – Sobre a consistência da aplicação de análise dimensional direcional à camada superficial

5.9.1 – Introdução

Num trabalho de grande importância teórica e grande volume de dados experimentais até então inéditos, Kader and Yaglom (1990) (daqui para frente, K&Y-1990) reintroduziram o conceito de análise dimensional direcional (ADD) em micrometeorologia, corroborando-o fartamente com medições realizadas no sítio de Tsimlyansk (atual Rússia) em condições extremamente instáveis no topo da camada superficial (CS). A essência da formulação teórica de Kader and Yaglom é a consideração de que os comprimentos ao longo da direção x e os comprimentos ao longo da direção z (as condições sendo uniformes e a turbulência, homogênea, em y) possuem dimensões físicas diferentes, L_x e L_z.

Para entendermos a análise dimensional direcional em ação de maneira simples, vamos considerar o momento de inércia de um retângulo de base b e altura h em relação ao seu centróide em torno do eixo x, com b paralelo a Ox e h paralelo a Oy; o seu valor é $I_{xx} = bh^3/12$. A menos do coeficiente $1/12$, deveria ser possível obter esta fórmula por meio de análise dimensional; entretanto, mesmo que nos atenhamos a expoentes inteiros, é impossível distinguir entre b^4, bh^3, b^2h^2, b^3h e h^4 no contexto de análise dimensional tradicional, uma vez que todas estas fórmulas possuem as mesmas dimensões (L^4). Já se supusermos que $[b] = L_x$, $[h] = L_y$, e $[I_{xx}] = L_xL_y^3$, a obtenção da forma correta é imediata.

De volta a K&Y-1990, algumas de suas consequências instigantes são: (a) algumas "constantes" de análise dimensional tradicional passam a possuir dimensões; notadamente, para a constante de von Kármán, $[\kappa] = L_z^{1/2}L_x^{-1/2}$; (b) passa a ser possível subdividir (e classificar) racionalmente a CS em sub-camada dinâmica (SDN), sub-camada dinâmico-convectiva (SDC) e sub-camada de convecção livre (SCL); em cada uma destas sub-camadas a forma da função de similaridade é determinada a menos de uma constante; (c) na SDC, surge uma nova escala de velocidade u_{**} com dimensões L_xT^{-1} que deve ser utilizada *apenas* para adimensionalizar os gradientes de velocidade horizontal média $d\overline{u}$ e as flutuações de velocidade horizontal u'.

Zilitinkevich (1994) (daqui para frente Z-1994) propôs uma versão diferente de ADD, em que a dimensão de uma grandeza é função não de sua direção no espaço, mas da origem de sua produção. Essencialmente, ele decompõe cada flutuação turbulenta de velocidade u' e w' em uma componente produzida mecanicamente e outra produzida pela convecção. Embora a interpretação de direcionalidade seja radicalmente diferente da de K&Y-1990, os resultados de Z-1994 em termos de funções de similaridade são muito parecidos. Na sequência será dada preferência à abordagem de K&Y-1990, por ser mais clara e mais simples. Conforme será mostrado, ambas as abordagens produzem resultados intrinsecamente inconsistentes entre as 3 sub-camadas da CS, apesar de seu sucesso em explicar o comportamento das funções de similaridade.

O objetivo deste trabalho *não* é apresentar resultados experimentais *nem* uma teoria totalmente nova sobre o comportamento da CS: os comportamentos das funções de similaridade são rigorosamente os mesmos de K&Y-1990. Deseja-se enfatizar as inconsistências da teoria (extremamente bem-sucedida!) de K&Y-1990: justamente devido ao seu sucesso, acreditamos que ela merece ser formulada de maneira consistente para toda a CS. Para que isto seja feito, é necessário (a) explicitar as escalas individuais dos 2 escalares mais importantes na atmosfera, temperatura e umidade, e (b) introduzir escalas de velocidade horizontal adicionais na SDN e na SCL no papel de variáveis independentes ou de controle nas formulações de análise dimensional. Esta tarefa não é elementar para a SCL, onde nos limitamos a estabelecer as condições que uma escala adequada de velocidade horizontal deve possuir.

Kader e Yaglom dão a seguinte definição, potencialmente muito útil, para a camada superficial:

$$z \lesssim 50 \text{ m} \quad \text{e} \quad z \lesssim 0{,}1 z_i \tag{5.100}$$

Nesta região, os balanços para *cada componente* da energia cinética turbulenta são

$$-\overline{w'u'}\frac{d\overline{u}}{dz} + \frac{1}{\overline{\rho}}\overline{p'\frac{\partial u'}{\partial x}} = \epsilon_{uu} + \frac{1}{2}\frac{\partial}{\partial z}\left(\overline{u'u'w'}\right), \tag{5.101}$$

$$\frac{1}{\overline{\rho}}\overline{p'\frac{\partial v'}{\partial y}} = \epsilon_{vv} + \frac{1}{2}\frac{\partial}{\partial z}\left(\overline{v'v'w'}\right), \tag{5.102}$$

$$\frac{g}{\overline{\theta}_v}\overline{w'\theta'_v} + \frac{1}{\overline{\rho}}\overline{p'\frac{\partial w'}{\partial z}} = \epsilon_{uu} + \frac{1}{2}\frac{\partial}{\partial z}\left(\overline{w'w'w'} + \frac{2}{\overline{\rho}}\wp\right), \tag{5.103}$$

onde os termos envolvendo flutuações de pressão no lado esquerdo são responsáveis pela redistribuição direcional de energia; repare que que a sua soma é

$$\frac{1}{\overline{\rho}}\left[\overline{p'\left(\frac{\partial u'}{\partial x} + \frac{\partial v'}{\partial y} + \frac{\partial v'}{\partial z}\right)}\right] = 0, \tag{5.104}$$

em virtude da equação da continuidade. Note que a soma de (5.101)–(5.103) recupera a equação de balanço de energia cinética turbulenta.

5.9.2 – A sub-camada dinâmica e as escalas individuais de temperatura e umidade

Na teoria clássica de similaridade de Monin-Obukhov, a sub-camada dinâmica é identificada como a região da camada superficial onde os efeitos de estratificação de densidade e produção convectiva de turbulência são desprezíveis diante da produção mecânica. Isto significa que o parâmetro de flutuabilidade $\beta = g/\overline{\theta}_v$ não entra na lista das variáveis que determinam as características da turbulência, as quais ficam então reduzidas aos fluxos cinemáticos de quantidade de movimento, $-\overline{w'u'}$ e temperatura virtual, $\overline{w'\theta'_v}$, além da própria distância até a superfície, $z - d_0$. Nestas circunstâncias, as escalas relevantes de velocidade (u_*) e temperatura potencial virtual (θ_{v*}) são

$$u_*^2 \equiv -\overline{w'u'}, \tag{5.105}$$

$$\theta_{v*} \equiv \overline{w'\theta'_v}\,/u_*. \tag{5.106}$$

A lista de adimensionalizações possíveis para gradientes e momentos de ordem 1, 2 e 3 inclui (sem ser exaustiva):

$$\frac{d\overline{u}}{dz} = A_{\overline{u}}\frac{u_*}{z-d_0}, \tag{5.107}$$

$$\frac{d\overline{\theta}_v}{dz} = A_{\overline{\theta}_v}\frac{\theta_{v*}}{z-d_0}, \tag{5.108}$$

$$\sigma_{\theta_v} = A_{\theta_v\theta_v}\theta_{v*}, \tag{5.109}$$

$$\sigma_w = A_{ww}u_*, \tag{5.110}$$

$$\sigma_u = A_{uu}u_*, \tag{5.111}$$

onde os A's são constantes. Na teoria clássica, $A_{\overline{u}} = A_{\overline{\theta}_v} = \kappa^{-1} = 2{,}5$ (Brutsaert, 1982). Note que (5.109)–(5.111) implicam que $\overline{\theta'_v\theta'_v}$, $\overline{w'w'}$ e $\overline{u'u'}$ são constantes em z na SDN — i.e.: a turbulência parece ser homogênea na vertical nesta sub-camada.

Para separar as escalas de temperatura e umidade, basta considerar a equação para a temperatura potencial virtual,

$$\theta_v = (1 + 0.61q)\theta, \tag{5.112}$$

onde q é a umidade específica e θ é a temperatura potencial; aplicando-se uma decomposição de Reynolds a θ_v, q e θ, e fazendo-se a média do produto das flutuações resultantes com w', obtém-se

$$\overline{\theta}_v = a\overline{\theta}, \tag{5.113}$$

$$\theta'_v = a\theta' + b\overline{\theta}q', \tag{5.114}$$

$$\theta_{v*} = a\theta_* + bq_*, \tag{5.115}$$

$$a = (1 + 0.61\overline{q}), \tag{5.116}$$

$$b = 0.61\overline{\theta}. \tag{5.117}$$

onde θ_* e q_* são definidos de forma análoga a (5.106).

Levando (5.113) e (5.114) em (5.108),

$$(1 + 0.61\overline{q})\frac{d\overline{\theta}}{dz} + 0.61\overline{\theta}\frac{d\overline{q}}{dz} = (1 + 0.61\overline{q})A_{\overline{\theta}_v}\frac{\theta_*}{z} + 0.61\overline{\theta}A_{\overline{\theta}_v}\frac{q_*}{z}. \tag{5.118}$$

Se os termos em $(1 + 0.61\overline{q})$ e $(0.61\overline{\theta})$ forem iguais dois a dois, segue-se que

$$\frac{d\overline{\theta}}{dz} = A_{\overline{\theta}}, \frac{\theta_*}{z} \tag{5.119}$$

$$\frac{d\overline{q}}{dz} = A_{\overline{q}}, \frac{q_*}{z} \tag{5.120}$$

com $A_{\overline{\theta}_v} = A_{\overline{\theta}} = A_{\overline{q}}$, isto é: os gradientes de temperatura potencial e umidade específica apresentam similaridade perfeita na SDN. O mesmo exercício de decomposição da temperatura potencial quando aplicado a (5.109) resulta em

$$a^2\,\overline{\theta'\theta'} + 2ab\,\overline{\theta'q'} + b^2\,\overline{q'q'} = A^2_{\theta_v\theta_v}\left(a^2\theta_*^2 + 2ab\theta_* q_* + b^2 q_*\right). \tag{5.121}$$

Supondo-se que a relações análogas a (5.109) sejam aplicáveis a θ e a q separadamente, segue-se que

$$\sigma_\theta^2 = A^2_{\theta\theta}\theta^2_{v*}, \tag{5.122}$$

$$\sigma_q^2 = A^2_{qq}q^2_*, \tag{5.123}$$

$$\overline{\theta'q'} = A^2_{\theta q}\theta_* q_*, \tag{5.124}$$

onde, mais uma vez, $A_{\theta\theta} = A_{qq} = A_{\theta q} = A_{\theta_v\theta_v}$, ou seja, as variâncias de temperatura e de umidade e a covariância entre ambas são perfeitamente similares na SDN. O conjunto das equações (5.122)–(5.124) implica

$$r_{\theta q} = \frac{\overline{\theta'q'}}{\sigma_\theta\sigma_q} = \pm 1, \tag{5.125}$$

isto é: a correlação entre as flutuações de temperatura e umidade é perfeita. Este tipo de resultado foi obtido pela primeira vez por Hill (1989), e depende fundamentalmente da hipótese de que as adimensionalizações do tipo de (5.108) e (5.109) valem tanto para θ e q individualmente como para qualquer combinação linear deles (inclusive a temperatura potencial); confirmações do resultado por outros meios foram depois obtidas para diversas condições de estabilidade (Dias and Brutsaert, 1996; McNaughton and Laubach, 1998; de Bruin et al., 1999)

Implicações de ADD para a SDN

Para Kader e Yaglom, a SDN é a região onde

$$\frac{1}{\overline{\rho}}\overline{p'\frac{\partial w'}{\partial z}} > \frac{g}{\overline{\theta}_v}\,\overline{w'\theta'_v}\,. \tag{5.126}$$

Mas

$$\frac{1}{\overline{\rho}}\overline{p'\frac{\partial w'}{\partial z}} \sim \frac{1}{\overline{\rho}}\overline{p'\frac{\partial u'}{\partial x}} \sim \frac{(\kappa u_*)^3}{z}. \tag{5.127}$$

Note que dimensionalmente

$$\left[\frac{(\kappa u_*)^3}{z}\right] = \frac{\left(L_z^{1/2}L_x^{-1/2}L_x^{1/2}L_z^{1/2}T^{-1}\right)^3}{L_z} = L_z^2T^{-3}. \tag{5.128}$$

Então a sub-camada dinâmica SDN deve ser a região onde

$$\frac{1}{z}\frac{(\kappa u_*)^3\overline{\theta}_v}{g\,\overline{w'\theta'_v}} > 1. \tag{5.129}$$

Kader e Yaglom definem portanto a SDN como a região onde

$$z < L_* \equiv \frac{(\kappa u_*)^3\overline{\theta}_v}{g\,\overline{w'\theta'_v}}. \tag{5.130}$$

É elementar mostrar que

$$\frac{L_*}{L_O} = \kappa^2 = 0{,}16. \tag{5.131}$$

Este é um excelente critério objetivo para a altura da sub-camada dinâmica.

Se $[u] = L_x T^{-1}$, $[w] = L_z T^{-1}$, $[\theta] = \Theta$, e $[q] = M_v M^{-1}$, onde Θ é a dimensão de temperatura, M é a dimensão de massa total de ar e M_v a dimensão de massa de vapor d'água, há várias consequências para a teoria de similaridade na SDN. Note que embora nos livros-texto seja usual apresentar a análise dimensional apenas em termos das 3 dimensões fundamentais "clássicas" em mecânica, M, L e T, a adoção de uma dimensão de temperatura independente é justificável em problemas em que a conversão de energia mecânica em térmica (ou vice-versa) não seja importante; analogamente, se não há reação química envolvendo a massa total de vapor d'água, é igualmente válido considerar M_v como uma dimensão independente da massa total de ar (Dias, 1986; Fischer et al., 1979). Esta interpretação "heterodoxa" de análise dimensional é necessária para a obtenção dos resultados clássicos da teoria de similaridade de Monin-Obukhov, e *análoga às extensões de direcionalidade para o comprimento* discutidas neste trabalho.

As consequências das hipóteses de dimensionalidade e de direcionalidade são então: $[u_*] = L_x^{1/2} L_z^{1/2} T^{-1}$; $[\theta_{v*}] = L_x^{-1/2} L_z^{1/2} \Theta(1 + M_v M^{-1})$; $[A_{\overline{u}}] = [A_{\overline{\theta}_v}] = [A_{\overline{\theta}}] = [A_{\overline{q}}] = L_x^{1/2} L_z^{-1/2}$; $[A_{\theta_v\theta_v}] = [A_{\theta\theta}] = [A_{qq}] = L_x L_z^{-1}$. Note portanto que as diversas constantes A's deixam de ser adimensionais e passam a ter dimensões envolvendo L_x e L_z. Em outras palavras, a aplicação de ADD na SDN leva a constantes *dimensionais* nas relações (5.107)–(5.111).

5.9.3 – A sub-camada dinâmico-convectiva: escalas individuais de temperatura e umidade

Nesta região, $z > L_*$ *ma non troppo*, a produção de turbulência por empuxo passa a ser da mesma ordem de grandeza que a produção mecânica. O parâmetro de flutuabilidade $g/\overline{\theta}_v$ deve portanto entrar na lista de variáveis que controlam a dinâmica da turbulência. Segundo Kader e Yaglom, u' e v' são produzidas mecanicamente, enquanto que w' é produzida por empuxo, enquanto que as trocas direcionais são relativamente pequenas. Isto conduz imediatamente a duas novas escalas de turbulência; a escala de velocidade convectiva

$$w_* = \left(\frac{g}{\overline{\theta}_v}\,\overline{w'\theta'_v}\,z\right)^{1/3} \tag{5.132}$$

e à escala de temperatura convectiva

$$\vartheta_{v*} = \frac{\overline{w'\theta'_v}}{w_*}. \tag{5.133}$$

Supondo, como é natural no contexto de ADD, que $[z] = L_z$ e $[g] = L_z T^{-2}$, segue-se que $[w_*] = L_z T^{-1}$, e $[\vartheta_{v*}] = \Theta(1 + M_v M^{-1})$. No entanto, como nesta região a produção mecânica *ainda* é importante, u_* também é uma das variáveis que controlam a turbulência desta sub-camada. Consequentemente, por analogia com (5.133), é possível formar uma escala de velocidade horizontal convectiva

$$u_{**} = -\frac{\overline{w'u'}}{w_*}, \tag{5.134}$$

cuja principal característica é possuir dimensões horizontais de comprimento: $[u_{**}] = L_x T^{-1}$. Agora é possível formar as seguintes relações adimensionais envolvendo as escalas acima, gradientes de grandezas médias estatísticas da turbulência:

$$\frac{d\overline{u}}{dz} = B_{\overline{u}} \frac{u_{**}}{z}, \tag{5.135}$$

$$\frac{d\overline{\theta}_v}{dz} = B_{\overline{\theta}_v} \frac{\vartheta_{v*}}{z}, \tag{5.136}$$

$$\sigma_{\theta_v} = B_{\theta_v\theta_v} \vartheta_{v*}, \tag{5.137}$$

$$\sigma_w = B_{ww} w_*, \tag{5.138}$$

$$\sigma_u = B_{uu} u_{**}. \tag{5.139}$$

Note como escalas diferentes de velocidade, u_{**} e w_*, são utilizadas para adimensionalizar flutuações (gradientes) envolvendo u e w, respectivamente. Estas previsões são um resultado original do trabalho de K&Y-1990: enquanto que na teoria clássica de estabilidade de Monin-Obukhov apenas a existência de funções adimensionais era prevista, aqui é possível prever a sua *forma*. Para demonstrar este fato, basta apresentar um exemplo, envolvendo o gradiente "adimensional" (a palavra precisa ser usada com cuidado à luz da ADD) de velocidade média: rearrumando (5.135) obtém-se

$$\begin{aligned}
\frac{z w_*}{u_*^2}\frac{d\overline{u}}{dz} &= B_{\overline{u}}, \\
\frac{1}{\kappa^{4/3}} \underbrace{\frac{\kappa z}{u_*}\frac{d\overline{u}}{dz}}_{\phi_\tau} \underbrace{\left(\frac{\kappa g z \,\overline{w'\theta'_v}}{\overline{\theta}_v u_*^3}\right)^{1/3}}_{-\zeta} &= B_{\overline{u}}, \\
\phi_\tau(\zeta) &= B_{\overline{u}} \kappa^{4/3} (-\zeta)^{-1/3}.
\end{aligned} \tag{5.140}$$

Esta equação contém a definição da variável de estabilidade de K&Y-1990, ζ, que é equivalente à variável de estabilidade de Obukhov exceto pela ausência da constante de von Kármán κ.

A extensão da teoria de K&Y-1990 para as escalas individuais de temperatura e umidade na SDC é imediata; sem repetir o desenvolvimento que se segue a (5.113)–(5.115), a escala convectiva de temperatura potencial virtual se decompõe naturalmente:

$$\vartheta_{v*} = (1 + 0.61\overline{q})\vartheta_* + (0.61\overline{\theta})\chi_*, \tag{5.141}$$

com

$$\vartheta_* = \overline{w'\theta'}\,/w_*, \tag{5.142}$$

$$\chi_* = \overline{w'q'}\,/w_*. \tag{5.143}$$

Implicações de ADD para a SDC

A SDC é a única das 3 sub-camadas da CS onde a aplicação de ADD não produz constantes dimensionais: de fato, todos os B's em (5.135)–(5.139) são adimensionais, como o leitor pode constatar facilmente. O outro fato notável é a consistência de sua aplicação: todas as flutuações (gradientes) envolvendo u são adimensionalizados por u_{**}, enquanto que todas as flutuações envolvendo w o são por w_*.

5.9.4 – A sub-camada de convecção livre

Nesta última e mais alta sub-camada da CS, argumenta-se com base no balanço de energia cinética turbulenta que u_* deixa totalmente de ser uma variável relevante (Wyngaard, 1973): a única escala de velocidade disponível para "adimensionalizar" gradientes e estatísticas turbulentas passa a ser w_*. Nesta região, $z \gg L_*$, é a produção por empuxo que agora alimenta as flutuações u' e v' além, naturalmente, de w'. Note como $\overline{p'/\overline{\rho}\partial w'/\partial z}$ troca de sinal entre a SDN, a SDC e a SCL. Por outro lado, não há novas escalas de temperatura potencial virtual, temperatura potencial ou umidade específica a se formar. Consequentemente, nesta sub-camada devemos ter:

$$\frac{d\overline{u}}{dz} = C_{\overline{u}}\frac{w_*}{z}, \tag{5.144}$$

$$\frac{d\overline{\theta}_v}{dz} = C_{\overline{\theta}_v}\frac{\vartheta_{v*}}{z}, \tag{5.145}$$

$$\sigma_{\theta_v} = C_{\theta_v\theta_v}\vartheta_{v*}, \tag{5.146}$$

$$\sigma_w = C_{ww}w_*, \tag{5.147}$$

$$\sigma_u = C_{uu}w_*. \tag{5.148}$$

Kader e Yaglom introduzem

$$L_{**} \equiv \frac{(\kappa_1 u_*)^3\overline{\theta}_v}{g\,\overline{w'\theta'_v}} \tag{5.149}$$

como o limite *inferior* da camada de convecção livre, onde

$$\kappa_1 = C_{\overline{u}}^{-1/2}. \tag{5.150}$$

Implicações de ADD para a SCL

Observe que agora flutuações u' e gradientes $d\overline{u}$ também são "adimensionalizados" por w_*; portanto, *alguns* dos C's acima *não* são adimensionais (à semelhança do que ocorre com os A's na SDN): $[C_{\overline{\theta}_v}] = [C_{\theta_v\theta_v}] = [C_{ww}] = 1$, mas: $[C_{\overline{u}}] = L_xL_z^{-1}$ e $[C_{uu}] = L_xL_z^{-1}$.

5.9.5 – Crítica da ADD e algumas correções formais

As previsões de ADD para a CS são amplamente confirmadas na SDC por dados experimentais (K&Y-1990): esta é a sub-camada onde seu teste é mais rigoroso, uma vez que o comportamento assintótico das funções de similaridade de Monin-Obukhov na SDN e na SCL já tinham sido previstos, e em boa parte confirmados, anteriormente. Uma novidade a partir dos dados experimentais

em K&Y-1990 foi a confirmação da previsão de (5.144) para $\frac{d\overline{u}}{dz}$, uma vez que as funções de similaridade empíricas anteriormente conhecidas (por exemplo, a bem conhecida formulação de Businger-Dyer) (Businger et al., 1971) não incluíam valores de ζ suficientemente altos que permitissem a identificação do seu comportamento na SCL.

Entretanto, este sucesso vem ao preço de tornar as formulações de similaridade para a SDN e a SCL dimensionalmente inconsistentes, uma vez que todos os A's e alguns dos C's passam a ser constantes *dimensionais*. Em outras palavras, a dimensionalidade de algumas destas constantes sugere que a teoria de ADD na forma utilizada em K&Y-1990 *deixou* de identificar algumas variáveis importantes na CS que poderiam torná-la totalmente consistente. Certamente, este não é um erro grave do ponto de vista da capacidade da teoria de *explicar* as observações, uma vez que as formulações para a SDN e a SCL são *anteriores* a K&Y-1990, na sua forma clássica pressupõem que os A's e os C's são todos adimensionais, e são bem sucedidas em explicar seus respectivos regimes de turbulência. O "defeito" a que nos referimos parece ser antes de mais nada puramente formal.

Correção de ADD para a sub-camada dinâmica

Na sub-camada dinâmica utilizando-se apenas as variáveis $\overline{w'u'}$, $\overline{w'\theta'}$ e z é impossível produzir variáveis com dimensões L_xT^{-1} ou L_zT^{-1}, isto é: com dimensões de velocidade horizontal ou velocidade vertical. Portanto, para tornar a ADD consistente na SDN é indispensável introduzir uma nova escala de velocidade; além disso, esta escala precisa estar associada a uma hipótese sobre o seu comportamento em função da altura z. Uma lista completa e compatível com a teoria clássica de Monin-Obukhov é: $\{u_* = -\overline{w'u'},\ z,\ \theta_{v*} = \overline{w'\theta'_v}/u_*,\ \sigma_u = (\overline{u'u'})^{1/2}\}$. Note que nesta abordagem σ_u é uma variável *independente* que introduz a necessária dimensão L_x na lista de dimensões da SDN; note também que além da hipótese de fluxo constante, $\partial\,\overline{w'u'}/\partial z = 0$, será necessário supor o mesmo para a variância da velocidade horizontal: $\partial\overline{u'u'}/\partial z = 0$. Com a introdução formal de $\overline{u'u'}$ na lista de variáveis de controle, obtém-se imediatamente as seguintes formulações dimensionais alternativas a (5.107)–(5.110):

$$\frac{d\overline{u}}{dz} = A'_{\overline{u}}\frac{\sigma_u}{u_*}\frac{u_*}{z}, \tag{5.151}$$

$$\frac{d\overline{\theta}_v}{dz} = A'_{\overline{\theta}_v}\frac{\sigma_u}{u_*}\frac{\theta_{v*}}{z}, \tag{5.152}$$

$$\sigma_{\theta_v} = A'_{\theta_v\theta_v}\frac{\sigma_u}{u_*}\theta_{v*}, \tag{5.153}$$

$$\sigma_w = A'_{ww}\frac{u_*}{\sigma_u}u_*. \tag{5.154}$$

Finalmente, é possível *definir* uma variável dependente na SDN:

$$\kappa \equiv \frac{u_*}{A'_{\overline{u}}\,\sigma_u} \tag{5.155}$$

que é numericamente igual à constante de von Kármán da teoria clássica (não-direcional): neste sentido, justifica-se a afirmação encontrada em K&Y-1999 de que κ é uma variável; na SDN, κ é constante em z.

Correção de ADD para a sub-camada de convecção livre

Assim como ocorre na SDN, para que a ADD forneça previsões consistentes na SCL, é preciso retirar o desvio-padrão da velocidade vertical (ou alguma outra escala de velocidade horizontal alternativa) da lista de variáveis dependentes de w_*, e elevá-la ao *status* de variável independente de controle da turbulência. É importante lembrar aqui que o objetivo deste trabalho não é a previsão de novos comportamentos físicos (isto foi feito em K&Y-1990), mas reinterpretar formalmente a teoria de ADD (assim como feito em Z-1994); portanto, não está em discussão, por exemplo, a validade de (5.144) ou (5.148) (cujas constantes $C_{\overline{u}}$ e C_{uu}, por possuírem dimensões segundo a ADD, as tornam formalmente inconsistentes. O objetivo é *reinterpretar* estas constantes de maneira que surja uma formulação de ADD totalmente consistente incluindo apenas constantes adimensionais, variáveis independentes ou de controle (que variam em cada sub-camada) e demais variáveis "dependentes" da turbulência.

Consequentemente, uma vez que (5.144) e (5.148) possuem confirmação experimental, é forçoso não somente incluir σ_u na lista de variáveis de controle, mas também admitir que σ_u e w_* possuem o mesmo comportamento $\sim z^{1/3}$. Estas equações então podem ser reescritas (lembrando que (5.145)–(5.147) já são dimensionalmente consistentes):

$$\frac{d\overline{u}}{dz} = C'_{\overline{u}} \frac{\sigma_u}{w_*} \frac{w_*}{z}, \tag{5.156}$$

$$\sigma_u \sim z^{1/3}. \tag{5.157}$$

É importante observar também que devido ao argumento físico de que a importância relativa da produção mecânica é assintoticamente nula na SCL, não é possível utilizar em hipótese alguma u_* na tentativa de "construir" escalas horizontais de velocidade nesta camada. Neste sentido, (5.157) é ao mesmo tempo uma *consequência* da teoria clássica e uma hipótese necessária (que precisa ser validada independentemente) para que a ADD possa ser aplicada.

5.10 – Conclusões

A teoria de K&Y-1990 é um dos exemplos mais bem-sucedidos de aplicação de análise dimensional a problemas da camada-limite atmosférica. Ao reduzir o número de graus de liberdade das funções de similaridade na CS em 1, ela permitiu a previsão acurada da dependência funcional destas funções com a variavel de estabilidade ζ de Obukhov, restando apenas constantes a determinar.

Para obter este sucesso, entretanto, foi necessário conviver com uma mistura de constantes dimensionais nas sub-camadas dinâmica e de convecção livre e adimensionais (na "nova" sub-camada dinâmico-convectiva, de acordo com a nova teoria). Além do mais, algumas escalas da teoria clássica, como por exemplo θ_{v*} possuem agora dimensões que envolvem L_x e L_z, e não apenas Θ. Embora este estado de coisas não seja impeditivo do sucesso da teoria, ele é certamente indesejável do ponto de vista formal: *por que a análise dimensional direcional deveria "funcionar" com constantes à sua vez dimensionais e adimensionais em diferentes partes da camada superficial*?

Inicialmente, estendemos a formulação de K&Y-1990, que foi feita apenas com a temperatura (potencial), para o caso mais geral de temperatura (potencial) virtual: isto dá lugar naturalmente à bem-conhecida escala q_* de umidade e a uma nova escala convectiva de umidade, que denominamos χ_*.

Nós procurarmos também reformular a ADD com o objetivo de obter um conjunto de constantes uniformemente adimensionais em toda a CS. Este esforço foi bem-sucedido na SDN, onde a hipótese de homogeneidade vertical da turbulência, que é bem confirmada experimentalmente, pode ser utilizada par fornecer a escala de velocidade horizontal faltante nesta sub-camada. A SDN já possui uma formulação totalmente consistente em K&Y-1990, e portanto não são necessárias modificações. O problema mais difícil de reformulação está na SCL: ali, o impedimento (*físico*: a produção mecânica de turbulência é desprezível) de se utilizar u_* como uma variável torna a busca de uma escala alternativa de velocidade horizontal mais complicada. Dado o sucesso das formulações de convecção livre (diga-se de passagem, bem anteriores à teoria de K&Y-1990), e admitindo-se que a ADD seja uma teoria válida, é forçoso que tal escala exista. Sua principal característica deverá ser uma dependência funcional com z igual à experimentada por w_*.

5.11 – Evolution of the measurement technology of H_2O, CO_2, and CH_4 with the ECM

According to Baldocchi (2003), the first measurements of scalar turbulent fluxes in the atmosphere were made by Swinbank (1951). The fluxes in question were the sensible heat flux H and the latent heat flux LE; the scalars were temperature θ and water vapor pressure e. The humidity sensor actually measured the wet-bulb temperature, then

> *The psychrometric element consists of two fine wet-bulb thermocouples built into an electrical network so designed that it simulates the behavior of Regnault's psychrometric equation for small changes in the variables (vapor pressure, saturation vapor pressure at the wet-bulb temperature, and the wet-bulb depression). The output of the circuit gives a measure of the fluctuations of vapor pressure practically linear over the range of variation that occurs naturally.*

In other words, the Swinbank apparatus included an analog computer that converted the measurements of dry and wet bulb temperature to water vapor pressure fluctuations in real time.

As one would expect in any seminal , and in hindsight, many limitations can be found in this first attempt of flux measurement by Swinbank: the averaging time, 5 minutes, was too short; the measurement of water vapor concentration fluctuations was done with thermocouples of dry and wet bulb, which certainly limited their response time, and the frequency of the measurements, after digitizing of the graphical records, was only 1 Hz (currently, measurement frequencies of at least 10 Hz are used in the eddy covariance method, and averaging times of at least 10 minutes are used, 30 minutes being the most commonly found averaging time).

The works of Baumgartner (1969) and Deanmead (1969) among others at the same time, report the measurement of *average* concentrations of CO_2, and inferred the fluxes using a flux-gradient method.

CO_2 flux measurements with the eddy covariance method, however, only became possible in the 1970's. The first measurements seem to be due to Desjardins (1974). The vertical velocity sensor was a propeller anemometer, and air was pumped through a closed-path CO_2 analyser. Strictly speaking, the method wasn't exactly what we call today the eddy covariance method, since the system integrated the vertical movements registered by the propeller anemometer. Some preliminary results obtained with the CO_2 flux measurements were shown, along with discussions about measurements performed over naked soil, and over hay. Numerous limitations of the anemometer used were discussed.

In the same year, Desjardins and Lemon (1974) analyzed many of the uncertainty sources in the CO_2 measurement, which are still subject of research now.

Leuning et al. (1982) performed measurements of CO_2 flux with the flux-gradient method and with the eddy covariance method. They found that the covariance $\overline{w'\rho_c'}$ produced incoherent results and disagreed with the flux-gradient method. This provided the first verification of the importance of the WPL correction (Webb et al., 1980), and also allowed the authors to identify that previous works had already proposed similar corrections to the WPL correction (Bakan, 1978; Jones and Smith, 1978), but with incorrect boundary conditions. Leuning et al. (1982) observed that in a posterior note, Smith and Jones (1979) recognized that the correct condition was originally proposed by Webb and Pearman (1977), which corresponds to the equation (6.27) of this text.

Here, it is remarkable that corrections for the CO_2 measurements with the eddy covariance method were already being considered in 1976, a very short time after the pioneering measurements of Desjardins (1974).

Fundamental problems identified by Leuning et al. (1982) and that somehow persist to this day are the alignment of the anemometer, the correction for air density through temperature fluctuations, which were later studied by Webb et al. (1980), the non-stationarity of the atmosphere during the measurement period, and their time average. Some of these subjects are the theme of the next session.

The effective implementation of the ECM for the measurement of turbulent gas fluxes depends critically on the gas analyzers. In the mid 1970's, gas analyzers for water vapor Buck (1976) and CO_2 Desjardins (1974) were emerging, and from then on the measurement of water vapor and CO_2 has become increasingly common in meteorological experiments.

Another substantial process has been the gradual substitution of closed-path sensors, in which the has is aspirated through a tube and measured in a closed chamber inside the analyzer, with open-path sensors, in which the gas is measured along an open path, between and emissor and a receptor, in the atmosphere itself. The general principle of these sensors is the absorption by the gas of part of the radiation emitted. As always, the measurement is harder the smaller the gas concentrations are.

The tendency is always to initially use slow sensors, only capable of measuring mean concentrations; moving to the use of closed-path fast sensors, and finally reaching a stage in which the open-astsensorsareavailable. Anexcellentrevisiono the evolution of the CO_2 measurement technologies can be found in Baldocchi (2003).

6

Turbulence data processing

6.1 – The separation of the average and the fluctuation

There is no universally accepted methodology for the definition of what represents the "average" $\overline{a}$ and the fluctuation a' of a variable a measured in a turbulent flow. The usual practice is to perform some kind of filtering of the original measured data, $a(t)$, initially producing a component $\overline{a}(t)$, and then to extract the fluctuation $a'(t)$ by (3.1). The problem is that in practice there are many different ways to calculate $\overline{a}(t)$. Figure 6.1-a shows a series of CO_2 concentrations measured at 2 meters above a turf farm in Tijucas do Sul, PR, in 2011-02-17 between 10:30 and 10:40 h. This 10-minute series will be used to illustrate some of the most common averaging procedures in what follows.

Block averages. The block average was defined in (3.9). As we know, the value $\overline{a}$ calculated remains constant for $-T/2 < t < T/2$. The fluctuation $a'(t)$ is calculated around this constant average. Figure 6.2-a shows the fluctuations of CO_2 density after the extraction of a block average. Essentially, it is the same figure 6.1-a, with the average shifted to zero. Note the pronounced negative asymmetry of ρ_c'.

Running average. This is equation (3.15): the value of $\overline{a}(t)$ varies continuously over time, and the fluctuation $a'(t)$ is calculated around this variable value. Figure 6.1-b shows the running average calculated with $P = 2\,\text{min}.$. Note that, unless the data of 10 minutes earlier or later are available, is not possible to calculate the running average for $t < 1\,\text{min}.$ or for $t > 9\,\text{min}.$. At these ends, the running average is replaced by the block average of the first 2 minutes and the last 2 minutes.

Figure 6.2-b shows the extracted fluctuations around the mobile averaging.

Linear first-order recursive filter. This is one of the most widely used procedure, perhaps because it is equivalent to analog filtering of a signal using a RC circuit. For a continuous function, the linear first-order recursive filter 1 is the solution of the differential equation

$$\frac{d\overline{a}}{dt} + \frac{1}{P}\overline{a} = \frac{1}{P}a(t). \tag{6.1}$$

In 6.1, P is the filter's "window": in practice, recommendation (3.16) remains valid also for a recursive filter.

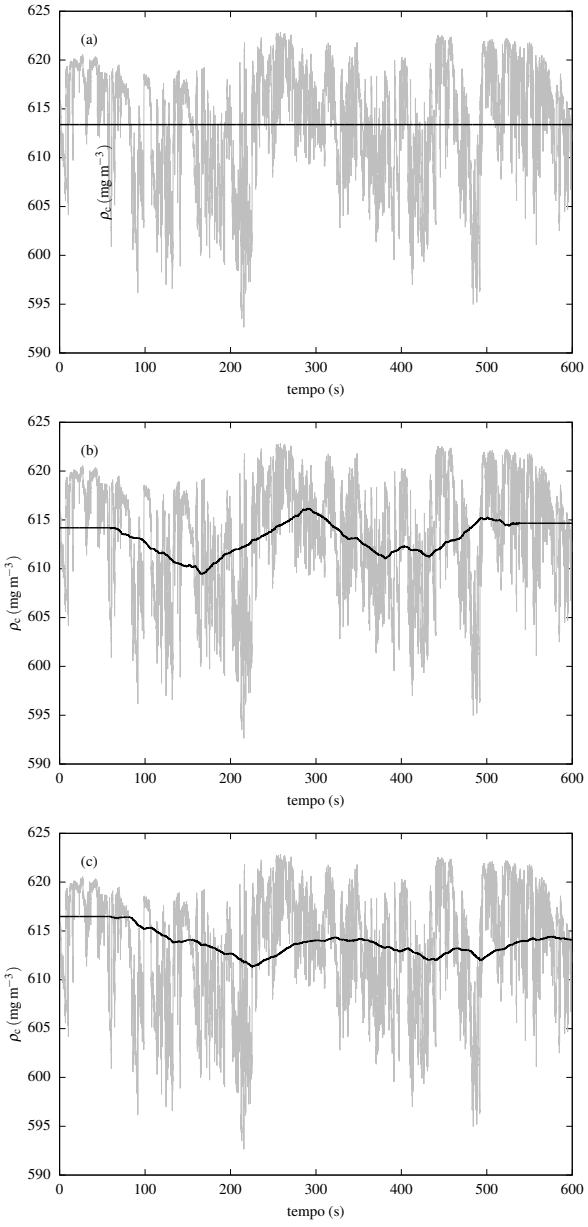

Figure 6.1: 10 minutes of CO_2 concentration measurements over a grass surface in Tijucas do Sul, PR, on 02/17/2011, 10:30 - 10: 40; (a) raw series and block average; (b) Running average with $P = 2$ min. (c) Low-pass recursive filter with $P = 2$ min..

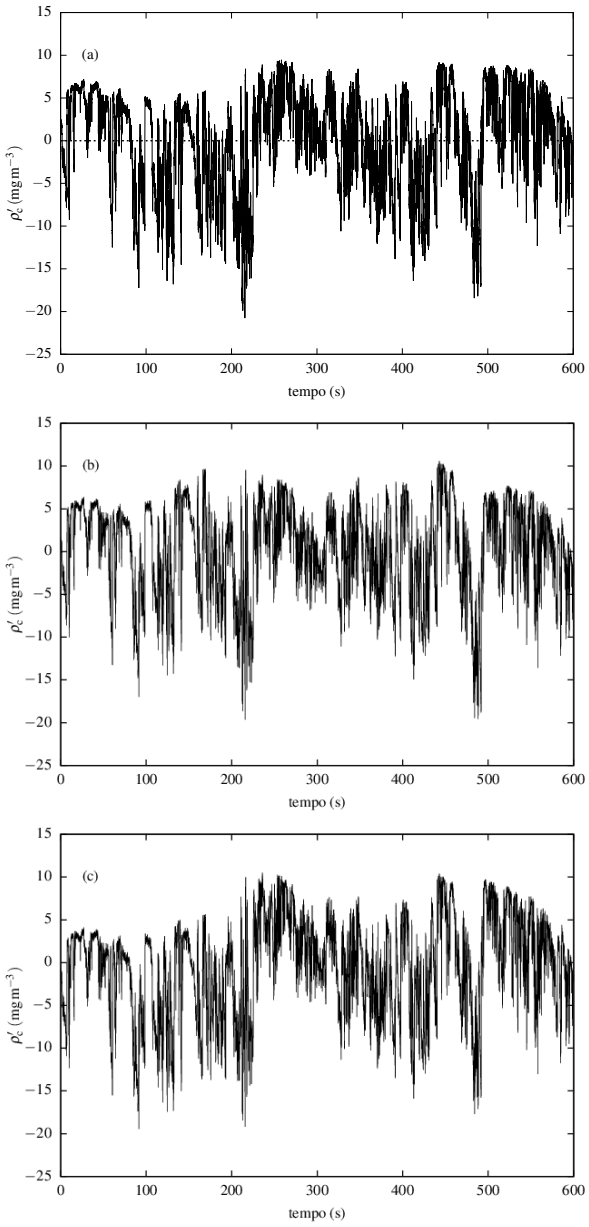

Figure 6.2: Fluctuations of ρ_c': (a) around a block average; (b) around a running average of 2 minutes; (c) around a low-pass filter of 2 minutes.

Figure 6.1-c shows the resut of applying the recursive filter (low-pass) to the CO_2 series. The first minute is used to "warm up" the filter, with a block average (1 minute), during which the fluctuations are calculated around the constant average. After this time, we apply (6.1) in the discretized form

$$\overline{a}_{n+1} = \frac{\Delta t}{P} a_{n+1} + \left(1 - \frac{\Delta t}{P}\right) \overline{a}_n. \tag{6.2}$$

Figure 6.2-c shows the CO_2 fluctuations around the low-pass filter.

It's important to observe, in figure 6.2, that the fluctuations arising from the the different ways of calculating the average are *different* (although in this case it's hard to notice without close scrutiny). In particular, for the running averag and the low-pass filter, *the sample mean of the fluctuations is no longer identically null*. In these cases, it's common to do additional post-processing, subtracting the residual sample mean from these series.

The calculation of averages is ultimately subjective and the result of a personal decision. Consequently, what is considered "mean" and "fluctuation" varies according to the method used; the corresponding statistics will also vary, as well as turbulent fluxes like $\overline{w'\rho_c'}$.

6.2 – Coordinate rotation

The Monin-Obukhov similarity theory, MOST, assumes a stationary and horizontally homogeneous flow. Under these conditions, it is assumed that the average velocity vector is constant and strictly horizontal, and it is common practice to align the Ox axis with this direction. Therefore, it is usual to write

$$\overline{\boldsymbol{u}} = [\overline{u} \quad 0 \quad 0]^\intercal \tag{6.3}$$

for the coordinates of the average wind velocity. Horizontal homogeneity also implies that there are no Reynolds shear stresses in the directions xy and yz:

$$\overline{u'v'} = 0, \qquad \overline{v'w'} = 0. \tag{6.4}$$

Under these idealized conditions, the Reynolds tensor simplifies to

$$\boldsymbol{\tau} = \begin{bmatrix} \overline{u'u'} & 0 & \overline{u'w'} \\ 0 & \overline{v'v'} & 0 \\ \overline{u'w'} & 0 & \overline{w'w'} \end{bmatrix}. \tag{6.5}$$

Then, the turbulent stress vector in the horizontal plane whose normal is $\boldsymbol{k}$ is

$$\boldsymbol{t} = \boldsymbol{k}^\intercal \cdot \boldsymbol{\tau} = \begin{bmatrix} 0 & 0 & 1 \end{bmatrix} \begin{bmatrix} \overline{u'u'} & 0 & \overline{u'w'} \\ 0 & \overline{v'v'} & 0 \\ \overline{u'w'} & 0 & \overline{w'w'} \end{bmatrix} = \begin{bmatrix} \overline{u'w'} \\ 0 \\ \overline{w'w'} \end{bmatrix}. \tag{6.6}$$

Therefore, under ideal conditions, the horizontal component of $\boldsymbol{t}$ is aligned with $\overline{\boldsymbol{u}}$. This makes sense physically, since we expect that the direction of the shear stresse is the same (with the opposite sign) as that of the wind velocity.

Given two successive rotation between the bases

$$\begin{aligned} E &= (\boldsymbol{e}_1, \boldsymbol{e}_2, \boldsymbol{e}_3), \\ F &= (\boldsymbol{f}_1, \boldsymbol{f}_2, \boldsymbol{f}_3), \qquad \text{e} \\ G &= (\boldsymbol{g}_1, \boldsymbol{g}_2, \boldsymbol{g}_3), \end{aligned}$$

the relations between the vectors of these bases are

$$\boldsymbol{f}_j = C_{ij}\boldsymbol{e}_i, \tag{6.7}$$

$$\boldsymbol{g}_k = D_{jk}\boldsymbol{f}_j = D_{jk}C_{ij}\boldsymbol{e}_i = C_{ij}D_{jk}\boldsymbol{e}_i, \tag{6.8}$$

where $\boldsymbol{C}$ and $\boldsymbol{D}$ are the respective rotation matrices. Therefore, the rotation matrix from E to G is the product

$$\boldsymbol{CD}$$

in this order. In Figure 6.3 we see two successive rotations: the first of an angle $+\alpha$ around z_E in the horizontal plane of basis E which aligns the horizontal wind velocity vector with the axis x_F; the second of a vertical angle β around y_F which aligns the "total" velocity vector of the average wind $\overline{\boldsymbol{u}}$ with the axis x_G.

The equations for the components of the rotation matrices are

$$C_{ij} = (\boldsymbol{e}_i \cdot \boldsymbol{f}_j), \tag{6.9}$$

$$D_{jk} = (\boldsymbol{f}_j \cdot \boldsymbol{g}_k). \tag{6.10}$$

In basis E, the coordinates of the vectors $\boldsymbol{e}_i$ and $\boldsymbol{f}_j$ are:

$$\begin{array}{lll} [1,0,0]^\intercal & [0,1,0]^\intercal & [0,0,1]^\intercal, \\ [\cos\alpha, \operatorname{sen}\alpha, 0]^\intercal & [-\operatorname{sen}\alpha, \cos\alpha, 0]^\intercal, & [0,0,1]^\intercal. \end{array}$$

(Note that, in figure 6.3, the angle α is *positive*, because represents a positive rotation around z_E.) Therefore,

$$\boldsymbol{C} = \begin{bmatrix} \cos\alpha & -\operatorname{sen}\alpha & 0 \\ \operatorname{sen}\alpha & \cos\alpha & 0 \\ 0 & 0 & 1 \end{bmatrix} \tag{6.11}$$

In basis F, the coordinates of the vectors $\boldsymbol{f}_j$ and $\boldsymbol{g}_k$ are:

$$\begin{array}{lll} [1,0,0]^\intercal & [0,1,0]^\intercal & [0,0,1]^\intercal, \\ [\cos\beta, 0, -\operatorname{sen}\beta]^\intercal & [0,1,0]^\intercal, & [\operatorname{sen}\beta, 0, \cos\beta]^\intercal. \end{array}$$

(Note, in figure 6.3, that the angle β is *negative*, because it represents a negative rotation around y_F.) Therefore,

$$\boldsymbol{D} = \begin{bmatrix} \cos\beta & 0 & \operatorname{sen}\beta \\ 0 & 1 & 0 \\ -\operatorname{sen}\beta & 0 & \cos\beta \end{bmatrix} \tag{6.12}$$

The "total" rotation matrix, given by the product $\boldsymbol{CD}$ will be

$$\begin{bmatrix} \cos\alpha\cos\beta & -\operatorname{sen}\alpha & \cos\alpha\operatorname{sen}\beta \\ \cos\beta\operatorname{sen}\alpha & \cos\alpha & \operatorname{sen}\alpha\operatorname{sen}\beta \\ -\operatorname{sen}\beta & 0 & \cos\beta. \end{bmatrix}$$

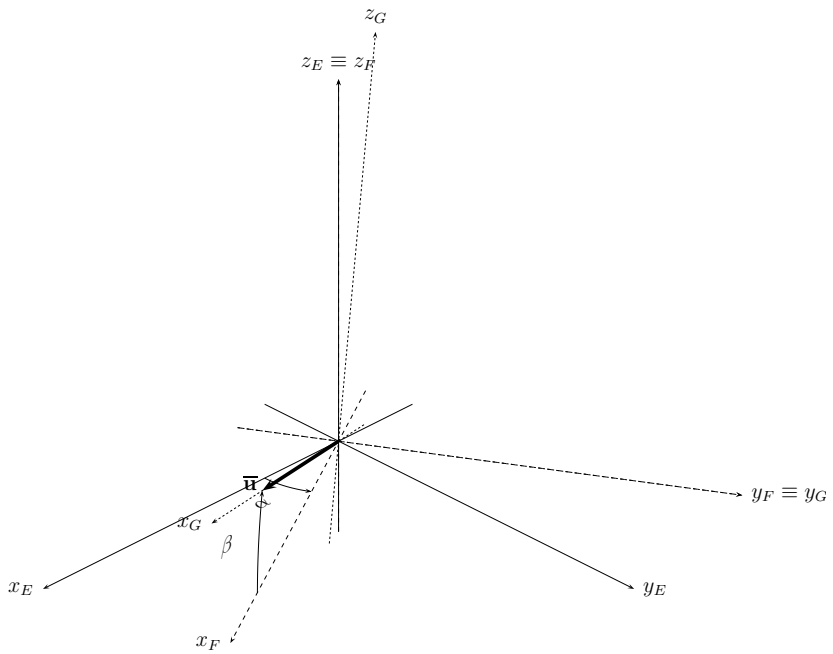

Figure 6.3: 2D coordinate rotation for the alignment of the wind velocity

Finally, the coordinates of the wind velocity vector in basis E, given by $[u, v, w]_E^\intercal$ will be rotated to basis G according to

$$\boldsymbol{u}_G = \boldsymbol{D}^\intercal \boldsymbol{C}^\intercal \boldsymbol{u}_E, \tag{6.13}$$

that is,

$$\begin{bmatrix} u \\ v \\ w \end{bmatrix}_G = \begin{bmatrix} \cos\alpha\cos\beta & \cos\beta\,\mathrm{sen}\,\alpha & -\mathrm{sen}\,\beta \\ -\mathrm{sen}\,\alpha & \cos\alpha & 0 \\ \cos\alpha\,\mathrm{sen}\,\beta & \mathrm{sen}\,\alpha\,\mathrm{sen}\,\beta & \cos\beta \end{bmatrix} \begin{bmatrix} u \\ v \\ w \end{bmatrix}_E . \tag{6.14}$$

The angles α and β are easily calculated from $\overline{u}$, $\overline{v}$ and $\overline{w}$ measured in basis E: typically, this is the reference system connected to a sonic anemometer installed in the field and carefully leveled, so that the axis z_E is as vertical as possible. These angles are

$$\alpha = +\,\mathrm{arctg2}\,(\overline{v}_E, \overline{u}_E)\,, \tag{6.15}$$

$$\beta = -\,\mathrm{arctg2}\left(\overline{w}_E, \sqrt{\overline{u}_E^2 + \overline{v}_E^2}\right) \tag{6.16}$$

(remember that angle β is negative in figure 6.3). The function $\mathrm{arctg2}(y, x)$ gives the angle formed with axis x by a two-dimensional vector (x, y) (notice to the order); in the programming languages C, MATLAB and Python, arctg2 is implemented as `atan2(y,x)`; in FORTRAN, as `ATAN2(Y,X)`.

The scalar fluxes should be rotated similarly. In particular, if η' is a density fluctuation, mixing ratio, temperature, etc., of a scalar, equation (6.14) is almost completely repeated:

$$\begin{bmatrix} \overline{u'\eta'} \\ \overline{v'\eta'} \\ \overline{w'\eta'} \end{bmatrix}_G = \begin{bmatrix} \cos\alpha\cos\beta & \cos\beta\,\mathrm{sen}\,\alpha & -\mathrm{sen}\,\beta \\ -\mathrm{sen}\,\alpha & \cos\alpha & 0 \\ \cos\alpha\,\mathrm{sen}\,\beta & \mathrm{sen}\,\alpha\,\mathrm{sen}\,\beta & \cos\beta \end{bmatrix} \begin{bmatrix} \overline{u'\eta'} \\ \overline{v'\eta'} \\ \overline{w'\eta'} \end{bmatrix}_E . \tag{6.17}$$

The change of basis for the Reynolds stress tensor is a little more elaborate. Defining the full tensor,

$$\boldsymbol{\tau} \equiv \overline{\boldsymbol{u}'\boldsymbol{u}^\top} = \begin{bmatrix} \overline{u'u'} & \overline{u'v'} & \overline{u'w'} \\ \overline{v'u'} & \overline{v'v'} & \overline{v'w'} \\ \overline{w'u'} & \overline{w'v'} & \overline{w'w'} \end{bmatrix}, \tag{6.18}$$

it follows from (6.13) that

$$\boldsymbol{\tau}_G = \boldsymbol{D}^\top \boldsymbol{C}^\top \boldsymbol{\tau}_E \boldsymbol{C}\boldsymbol{D}. \tag{6.19}$$

The coordinate rotations shown in this section form the basis of the data processing of scalar fluxes and momentum measured in micrometeorological experiments. A third rotation is possible, which makes $\overline{v'w'}_G = 0$, but its use is questionable and many authors consider it "non-physical" (Finnigan et al., 2003).

An more recent alternative, the *planar fit method* of Wilczak et al. (2001), decomposes the rotations in a sequence of two, one of them (analogous to the $\boldsymbol{D}$ rotation in this text) being applied to every micrometeorological block available followed by a rotation (analogous to the $\boldsymbol{C}$ rotation in this text) applied separetely to each block, to align the horizontal wind vector with the final x axis. According to the authors, the method minimizes the errors in the calculation of the turbulent shear stresses. The method calculates a mean offset in the vertical axis (typically smaller then the accuracy of the sonic anemometers) with a least squares method, and it has been gaining wide acceptance.

6.2.1 – The WPL correction for the average vertical velocity

A quick inspection of table 2.1 shows that $\rho_c \ll \rho$, and that

$$\rho \approx \rho_s + \rho_v \tag{6.20}$$

is an excellent approximation. The state equation for air will be (approximately)

$$p = [\rho_s R_s + \rho_v R_v]T. \tag{6.21}$$

Now, applying the Reynolds decomposition to all of the quantities in (6.21), and neglecting the higher-order products of fluctuations, we have

$$\begin{aligned} \overline{p} + p' &= (\overline{\rho}_s + \rho_s')R_s(\overline{T} + T') + (\overline{\rho}_v + \rho_v')R_v(\overline{T} + T') \\ &= (\overline{\rho}_s R_s + \overline{\rho}_v R_v)\overline{T} + \overline{\rho}_s R_s T' + \rho_s' R_s \overline{T} + \overline{\rho}_v R_v T' + \rho_v' R_v \overline{T}. \end{aligned} \tag{6.22}$$

This allows an obvious interpretation for $\overline{p}$ and p':

$$\overline{p} = (\overline{\rho}_s R_s + \overline{\rho}_v R_v)\overline{T}, \tag{6.23}$$

$$p' = (\overline{\rho}_s R_s + \overline{\rho}_v R_v)T' + \overline{T}(R_s \rho_s' + R_v \rho_v'). \tag{6.24}$$

Making the observation that, in the surface layer, the pressure fluctuation can be neglected *vis-à-vis* the temperature and density fluctuations (Fleagle and Businger, 1980) (see also the discussion leading to (4.44)),

$$0 = (\overline{\rho}_s R_s + \overline{\rho}_v R_v)T' + \overline{T}(R_s \rho_s' + R_v \rho_v'). \tag{6.25}$$

Multiplying (6.25) by the vertical velocity fluctuation w', taking a time average average and using Reynolds' postulates, we obtain

$$0 = (\overline{\rho}_s R_s + \overline{\rho}_v R_v)\overline{w'T'} + \overline{T}(R_s\overline{w'\rho_s'} + R_v\overline{w'\rho_v'}). \tag{6.26}$$

Note here a difficulty in this derivation: as already mentioned, strictly speaking, the Reynolds postulates do not apply fully to the block and running averages — see (3.14) and (3.19)–(3.21) — and its approximate validity must be assumed. To the best of our knowledge, a detailed analytical evaluation of the effects of these approximations hasn't been done.

Equation (6.26) plays a central role in the WPL approximation. In fact, applying Reynolds's decomposition to (3.40),

$$\begin{aligned} \overline{w\rho_s} = \overline{w}\,\overline{\rho_s} + \overline{w'\rho_s'} = 0 \Rightarrow \\ \overline{w} = -\frac{\overline{w'\rho_s'}}{\overline{\rho_s}}. \end{aligned} \tag{6.27}$$

Note that $\overline{w}$ can be effectively calculated from (6.26)–(6.27), using measurements of $\overline{w'T'}$ and of $\overline{w'\rho_v'}$. A fact rarely mentioned is that the WPL correction stems from the hypothesis of a non-null value of $\overline{w}$; however, in most measurements turbulent fluxes using the eddy covariance method, it is common to apply a coordinate rotation, whose effect is precisely to force $\overline{w} = 0$. This produces an apparent conflict between simultaneous application of the coordinate rotation and the WPL correction (Massman and Lee, 2002; Dias et al., 2007). However, notice also that the vertical velocity value $\overline{w}$ estimated by the WPL correction is *very small*; in fact, it is smaller than the accuracy of the measurements using sonic anemometers (Finnigan, 2009). In practice, therefore, the procedure of first applying a coordinate rotation that makes $\overline{w} = 0$, and *then* applying the WPL correction which is equivalent to stipulate a small value of $\overline{w}$ — too small to be measured with the currently available measuring instruments — is justifiable.

Continuing, now we will calculate the water vapor mass flux taking into account (6.27), this is, taking into account the WPL correction.

For the water vapor mass flux E, start from (5.7) and apply the Reynolds decomposition:

$$E = \overline{w\rho_v} = \overline{w}\,\overline{\rho_v} + \overline{w'\rho_v'}. \tag{6.28}$$

Typically, the eddy covariance method generates the second term in (6.28); the WPL correction consists of calculating, and adding, the first term. For this, we calculate $\overline{w}$ explicitly. From (6.26),

$$\begin{aligned} \overline{w'\rho_s'} = -\frac{1}{\overline{T}}\left[\overline{\rho_s} + \frac{R_v}{R_s}\overline{\rho_v}\right]\overline{w'T'} - \frac{R_v}{R_s}\overline{w'\rho_v'} \Rightarrow \\ \overline{w} = \frac{1}{\overline{\rho_s}}\left\{\frac{1}{\overline{T}}\left[\overline{\rho_s} + \frac{R_v}{R_s}\overline{\rho_v}\right]\overline{w'T'} + \frac{R_v}{R_s}\overline{w'\rho_v'}\right\}. \end{aligned} \tag{6.29}$$

Putting $\mu = R_v/R_s$, and taking expression (6.28) to E,

$$\begin{aligned}
E &= \frac{\overline{\rho_v}}{\overline{\rho_s}} \left\{ \frac{1}{\overline{T}} \left[\overline{\rho_s} + \frac{R_v}{R_s} \overline{\rho_v} \right] \overline{w'T'} + \frac{R_v}{R_s} \overline{w'\rho_v'} \right\} + \overline{w'\rho_v'} \\
&= \overline{\rho_v} \left\{ \left(1 + \mu \frac{\overline{\rho_v}}{\overline{\rho_s}} \right) \frac{\overline{w'T'}}{\overline{T}} \right\} + \frac{\overline{\rho_v}}{\overline{\rho_s}} \mu \overline{w'\rho_v'} + \overline{w'\rho_v'} \\
&= \overline{\rho_v} \left(1 + \mu \overline{r_v} \right) \frac{\overline{w'T'}}{\overline{T}} + \left(1 + \mu \overline{r_v} \right) \overline{w'\rho_v'} \\
&= \left(1 + \mu \overline{r_v} \right) \left[\overline{w'\rho_v'} + \overline{\rho_v} \frac{\overline{w'T'}}{\overline{T}} \right],
\end{aligned} \tag{6.30}$$

where

$$\overline{r_v} = \frac{\overline{\rho_v}}{\overline{\rho_s}} \tag{6.31}$$

is the mixing ratio for water vapor. Equation (6.30) is the expression obtained by Webb et al. (1980) for the correction of the water vapor turbulent flux.

Now, proceeding to the case of a greenhouse gas such as CO_2, start from (5.9) and apply the Reynolds decomposition:

$$\begin{aligned}
F_c &= \overline{w}\,\overline{\rho_c} + \overline{w'\rho_c'} \\
&= \left\{ -\frac{\overline{w'\rho_s'}}{\overline{\rho_s}} \right\} \overline{\rho_c} + \overline{w'\rho_c'} \\
&= -\frac{\overline{\rho_c}}{\overline{\rho_s}} \left\{ -\frac{1}{\overline{T}} (\overline{\rho_s} + \mu \overline{\rho_v}) \overline{w'T'} - \mu \overline{w'\rho_v'} \right\} + \overline{w'\rho_c'} \\
&= \overline{r_c} \left[\overline{\rho_s} (1 + \mu \overline{r_v}) \frac{\overline{w'T'}}{\overline{T}} + \mu \overline{w'\rho_v'} \right] + \overline{w'\rho_c'} \\
&= \frac{\overline{\rho_c}}{\overline{\rho_s}} \overline{\rho_s} (1 + \mu \overline{r_v}) \frac{\overline{w'T'}}{\overline{T}} + \mu \overline{r_c}\, \overline{w'\rho_v'} + \overline{w'\rho_c'} \\
&= \overline{\rho_c} (1 + \mu \overline{r_v}) \frac{\overline{w'T'}}{\overline{T}} + \mu \overline{r_c}\, \overline{w'\rho_v'} + \overline{w'\rho_c'},
\end{aligned} \tag{6.32}$$

where

$$\overline{r_c} = \frac{\overline{\rho_c}}{\overline{\rho_s}} \tag{6.33}$$

it is the mixing ratio for CO_2.

For measurements of greenhouse gases fluxes, it is essential to apply the WPL correction.

6.3 – Energy fluxes and greenhouse gas measurements in different biomes

This section presents a brief review of some results of CO_2 fluxe measurements performed in many parts of the world. The goal is not to produce a comprehensive review of this type of measurement, but to provide a connection with the material of the previous sections through some examples and critical discussions of these measurements.

6.3.1 – BOREAS

The BOREAS project (*Boreal Ecosystem - Atmosphere Study*) took place in the central region of Canada as part of NASA's Earth Science Research and Analysis program, with the goal of understanding the interactions between the boreal forest's biome and the atmosphere. A part of this project consisted in flux measurements of energy, water, carbon and other gases, in order to support the climate change and the global warming studies. The field phase of this project happened between 1993 and 1997 (Sellers et al., 1997). The boreal regions correspond to the largest ecosystems in the world, covering something between 6 and 8.5% of the planet's land surface (Simpson et al., 1997), which makes this project an extremely important one for global change research.

The CO_2 flux measurements were performed at micrometeorological towers erected in various sites throughout the boreal forest. Besides the measurement of mean meteoroloogical data such as temperature, humidity and pressure, the towers also quantified the turbulent exchange of energy and mass between the the forest and the atmosphere, mostly by means of the eddy covariance method. The measurements were always performed a few above the canopy, using tridimensional sonic anemometers and open-path infrared gas analysers with a frequency of 15 Hz. The fluctuations were calculated by means of a recursive filter with a time constant equal to 400 s; a coordinate rotation was performed to make the mean vertical velocity of each block equal to zero; and the WPL correction was applied.

From the field measurements performed in this experiment, the CO_2 flux in the boreal forest varied from an absorption of 130 $g_C\,m^{-2}ano^{-1}$ in the "southern old aspen" region to an emission of 50 $g_C\,m^{-2}ano^{-1}$ in the "northern old black spruce" region (Sellers et al., 1997).

Simpson et al. (1997) presented the results obtained in the studies of methane and nitrous oxide exchange between the "aspen" boreal forest and the atmosphere. The emission of nitrous oxide in this type of forest is associated with the bacterial processes of nitrification and denitrification occurring in the soil, whereas methane is produced in the anaerobic microbial decomposition of organic matter, and consumed by oxidizing bacteria in aerobic conditions.

The measurements of Simpson et al. (1997) were made in a sequence of 5 consecutive months, in a 40 m high tower, over a forest approximately 21 m high. The method used for the CH_4 and N_2O fluxe measurements was the flux-gradient method, based on the MOST, in which the scalar flux is given by:

$$F = 1{,}3\frac{u_*\kappa(\overline{\rho_{\chi 1}} - \overline{\rho_{\chi 2}})}{\ln\left(\frac{z_2-d}{z_1-d}\right) - [\Psi_F(\zeta_2) - \Psi_F(\zeta_1)]}. \tag{6.34}$$

In this case, the same similarity functions for both CH_4 and N_2O temperature gradients were used. Compare (6.34) with the definition of fluxes and turbulence scales in (5.5)–(5.9), and with (5.24). For the stability functions Ψ_F, Simpson et al. (1997) used the same equations presented in section 5.3.

It is important to note that Simpson et al. (1997) applied a correction factor of 1,3 in (6.34), with a somewhat questionable justification based on the contributions of convective circulation cells to the surface fluxes. Strictly speaking, this kind of adjustment is often applied in an *ad hoc* way to force the closing of the

surface energy balance (Twine et al., 2000), but a systematic approach to explain the lack of closure of the energy balance has not been attained yet; in this sense it is worth mentioning the works of Sakai et al. (2001) and Finnigan et al. (2003) about the contribution of the mesoscale components to the surface fluxes.

For the measurement of high-frequency data, a sonic anemometer (20cm path Kaijo-Denki DAT-310) was used, placed at 39,1 m, and run at a frequency of 100 Hz with 20-Hz block averaging, undergoing a coordinate rotation to eliminate the mean vertical velocity. The gas concentration difference between two levels was measured with two Campbell Scientific Inc. *Tunable diode laser Trace Gas Analysis System* sensors, placed at $z_2 = 37{,}5$ m and $z_1 = 26{,}8$ m. The measured fluxes were $1{,}4 \pm 0{,}5\,\mathrm{ng\,m^{-2}\,s^{-1}}$ and $15{,}7 \pm 2{,}8\mathrm{ng\,m^{-2}\,s^{-1}}$ respectively for CH_4 and N_2O, for the 5-month period.

CH_4 flux measurements using the same technique were also made in the "southern boreal fen" region, and CH_4 emission rates of the order of $2250\,\mathrm{ng\,m^{-2}\,s^{-1}}$ were obtained (Simpson et al., 1997), which is expected due to the anaerobic characteristic of this type of ecosystem.

6.3.2 – LBA

The Large-Scale Biosphere-Atmosphere Experiment in Amazonia was an international research conducted in the brazilian amazon forest between 1995 and 2005. It had the goal of understanding the carbon and other nutrient's dynamics between the forest and the atmosphere, and CO_2 flux studies were made using, among others, the eddy covariance method.

Miller et al. (2004) made a study that compared the eddy covariance method, with some of its correction alternatives, with biometric inventories performed in the region. The measurements were made in the *Floresta Nacional Tapajós*, 70 km south of Santarém PA, a typical dense tropical forest region (average canopy height: 35 to 40 m), on a plateau that extends for many kilometers.

The biometric inventories are measurements of biomass that exists in a given region, and when they are continued for several years, they allow estimates of the carbon balance in the period. Miller et al. (2004) used three existing inventories in the region to estimate the carbon balance for 16 years (1984-2000) in the area in which the measurements of eddy covariances were undertaken.

The eddy covariance method applied by the authors consisted in the measurement of the turbulent CO_2 flux at a 64 m-high tower. The high frequency measurements of wind velocity were made by a three-axis sonic anemometer. The molar density of CO_2 and H_2O were measured independently by two analysers: an infrared open path gas analyser, and a closed path one. The latter sampled air through a teflon PFA overheated tube (65° C) with 9,5 mm of internal diameter. All of the measurements were performed at 4 Hz, and the delay time of the closed path analyser was 11,75 s for CO_2 and 12,75 s for H_2O. Two different methods were also used, named method (1) and method (2), for the calculation of CO_2 and H_2O concentrations (for further details, check Miller et al. (2004)).

Table 6.1: Results obtained by Miller et al. (2004) for CO_2 fluxes in Amazônia (a positive sign indicates an emission). CP ="closed path"; OP = "open path".

Method of measurement/correction	Flux ($Mg_C\,ha^{-1}\,year^{-1}$)
biometric	$0,8 \pm 2,0$
CP, 30-min, without *detrending*, w/ cor. alta frequência	$-3,9$
CP, 30-min, without *detrending*, wo/ cor. alta frequência	$-4,2$
OP, 30-min, without *detrending*, w/ WPL	$-10,0$
OP, 30-min, without *detrending*, wo/ WPL método (1)	$-5,5$
OP, 30-min, without *detrending*, w/ WPL método (2)	$-5,0$
CP, 120-min, without *detrending*, w/ cor. alta frequência	$-3,5$
OP, 30-min, with *detrending*, w/ WPL método (2)	$-4,8$
CP, 30-min, without *detrending*, w/ cor. alta frequência, $u_* < 0{,}2\,m\,s^{-1}$	$+0,4$
CP, 30-min, without *detrending*, w/ cor. alta frequência, $u_* < 0{,}3\,m\,s^{-1}$	$+2,0$

For the closed-path analyzer, it was necessary to apply a correction for the loss of the high frequency fluctuations, which was made on the basis of the similarity between temperature and CO_2 and H_2O, by means of a first-order filter that simulates the attenuation of the fluctuations in the tube. The time constant were found by comparing the spectra of temperature and CO_2 or temperature and H_2O, and the result obtained was a time constant of 0,4 s for CO_2 and of 0,9 s for H_2O.

The effect of the loss low-frequency flux components by the average used to estimate the fluxes, as well as the effect of the linear detrending, were also discussed by the authors. They tested 30-min. averages and 2-hour averages, to assess the effect of the time-averaging period, and also compared the results obtained with and without linear detrending.

On last correction of the flux data was applied to "calm" periods, when the eddy covariance method is not able to measure the CO_2 flux. The correction, which is standard, consisted of appliying a filter based on the friction velocity values u_*: whenever the measured u_* was below a certain cutoff value, the measured fluxes were replaced by model values based on soil and plants respiration as a function of easily-measured variables such as soil temperature.

The obtained results comparing all the correction possibilities and the biometric results are presented in table 6.1. The results give an important idea of the dispersion of results that can be obtained at a single site from measurements with the ECM.

The evidence that the CO_2 flux is underestimated during nights with low turbulence is confirmed in other measurements made in the project, as the work presented in Culf et al. (1997) and in the paper by Chambers et al. (2004). Miller et al. (2004) also conclude that using of 30 min or 2 h in the calculation of averages did not produce significant differences, as well as the utilization of methods (1) and (2) in the WPL correction. In general, the measurements using closed- and open-path analyzers were shown to be similar, and the result considered by the authors as the most correct is a CO_2 flux of $+0{,}4 MgC\,ha^{-1}\,ano^{-1}$, a result

consistent with the biomass inventory. It is important to emphasize that the large error associated with the biometric measurements is due to the fact that smaller plants are neglected in the study, which can represent a large part of the carbon balance of the region.

6.3.3 – ChinaFLUX

Yu et al. (2006) present an overview of ChinaFLUX (Chinese Research Network for Fluxes in Terrestrial Ecosystems), a network of micrometeorological measurements of fluxes of CO_2, water vapor and energy between the biosphere and the atmosphere for long periods using chambers and the Eddy Covariance Method. The ECM, used in 8 different places, had as a focus the measurement of water vapor and CO_2 while the chamber method, used in 17 places, emphasized CH_4 and N_2O measurements.

The measurements using the ECM were performed in 3 places over, 4 places over tall forest in 1 place over an agriculture area with crop rotation (wheat and corn). The standard set of equipments in these micrometeorological stations consisted of an open-path infrared gas analyzer model *Li-Cor* LI-7500 (measuring H_2O and CO_2), a sonic anemometer *Campbell* CSAT3 (measuring the three components of the wind velocity and temperature), and a datalloger storing the measurements at 10 Hz. The fluxes were calculated using block averages of 30 minutes, and were corrected with the WPL correction.

The eddy covariance measurements were supplemented with a 6-level CO_2/H_2O and a 7-level CO_2 profiling system, also custom-designed by Campbell Scientific Inc., at the crop/grassland sites and the forest sites, respectively. Standard meteorological measurements included air humidity, wind speed and direction, four components of the net radiation, photosynthetically active radiation, soil heat flux, soil temperature, and soil moisture.

In one of the forests there were four-level measurements, allowing investigations about the fluxes footprint (Leclerc and Thurtell, 1990), advection effects, vertical divergence of turbulents fluxes and aerodynamic interference from the tower.

In two forests open and closed path sensors were compared, and the resulting fluxes from the two sensors were considered similar.

In an agricultural area, techniques of *ensemble blocks* were applied and ogives (Sun et al., 2006) were calculated to determine the contribution of the low frequencies to the fluxes (see above the comments on the analysis of Sakai et al. (2001) and Finnigan et al. (2003)), under the argument that the inclusion of the components of low frequency can improve the energy balance closure. However, averages over periods greater than 30 minutes did not always improve the results.

Other results reported in Yu et al. (2006) are not surprising, considering what we have already reviewed earlier:

- Daytime observations are less affected than nighttime ones.
- Daytime data are less affected by the ground roughness than nighttime data.
- Measurements with the ECM showed discrepancies and uncertainties mainly during nights and over complex terrain.

6.4 – Cerrado

da Rocha et al. (2002) used the ECM for measurement of the CO_2 flux on a savanna (Cerrado Sensu stricto) near the city of Santa Rita do Passa-Quatro (SP) between october of 2000 and march of 2002. The measurements were performed from a 21 m-high tower equipped with sensors to measure meteorological variables besides a set of high-frequency sensors consisting of a sonic anemometer (A1012R *Gill Solent*), an infrared gas analyser for CO_2 and H_2O (*Li-cor* 6262) and an air sampling system. The micrometeorological measurements were made at 5 Hz. The fluxes were calculated for periods of 30 minutes using coordinate rotation and algorithms for the loss of the high frequencies described in Moncrieff et al. (1997).

Nocturnal fluxes were filtered for the cutoff values of u_*, as proposed by Goulden et al. (2006); considering cutoff values of $0,2\,\mathrm{m\,s^{-1}}$ and $0,5\,\mathrm{m\,s^{-1}}$, the CO_2 balance results in $-0,5\,\mathrm{t_C\,ha^{-1}\,year^{-1}}$ and $+3,2\,\mathrm{t_C\,ha^{-1}\,year^{-1}}$. The authors conclude that the cerrado is a small source of CO_2, with a net $+0,1\,\mathrm{t_C\,ha^{-1}\,year^{-1}}$ emission rate.

6.5 – Conclusions

With various decades of effective use around the globe, the micrometeorological methods of flux-gradient and eddy covariance constitute a practical tool for the measurement of greenhouse gas surface fluxes.

Even with the almost enthusiastic adoption of the ECM by the ecological community, and its great utility for studying the physiology of ecosystems (Baldocchi, 2003), significant challenges still have to be overcome, including a better understanding of all the time scales that contribute to the surface fluxes, and their relation with atmospheric stability; of the surface energy balance; of the effects of advection and their relation with complex topography; of the non-stationarity; and of the intermittency of the nocturnal turbulence.

The continuous technological advance of the sensors, and their corresponding diminishing costs, have made the ECM widely available and allowed the generation of a large flux data base. This massive experimental approach has generated in the last decades a heretofore unseen volume of knowledge on the physics, chemistry and biology of numerous terrestrial ecosystems.

The availability of more sensors, at a relatively low cost; the increase of computer resources; and the quantitative and qualitative improvement of human resources in micrometeorology research permit an optimistic assessment of the ECM and the FGM application potential in greenhouse gas studies.

The physical hypotheses of the micrometeorological methods and their current limitations were emphasized here so that in new experiments the experimental apparatus and the theoretical analysis can provide advances in their application and in the reliability of their results.

7

Energy fluxes at the surface of the Earth

7.1 – The movement of the Earth

The Earth goes around the Sun in a trajectory that is approximately elliptical. The plane of the trajectory is called the ecliptic plane. In figure 7.1, the distance OA = r_0 is the major semi-axis of the ellipse. It is a unit of length in astronomy: the Astronomical Unit (AU).

The points A, B, C, D, A′, B′, C′ and D′ are outstanding points of the annual movement of the planet around the Sun. A marks the perihelion, the point where the planet is closest to the Sun. By the same token, C marks the afelion, the point where the planet is farthest from the Sun. The dates for these points vary slightly from year to year. Table 7.1, valid for 2020; it has been retrived from United States Naval Observatory (2019).

The material described here has been collected from several points. Perhaps the most authoritative is the paper by van Flandern and Pulkkinen (1979), and a very detailed guide for the calculation of the Sun's declination and the distance Sun-Earth can be found in Schlyter (2019).

Table 7.1: Outstanding days in the Earth's orbit for 2020.

Point	date/time (UTC)	Name
A	January 5, 2020, 07:48	Perihelion
B	April 5, 2020, 19:48	$r/r_a = 1$
C	July 4, 2020, 11:35	Aphelion
D	October 5, 2020,19:48	$r/r_a = 1$
A′	December 21, 2020, 10:02	Winter Solstice
B′	March 20, 2020, 03:50	Spring Equinox
C′	June 20, 2020, 21:44	Summer Solstice
D′	September 22, 2020	Autumn Equinox

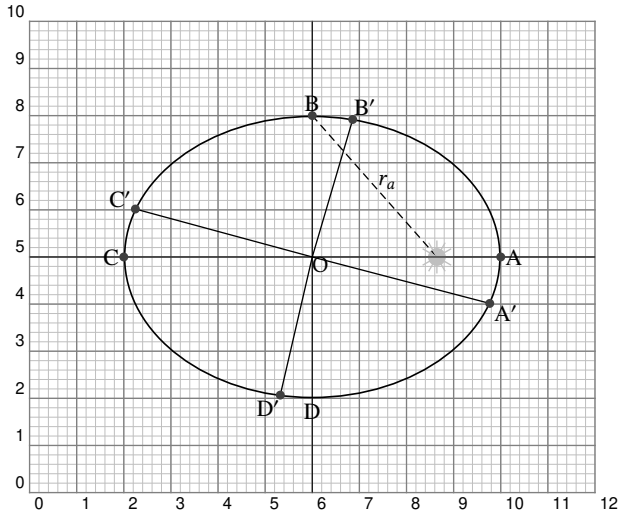

Figure 7.1: The Earth's trajectory around the Sun.

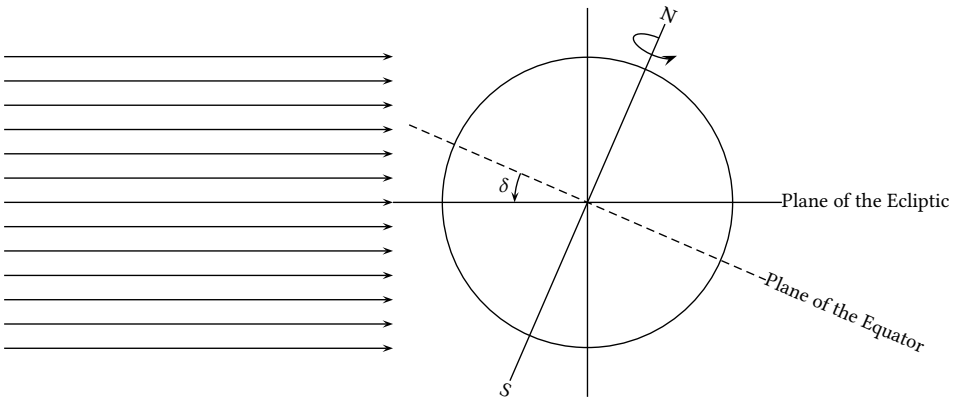

Figure 7.2: The position of the planet Earth with respect to the incidence of the Sun's rays around the Northern Hemisphere Solstice.

In figure 7.1, the semi-major axis of the ellipse is r_a, and the semi-minor axis is r_b. The distance between the Sun and the Earth at any point in the trajectory is r. The value of r_a is defined in Astronomy as the *Astronomical Unit*, AU. The Sun's *declination* with respect to the Earth is the angle δ between the plane of the Equator and the plane of the Ecliptic, measured perpendicularly to the latter.

The cause for the changing seasons is not the variation in the distance Sun-Earth r, but rather the inclination of the axis of rotation of the planet in relation to the plane of the ecliptic, and the consequent change in the Sun's declination.

For example, figure 7.2 shows the situation of the planet with respect to the incidence of the Sun's rays around the Winter Solstice (Norther Hemisphere). At this point in the planet's trajectory, most of that incidence is on the Southern Hemisphere, where it is the begginning of Summer. The opposite situation will happen around the Summer Solstice (Norther Hemisphere).

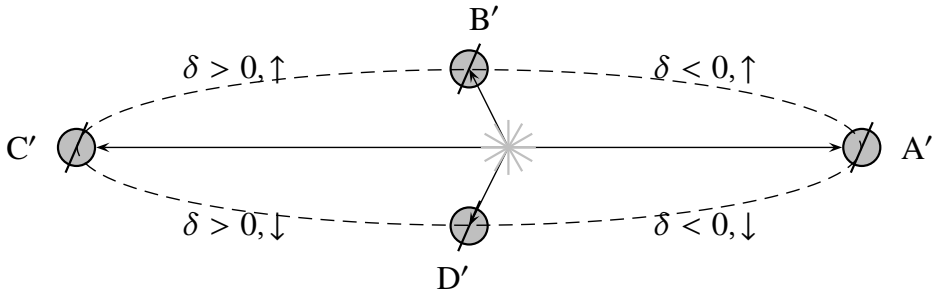

Figure 7.3: The incidence of the rays of the Sun on the Earth around the year. The sign of the Sun's declination δ is indicated between the points A′, B′, C′ and D′, as well as the sign of its rate of change, indicated as positive (↑) or negative (↓).

The situation around the year is shown in Figure 7.3. Note that the figure is not drawn accurately; it does however show the essential elements in terms of how the Sun's rays' incidence changes around the year. The 4 points emphasized are the solstices and the equinoxes. During the solstices, the Sun's rays are at maximum incidence on either hemisphere, and this determines the beginning of Summer and Winter. On the other hand, at the equinoxes, the Sun's rays fall perpendicularly to the Equator (hence their names).

Relatively low precision formulae for the values of δ and r/r_a at a given date are given by van Flandern and Pulkkinen (1979). These formulae are converted into a Python function (`ddse`) in listing 7.1.

Listing 7.1: `sunearth.py` — Calculation of distance and declination of Sun as a function of date.

```
from math import pi, modf, sin, cos, asin, sqrt, atan2
TwoPi = 2*pi
# ------------------------------------------------------------------------
# ddse
#
# version: 2019-05-04T13:46:15
#
# ------------------------------------------------------------------------
def ddse(yea,mon,day):
    '''
    ddse: declination and distance sun-earth a funcion of
    (year, month, day)

    based on

    Van Flandern, T. C. and Pulkkinen, K. F. (1979) "Low Precision
    Formulae for Planetary Positions" - The Astronomical Journal
    Supplement Series, 41,391:411.
    '''
# ------------------------------------------------------------------------
    assert(isinstance(yea,int))
    assert(isinstance(mon,int))
    assert(isinstance(day,int))
# ------------------------------------------------------------------------
# At GMT noon: this is done with purely integer arithmetic
# ------------------------------------------------------------------------
    JD = 367 * yea - ( 7 * (yea + (mon + 9) // 12 ) // 4 ) \
       + ( 275 * mon // 9 + day ) + 1721014
    # JD = + 367 * yea \
```

```
30      #       - 7*(yea + (mon + 9)//12)/4 \
31      #       - 3*((yea + (mon - 9)//7)//100 + 1)//4 \
32      #       + 275*mon//9 + day + 1721029
33  # ------------------------------------------------------------------------
34  # Obtains tee,
35  # TT == thousands of Julian years from 2000
36  # TC == hundreds of Julian years from 1900
37  # ------------------------------------------------------------------------
38      tee = float(JD - 2451545.0 + 0.5) ;
39  #   TT = tee/365250.0
40      TC = tee/36525.0 + 1.0 ;
41  #   TC = 10.0*TM + 1.0
42  # ------------------------------------------------------------------------
43  # other variables
44  # ------------------------------------------------------------------------
45      LS = 0.779072 + 0.00273790931 * tee  # mean longitude, Sun
46      GS = 0.993126 + 0.00273777850 * tee  # mean anomaly, Sun
47      G5 = 0.056531 + 0.00023080893 * tee  # mean anomaly, Jupiter
48      OM = 0.347343 - 0.00014709391 * tee  # longitude of lunar ascending mode
49  # ------------------------------------------------------------------------
50  # the eccentricity of the Earth comes from a different source:
51  # http://www.jgiesen.de/kepler/eccentricity.html
52  # ------------------------------------------------------------------------
53  # ec = +0.0167086342 - 0.0004203654*TT - 0.0000126734*TT**2 \
54  #      +0.0000001444*TT**3 -0.0000000002*TT**4 + 0.0000000003*TT**5
55  # ------------------------------------------------------------------------
56  # extracts fractional part
57  # ------------------------------------------------------------------------
58      (LS,ipart) = modf(LS)
59      (GS,ipart) = modf(GS)
60      (G5,ipart) = modf(G5)
61      (OM,ipart) = modf(OM)
62  # ------------------------------------------------------------------------
63  # converts to radians
64  # ------------------------------------------------------------------------
65      LS = LS * TwoPi
66      GS = GS * TwoPi
67      G5 = G5 * TwoPi
68      OM = OM * TwoPi
69  # ------------------------------------------------------------------------
70  # obtains VS
71  # ------------------------------------------------------------------------
72      VS = + 0.39785 * sin( LS ) \
73           - 0.01000 * sin( LS - GS ) \
74           + 0.00333 * sin( LS + GS ) \
75           - 0.00021 * TC * sin( LS ) \
76           + 0.00004 * sin( LS + 2.0 * GS ) \
77           - 0.00004 * cos( LS ) \
78           - 0.00004 * sin( OM - LS ) \
79           + 0.00003 * TC * sin( LS - GS )
80  # ------------------------------------------------------------------------
81  # obtains US
82  # ------------------------------------------------------------------------
83      US = + 1.0 \
84           - 0.03349 * cos( GS ) \
85           - 0.00014 * cos( 2.0 * GS ) \
86           + 0.00008 * TC * cos( GS ) \
87           - 0.00003 * sin( GS - G5 )
88  # ------------------------------------------------------------------------
89  # Sun's declination
90  # ------------------------------------------------------------------------
91      delta = asin( VS / sqrt(US) ) ;
92  # ------------------------------------------------------------------------
93  # distance Sun-Earth in the form (r/a) where a is the length
94  # of the largest semi-axis of the Earth's orbit, i.e.: the equivalent
95  # to one astronomical unit, and r is the Sun-Earth distance
96  # ------------------------------------------------------------------------
97      rr = 1.00021 * sqrt( US )
98      return (delta,rr)
99
100 # ------------------------------------------------------------------------
101 # sunman
102 #
```

```
# version of 2019-04-23T09:58:05
# ------------------------------------------------------------------------
def sunman(yea,mon,day,sec=0.0):
    '''
    sunman: only the sun mean anomaly a funcion of (year, month,day)

    based on

    Van Flandern, T. C. and Pulkkinen, K. F. (1979) "Low Precision
    Formulae for Planetary Positions" - The Astronomical Journal
    Supplement Series, 41,391:411.
    '''
# ------------------------------------------------------------------------
    assert(isinstance(yea,int))
    assert(isinstance(mon,int))
    assert(isinstance(day,int))
# ------------------------------------------------------------------------
# At GMT noon: this is done with purely integer arithmetic
# ------------------------------------------------------------------------
    JD = + 367 * yea \
         - 7*(yea + (mon + 9)/12)/4 \
         - 3*((yea + (mon - 9)/7)/100 + 1)/4 \
         + 275*mon/9 + day + 1721029
# ------------------------------------------------------------------------
# trying to get more accuracy by calculating seconds
# ------------------------------------------------------------------------
    JD = float(JD + sec/86400.0)
# ------------------------------------------------------------------------
# Obtains tee,
# ------------------------------------------------------------------------
    tee = float(JD - 2451545.0) ;
# ------------------------------------------------------------------------
# other variables
# ------------------------------------------------------------------------
    GS = 0.993126 + 0.00273777850 * tee  # mean anomaly, Sun
    (GS,ipart) = modf(GS)
# ------------------------------------------------------------------------
# converts to radians
# ------------------------------------------------------------------------
    GS = GS * TwoPi
    return(GS)
```

7.2 – The declination of the Sun seen from the Earth

Figure 7.4 shows the incidence of the Sun's rays seen from the Earth. The plane of the Equator is Oxy, and Oyz is perpendicular to the plane of the Ecliptic, which is not shown, but contains the line OS connecting the center of the Earth to the center of the Sun: the Sun's declination δ is the angle between the planes of the Ecliptic and the Equator, and is indicated in the figure. Because the Sun is very far away, all rays can be assumed to be parallel. At point P on the surface of the Earth, a ray comes along PS′, and the Sun is effectively seen as in position S′. The position of P is given by the *hour angle* h, which is the angular distance to the solar noon, and the latitude φ.

The vertical through P is given by the unit vector $\boldsymbol{n}$, and the direction towards the Sun at P is given by the unit vector $\boldsymbol{m}$. By definition, the Zenith angle Z is the angle between $\boldsymbol{m}$ and $\boldsymbol{n}$. From figure 7.4, one obtains

$$\boldsymbol{m} = (0, \cos\delta, \sin\delta), \tag{7.1}$$

$$\boldsymbol{n} = (\cos\varphi \sin h, \cos\varphi \cos h, \sin\varphi), \tag{7.2}$$

whence

$$\boldsymbol{m} \cdot \boldsymbol{n} = \cos Z = \cos\delta \cos\varphi \cos h + \sin\delta \sin\varphi. \tag{7.3}$$

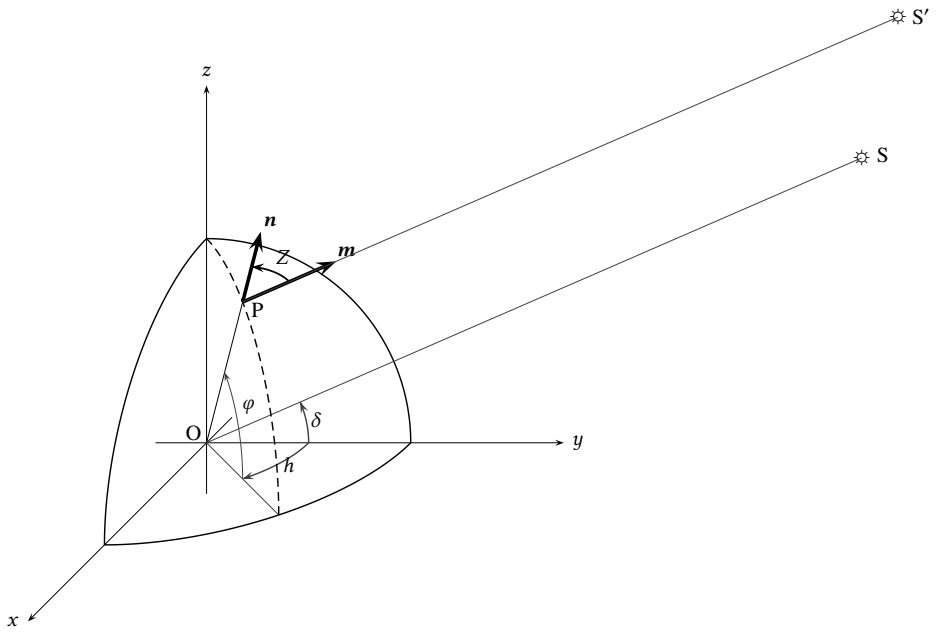

Figure 7.4: The declination of the Sun.

Several useful relationships can be derived with the help of (7.3):

a) The angle H covered between sunrise, when $\boldsymbol{n} \parallel Oxz$ and $\cos Z = 0$, and the solar noon is given by

$$\begin{aligned} 0 &= \cos\delta\cos\varphi\cos H + \sin\delta\sin\varphi \;\Rightarrow \\ \cos H &= -\operatorname{tg}\varphi\operatorname{tg}\delta. \end{aligned} \tag{7.4}$$

From (7.4) one obtains the length of daylight in hours, N:

$$\frac{H}{\pi/2} = \frac{N}{12} \qquad \Rightarrow \qquad N = \frac{24H}{\pi}. \tag{7.5}$$

b) The latitude φ_p of the polar night is the point where $H = 0$:

$$\operatorname{tg}\varphi_p = -\operatorname{cotg}\delta \qquad \Rightarrow \qquad \varphi_p = \frac{\pi}{2} - \delta. \tag{7.6}$$

c) At the poles,

$$\cos Z = \sin\delta \qquad \Rightarrow \qquad \frac{\pi}{2} - Z = \delta,$$

so that the Sun's elevation is practically constant during the day.

d) At solar noon,

$$\begin{aligned} \cos h &= 1, \\ \cos Z &= \cos\delta\cos\varphi + \sin\delta\sin\varphi \\ &= \cos(\varphi - \delta) \;\Rightarrow \\ Z &= \varphi - \delta. \end{aligned} \tag{7.7}$$

7.3 – Radiaton

The flux of energy per unit area associated with different wavelengths is called *irradiance*, and given in units of W m^{-2} in the SI. The wavelength of the radiation depends on the temperature of the emitting body; at temperature T, a black body emits a spectrum of radiation whose peak is given by Wien's law,

$$\lambda_m = \frac{\alpha}{T}, \tag{7.8}$$

where $\alpha = 2897.0\,\mu\text{m K}$ (Fleagle and Businger, 1980, p. 217).

Solar radiation, emmited by the Sun at a temperature close to 6 000 K, covers a range of wavelengths $\lambda \sim 0.3$–$3\,\mu m$, and reaches the top of the atmosphere of the Earth. The *solar constant* $R_{s0} \approx 1354\,\text{W m}^{-2}$ is the irradiance in the direction of the Sun's rays at a distance of $1\,\text{AU} = r_a$ of the Sun. The irradiance on a direction perpendicular to the top of the Atmosphere at a given day and latitude is the *extra-atmospheric solar irradiance*, and is given by

$$R_{sea} = R_{s0}\left(\frac{r_a}{r}\right)^2 \cos Z. \tag{7.9}$$

The mean value of R_{sea} over 24 hours is a useful quantity, that can later be used to estimate the solar irradiance reaching the surface of the Earth.

$$\begin{aligned} R_{sea}(t) &= R_{s0}\left(\frac{r_a}{r}\right)^2 \left[\sin\delta\sin\varphi + \cos\delta\cos\varphi\cos h(t)\right]; \\ \langle R_{sea}\rangle &= \frac{1}{D}\int_0^T R_{sea}(t)\,\mathrm{d}t, \end{aligned} \tag{7.10}$$

where $D = 86400\,\text{s}$ is the duration of the day, and T is the duration of sunlight, with time t measured from sunrise to sunset. But

$$D = \frac{2\pi}{\omega}, \tag{7.11}$$

$$\omega \mathrm{d}t = \mathrm{d}h, \tag{7.12}$$

where ω is the angular velocity of Earth, whence

$$\begin{aligned} \langle R_{sea}\rangle &= \int_{-H}^{+H} \frac{\omega}{2\pi} R_{s0}\left(\frac{r_a}{r}\right)^2 \left[\sin\delta\sin\varphi + \cos\delta\cos\varphi\cos h(t)\right] \frac{\mathrm{d}h}{\omega} \\ &= \left(\frac{r_a}{r}\right)^2 \frac{R_{s0}}{\pi}\left[H\sin\delta\sin\varphi + \cos\delta\cos\varphi\sin H\right]. \end{aligned} \tag{7.13}$$

The solar or *short wave* irradiance R_s reaching the surface of the Earth is most of the time less than R_{sea}. Ideally, it should be measured directly with *piranometers*, but historically it has been estimated by measurements of *bright sunshine duration* n (usually in hours), through Prescott's equation (Brutsaert, 1982):

$$\langle R_s\rangle = \langle R_{sea}\rangle \left[a + b\frac{n}{N}\right], \tag{7.14}$$

with $a \sim 0.25$ and $b \sim 0.50$. Note that Prescott's equation is not able to predict values of R_s at a timescale of ~ 1 h, only at the 24-hour mean, because the duration of bright sunshine is an integrated measurement.

Besides solar radiation, the surface of the Earth also receives radiation emmited by the atmosphere, over wavelengths $\lambda \sim 3$–$100\,\mu m$, due to the fact that the emmiting sources are at temperatures of the order of 300 K. This *longwave* or *atmospheric* irradiance reaching the surface is R_a. Finally, the surface itself re-emits radiation back to the atmosphere; this is the emitted irradiance R_e.

The ratio of the reflected to the incoming solar irradiance is the *albedo* α of the surface; and the ratio of the absorbed to the incoming atmospheric irradiance is the *absortivity/emissivity* ϵ of the surface. The *net* irradiance is the total energy flux per unit area absorbed the the surface:

$$R_n = R_s(1 - \alpha) + \epsilon R_a - R_e. \tag{7.15}$$

7.4 – Atmospheric radiation

The estimation of incoming atmospheric (longwave) irradiance is a complicated business. It is usually split into two parts: the estimation of clear-sky atmospheric irradiance, R_{ac}, and the estimation of the increase due to the presence of clouds. Clear-sky atmospheric irradiance is usually obtained from equations with the form

$$R_{ac} = \epsilon_{ac}\sigma T_a^4. \tag{7.16}$$

(7.16) is obviously inspired by Stefan-Boltzmann's law for a gray body. It appears to have had a strictly empirical origin in the work of Brunt (1932), in the form

$$\epsilon_{ac} = 0.52 + 0.0065\sqrt{e_a} \tag{7.17}$$

(in SI units), but can be obtained from equations for radiative transfer in the atmosphere under certain simplifying assumptions. Perhaps the clearest, and one of the simplest, ways to derive it can be found in Brutsaert (1975). In principle, the longwave radiation reaching the surface can be found by integrating Schwarzchild's equation

$$\mathrm{d}I_\lambda = -k_\lambda(I_\lambda - B_\lambda(T)), \tag{7.18}$$

but an alternative that yields a faster analytical result is

$$R_{ac} = \int_0^\infty \sigma T^4 \frac{\mathrm{d}\epsilon_f}{\mathrm{d}u}\mathrm{d}u. \tag{7.19}$$

Consider now an exponential distribution for the temperature in the atmosphere,

$$T(z) = T_0 \exp\left(-\frac{\gamma z}{T_0}\right) \tag{7.20}$$

with $\gamma = 6.5\,\mathrm{K\,km^{-1}}$ and $T_0 = 288.15\,\mathrm{K}$. To a first approximation,

$$\frac{\mathrm{d}T}{\mathrm{d}z} = -\gamma, \tag{7.21}$$

so that

$$p = \rho R_d T, \tag{7.22}$$

$$\mathrm{d}p = -\rho g \mathrm{d}z, \tag{7.23}$$

$$\frac{\mathrm{d}p}{p} = \frac{g}{R_d T}\mathrm{d}z = \frac{g}{\gamma R_d}\frac{\mathrm{d}T}{T}, \tag{7.24}$$

$$\frac{p}{p_0} = \left(\frac{T}{T_0}\right)^{\frac{g}{\gamma R_d}}. \tag{7.25}$$

For water vapor,

$$\begin{aligned} e_0 &= \rho_{v0} R_v T, \\ \rho_{v0} &= \frac{e_0}{R_v T_0}, \\ \rho_v(z) &= \rho_{v0} \exp(-k_w z), \end{aligned} \tag{7.26}$$

with $k_w = 4.4 \times 10^{-4}\,\mathrm{m}^{-1}$. In Brutsaert (1975), the effective emissivity ϵ_f is written as a function of optical path

$$u = \int_0^z \rho_v(\zeta) \left(\frac{p}{p_0}\right)^{1/2} \mathrm{d}\zeta \tag{7.27}$$

as

$$\epsilon_f = A a^m, \tag{7.28}$$

with $A = 0.75$, $m = 1/7$ and

$$a = \frac{u}{\rho_w} \tag{7.29}$$

in cm of equivalent water (with $\rho_w = 1\,\mathrm{g\,cm}^{-3}$). It seems preferable, however, to use a version in which dimensionless factors appear more clearly. Therefore, let us put

$$\epsilon_f = \left(\frac{u}{u_0}\right)^m. \tag{7.30}$$

Then, equating (7.30) to (7.28) with (7.29),

$$u_0 = (0.75)^{-1/7} = 7.491541\,\mathrm{g\,cm}^{-2} = 74.91541\,\mathrm{kg\,m}^{-2}. \tag{7.31}$$

Differentiating (7.30),

$$\frac{\mathrm{d}\epsilon_f}{\mathrm{d}u} = \frac{m}{u_0}\left(\frac{u}{u_0}\right)^{m-1}. \tag{7.32}$$

With (7.32) and (7.19)–(7.20):

$$\begin{aligned} R_{ac} &= \int_{u=0}^{\infty} \sigma \left(T_0 \mathrm{e}^{-\gamma z/T_0}\right)^4 \frac{m}{u_0}\left(\frac{u}{u_0}\right)^{m-1} \mathrm{d}u \\ &= \int_{z=0}^{\infty} \sigma T_0^4 \mathrm{e}^{-4\gamma z/T_0} \frac{m}{u_0}\left(\frac{1}{u_0}\int_{\zeta=0}^{z} \rho_{v0}\left(\frac{p}{p_0}\right)^{1/2} \mathrm{d}\zeta\right)^{m-1} \rho_v \left(\frac{p}{p_0}\right)^{1/2} \mathrm{d}z. \end{aligned} \tag{7.33}$$

Now, with (7.20), (7.25) and (7.26):

$$\begin{aligned}
R_{ac} &= \int_{z=0}^{\infty} \sigma T_0^4 \mathrm{e}^{-4\gamma z/T_0} \frac{m}{u_0} \left(\frac{1}{u_0} \int_{\zeta=0}^{z} \rho_{v0} \mathrm{e}^{-k_w \zeta} \left(\frac{T}{T_0} \right)^{g/(2\gamma R_d)} \mathrm{d}\zeta \right)^{m-1} \rho_{v0} \mathrm{e}^{-k_w z} \left(\frac{T}{T_0} \right)^{g/(2\gamma R_d)} \mathrm{d}z \\
&= \int_{z=0}^{\infty} \sigma T_0^4 \mathrm{e}^{-4\gamma z/T_0} \frac{m}{u_0} \left(\frac{1}{u_0} \int_{\zeta=0}^{z} \rho_{v0} \mathrm{e}^{-\left(k_w + \frac{g}{2R_d T_0}\right)\zeta} \mathrm{d}\zeta \right)^{m-1} \rho_{v0} \mathrm{e}^{-\left(k_w + \frac{g}{2R_d T_0}\right) z} \mathrm{d}z \\
&= m \left(\frac{\rho_{v0}}{u_0} \right)^m \sigma T_0^4 \int_{z=0}^{\infty} \mathrm{e}^{-\left(\frac{4\gamma}{T_0} + k_w + \frac{g}{2R_d T_0}\right) z} \left(\int_{\zeta=0}^{z} \mathrm{e}^{-\left(k_w + \frac{g}{2R_d T_0}\right)\zeta} \mathrm{d}\zeta \right)^{m-1} \mathrm{d}z.
\end{aligned} \tag{7.34}$$

In order to simplify notation a little bit, let

$$k_1 = \frac{4\gamma}{T_0} + k_2, \tag{7.35}$$

$$k_2 = k_w + \frac{g}{2R_d T_0}; \tag{7.36}$$

then,

$$\begin{aligned}
R_{ac} &= m \left(\frac{\rho_{v0}}{u_0} \right)^m \sigma T_0^4 \int_{z=0}^{\infty} \mathrm{e}^{-k_1 z} \left(\int_{\zeta=0}^{z} \mathrm{e}^{-k_2 \zeta} \mathrm{d}\zeta \right)^{m-1} \mathrm{d}z \\
&= m \left(\frac{\rho_{v0}}{u_0 k_2} \right)^m \sigma T_0^4 \int_{z=0}^{\infty} \mathrm{e}^{-k_1 z} \left(1 - \mathrm{e}^{-k_2 z} \right)^{m-1} k_2 \, \mathrm{d}z.
\end{aligned} \tag{7.37}$$

Now introduce the change of variables

$$t = \mathrm{e}^{-k_2 z}, \tag{7.38}$$

$$\mathrm{d}t = -k_2 \mathrm{e}^{-k_2 z} \mathrm{d}z, \tag{7.39}$$

to obtain

$$\begin{aligned}
R_{ac} &= m \left(\frac{\rho_{v0}}{u_0 k_2} \right)^m \sigma T_0^4 \int_{z=\infty}^{0} \left(\mathrm{e}^{-k_2 z} \right)^{\frac{k_1}{k_2} - 1} \left(1 - \mathrm{e}^{-k_2 z} \right)^{m-1} k_2 \left(-\mathrm{e}^{-k_2 z} \right) \mathrm{d}z \\
&= m \left(\frac{\rho_{v0}}{u_0 k_2} \right)^m \sigma T_0^4 \int_{t=0}^{1} t^{\frac{k_1}{k_2} - 1} (1 - t)^{m-1} \, \mathrm{d}t \qquad (7.40) \\
&= \underbrace{\left[m \left(\frac{e_0}{u_0 k_2 R_v T_0} \right)^m B\left(\frac{k_1}{k_2}, m \right) \right]}_{\epsilon_{ac}} \sigma T_0^4. \qquad (7.41)
\end{aligned}$$

In SI units, Brutsaert's equation is

$$\epsilon_{ac} = 0.64 \left(\frac{e_a}{T_a} \right)^{1/7}. \tag{7.42}$$

Table 7.2: Cloudy-sky parameterisations

Parameterization	Experimental site
Jacobs (1978): $R_a = (1 + 0.26c)R_{ac}$	Baffin Island (Canada)

7.5 – Cloudiness effect on atmospheric irradiance

Atmospheric irradiance increases in the presence of clouds. A way to account for that is to write

$$R_a = \phi R_{ac}, \tag{7.43}$$

where ϕ is some function of the cloud cover. Bolz's equation, in terms of cloudiness, is

$$\phi = 1 + 0.22c^2 \tag{7.44}$$

where c is cloud cover, between 0 and 1, as reported in manually operated weather stations in *oktas*, or eights of sky clovered by clouds Wikipedia (2019). If c is not available, a surrogate is

$$c = 1 - n/N, \tag{7.45}$$

where n and N have been defined above. Again, (7.45) can only be used with (7.44) to derive daily averages of R_a.

More recent equations have been developed to estimate ϕ, and are shown in table 7.2, obtained from Duarte et al. (2006)

8

Turbulent diffusion

8.1 – Scales in turbulence

In a turbulent flow, it is not always clear what is meant by a "particle". There is a wealth of scales in fully developed turbulent flows, and a way to manage this wide range of scales is to define a few that differ significantly in their sizes. The *integral scale* is defined mathematically in terms of the autocorrelation function $\varrho(x)$ (usually of the longitudinal velocity component):

$$\ell = \int_0^\infty \varrho(x)\,\mathrm{d}x.$$

Taylor's microscale λ is defined in terms of the curvature of $\varrho(x)$ at the origin:

$$-\frac{2}{\lambda} \equiv \left.\frac{\mathrm{d}^2\rho}{\mathrm{d}x^2}\right|_{x=0}.$$

Finally, we have Kolmogorov's microscale:

$$\eta = (\nu^3/\epsilon)^{1/4}.$$

The classical particles of Fluid Mechanics have to be of size η or smaller: they can only "see" molecular diffusion, and smooth fields around them. On the other hand, "particles" of size λ "see" turbulent diffusion, and a considerably more agitated world around them.

8.2 – Turbulent diffusivity

Let us now define "turbulent diffusivity". If F is the turbulent flux of a scalar whose concentration is c, its turbulent diffusivity K at a point is *defined* as

$$F \equiv -\overline{\rho} K \frac{\mathrm{d}\overline{c}}{\mathrm{d}z}.$$

The overbars on the variables indicate Reynolds (1895) averages. Usually turbulent diffusivity is *modelled* with simple dimensional arguments, such as

$$K = c\sigma_w \ell,$$

where σ_w is a velocity scale (for instance, in this case we are thinking of the standard deviation of vertical velocity). The turbulent flux itself is usually defined by means of Reeynolds averages:

$$F = \overline{\rho w c} \approx \overline{\rho}\,\overline{w'c'},$$

as long as c is a mass concentration.

8.3 – Turbulent diffusion theory

Let us proceed to Taylor (1921)' s turbulent diffusion theory. We do it by following a particle (in Kolmogorov's sense) using a *Lagrangian* description of the flow:

$$Z(t) = Z(0) + \int_0^t W(t')\,\mathrm{d}t'. \tag{8.1}$$

Without loss of generality, assume $Z(0) \equiv 0$ (always), and

$$\overline{Z(t)} = 0. \tag{8.2}$$

Our averages now need also to be considered from a Lagrangian point of view, as averages over a large number of particles. If $Z_i(t)$ is the position of the $i^{\underline{\text{th}}}$ particle and we are emitting a large number N of particles,

$$\overline{Z(t)} = \frac{1}{N}\sum_{i=1}^{N} Z_i(t).$$

Consider now the mean square deviation of $Z(t)$ with respect to the origin. Clearly, this is a measure of how the particles will "disperse" around it. We are interested in the quantities

$$\overline{Z^2(t)}, \qquad \frac{\mathrm{d}}{\mathrm{d}t}\left[\overline{Z^2(t)}\right].$$

Proceeding,

$$\frac{\mathrm{d}}{\mathrm{d}t}\left[\overline{Z^2(t)}\right] = 2\overline{Z(t)\frac{\mathrm{d}Z}{\mathrm{d}t}}.$$

But

$$W(t) = \frac{\mathrm{d}Z}{\mathrm{d}t}; \tag{8.3}$$

Therefore,

$$\begin{aligned}\frac{\mathrm{d}}{\mathrm{d}t}\left[\overline{Z^2(t)}\right] &= 2\overline{Z(t)W(t)} \\ &= 2\overline{\left[\int_{t'=0}^{t} W(t')\,\mathrm{d}t'\right]W(t)} \\ &= 2\int_0^t \overline{W(t')W(t)}\,\mathrm{d}t'.\end{aligned}$$

Now if $W(t)$ is a *stationary* stochastic process,

$$\begin{aligned}&\overline{W(t')W(t)} = \overline{W(0)W(t-t')} \Rightarrow \\ &\frac{\mathrm{d}}{\mathrm{d}t}\left[\overline{Z^2(t)}\right] = 2\int_0^t \overline{W(0)W(t-t')}\,\mathrm{d}t'.\end{aligned}$$

To proceed further, we define the *Lagrangian autocorrelation function*,

$$\varrho_L(\tau) \equiv \frac{1}{\overline{W^2}}\overline{W(t)W(t+\tau)},$$

where we are assuming that $\overline{W^2}$, differently from $\overline{Z^2(t)}$, does not depend on t (which is the stationarity hypothesis for $W(t)$). With that,

$$\frac{\mathrm{d}}{\mathrm{d}t}\left[\overline{Z^2(t)}\right] = 2\overline{W^2}\int_0^t \varrho_L(\tau)\,\mathrm{d}\tau;$$
$$\overline{Z^2(t)} = 2\overline{W^2}\int_0^t\int_0^{t'} \varrho_L(\tau)\,\mathrm{d}\tau\mathrm{d}t'.$$

We now integrate by parts:

$$f(t') \equiv \int_0^{t'} \varrho_L(\tau)\,\mathrm{d}\tau;$$
$$\int_0^t f(t')\,\mathrm{d}t' = t'f(t')\Big|_0^t - \int_0^t t'\varrho_L(t')\,\mathrm{d}t';\Rightarrow$$
$$\overline{Z^2(t)} = 2\overline{W^2}\left[t\int_0^t \varrho_L(t')\,\mathrm{d}t' - \int_0^t t'\varrho_L(t')\,\mathrm{d}t'\right]$$
$$= 2\overline{W^2}t\int_0^t \left(1-\frac{t'}{t}\right)\varrho_L(t')\,\mathrm{d}t'. \tag{8.4}$$

At this point, we want to introduce the *Lagrangian integral scale*:

$$\mathscr{T}_L \equiv \int_0^\infty \varrho_L(\tau)\,\mathrm{d}\tau, \tag{8.5}$$

but does it exist? The safest bet seems to be to assume that $\varrho_L(t)$ belongs to the space L_1; this means to assume that

$$\int_0^\infty |\varrho_L(t)|\,\mathrm{d}t < \infty. \tag{8.6}$$

Assuming (8.6) ensures that $\mathscr{T}_L$ in (8.5) exists. We now change variables to

$$\tau = \frac{t'}{\mathscr{T}_L}, \tag{8.7}$$
$$\tau_L = \frac{t}{\mathscr{T}_L}, \tag{8.8}$$
$$\varrho_L^*(\tau) \equiv \varrho_L(\tau\mathscr{T}_L), \tag{8.9}$$

so that (8.4) becomes

$$\overline{Z^2(t)} = 2\overline{W^2(t)}\mathscr{T}_L t\int_{\tau=0}^{\tau_L}\left(1-\frac{\tau}{\tau_L}\right)\varrho_L^*(\tau)\,\mathrm{d}\tau. \tag{8.10}$$

Proceed with an *asymptotic analysis*: suppose that $\tau_L \ll 1$; then, there isn't enough "time" for $\varrho_L^*(\tau)$ to decrease very much from 1, and

$$\varrho_L(\tau) \approx 1 \;\Rightarrow$$
$$\overline{Z^2(t)} \approx 2\overline{W^2(t)}\mathscr{T}_L t\int_0^{\tau_L}(1-\frac{\tau}{\tau_L})\,\mathrm{d}\tau$$
$$= 2\overline{W^2(t)}\mathscr{T}_L t\times\frac{1}{2}\tau_L$$
$$= \overline{W^2}t^2\,\blacksquare \tag{8.11}$$

Consider now the case $\tau_L \gg 1$. The objective is to obtain a suitable approximation for the integral in (8.10). First, note that if (8.6) holds, then obviously

$$\int_0^\infty |\varrho_L^*(\tau)|\,\mathrm{d}\tau < \infty. \tag{8.12}$$

Next, a standard interpretation in stochastic processes is that under reasonable assumptions such as stationarity and ergodicity, a process becomes effectively decorrelated from itself in two integral time scales (Tennekes and Lumley, 1972, p. 213–214). This means that it is reasonable to expect ϱ_L^* to decrease to zero relatively fast from $\tau_L = 1$ onwards.

In the literature, in obtaining an approximation for (8.10), this is not always discussed at length. Pope (2000)'s presentation of this subject can be found in Chapter 12, p. 498–499, but there is no deep justification for his equation (12.154). Monin and Yaglom (1971) (Ch. 5, p. 543–544) do better. We quote from them:

> Let us now make the natural assumption that the Lagrangian correlation function $R_{ii}^{(L)}(s)$ approaches zero when $s \to \infty$, *and so rapidly that the following correlation time will exist* (...)

There is also some justification in Tennekes and Lumley (1972) (Ch. 6, Eqs. (6.4.11–6.4.12)). It is clear that Taylor's expression for large times (which we will obtain soon) is by no means only a mathematical derivation, but rather a result that requires "reasonable" assumptions that cannot be proved *a priori*.

Therefore, to proceed, *some* additional assumption is needed on $\varrho_L^*(\tau)$. From the foregoing discussion, an assumption as good as any is that there exists $g(\tau) = \tau^{-m}$ with $m > 1$ and such that $|\varrho_L^*(\tau)| \le g(\tau)$, $\tau \ge 1$ (note that $|\varrho_L^*(\tau)| \le 1$ always). Then, for $\tau_L \gg 1$,

$$\begin{aligned}\overline{Z^2(t)} &\approx \lim_{\tau_L\to\infty} 2\overline{W^2(t)}\mathscr{T}_L t \int_0^{\tau_L}\left(1-\frac{\tau}{\tau_L}\right)\varrho_L^*(\tau)\,\mathrm{d}\tau \\ &= 2\overline{W^2(t)}\mathscr{T}_L t\left[\int_0^\infty \varrho_L^*(\tau)\,\mathrm{d}\tau - \lim_{\tau_L\to\infty}\int_0^{\tau_L}\frac{\tau}{\tau_L}\varrho_L^*(\tau)\,\mathrm{d}\tau\right]\end{aligned} \tag{8.13}$$

The first integral in the brackets is equal to 1; for the second, we split the integration interval beteween $\tau \in [0,1)$ and $\tau \in [1,\infty)$. We have

$$\lim_{\tau_L\to\infty}\int_0^1 \frac{\tau}{\tau_L}\varrho_L^*(\tau)\,\mathrm{d}\tau = 0 \tag{8.14}$$

and

$$\begin{aligned}\left|\lim_{\tau_L\to\infty}\int_1^{\tau_L}\frac{\tau}{\tau_L}\varrho_L^*(\tau)\,\mathrm{d}\tau\right| &\le \lim_{\tau_L\to\infty}\int_1^{\tau_L}\left|\frac{\tau}{\tau_L}\varrho_L^*(\tau)\right|\mathrm{d}\tau \\ &\le \lim_{\tau_L\to\infty}\frac{1}{\tau_L}\int_1^{\tau_L}\tau g(\tau)\,\mathrm{d}\tau \\ &= \lim_{\tau_L\to\infty}\frac{1}{\tau_L}\int_1^{\tau_L}\tau^{-m+1}\,\mathrm{d}\tau.\end{aligned} \tag{8.15}$$

For $m \neq 2$,

$$\lim_{\tau_L\to\infty} \frac{1}{\tau_L}\int_1^{\tau_L} \tau^{-m+1}\,\mathrm{d}\tau = \lim_{\tau_L\to\infty} \frac{1}{\tau_L}\left[\frac{1}{-m+2}\tau^{-m+2}\right]_1^{\tau_L}$$
$$= \lim_{\tau_L\to\infty} \frac{1}{(-m+2)}\frac{1}{\tau_L}\left[\tau_L^{-m+2}-1\right] = 0. \tag{8.16}$$

For $m = 2$,

$$\lim_{\tau_L\to\infty} \frac{1}{\tau_L}\int_1^{\tau_L} \tau^{-m+1}\,\mathrm{d}\tau = \lim_{\tau_L\to\infty} \frac{1}{\tau_L}\Big[\ln(\tau)\Big]_1^{\tau_L}$$
$$= \lim_{\tau_L\to\infty} \frac{1}{\tau_L}\ln(\tau_L) = 0. \tag{8.17}$$

Together, (8.13)–(8.17) give

$$\lim_{\tau_L\to\infty} \int_0^{\tau_L} \frac{\tau}{\tau_L}\varrho_L^*(\tau)\,\mathrm{d}\tau = 0 \tag{8.18}$$

and the desired expression for $\overline{Z^2(t)}$ for $\tau_L \gg 1$ is

$$\overline{Z^2(t)} \approx 2\overline{W^2(t)}\mathscr{T}_L t. \tag{8.19}$$

In short, our results for the root mean square values of $Z(t)$ are

$$Z^{\mathrm{rms}} = W^{\mathrm{rms}} t, \qquad t \ll \mathscr{T}_L; \tag{8.20}$$
$$Z^{\mathrm{rms}} = W^{\mathrm{rms}}\sqrt{2\mathscr{T}_L t}, \qquad t \gg \mathscr{T}_L. \tag{8.21}$$

8.4 – The lagrangian concentration field

Let us change focus to the path of the Lagrangian particles. Each particle has a function of position in the form

$$\boldsymbol{x} = \boldsymbol{X}(\boldsymbol{\xi}, t),$$

where ξ is the position of the particle at $t = 0$, so that

$$\boldsymbol{\xi} = \boldsymbol{X}(\boldsymbol{\xi}, 0).$$

Therefore, at $t = 0$, $\boldsymbol{X}$ is the identity. In the absence of diffusion, the transport equation for a scalar whose concentration is c is

$$\frac{\mathrm{D}c}{\mathrm{D}t} = \frac{\partial c}{\partial t} + \sum_{i=1}^{3} u_i \frac{\partial c}{\partial x_i} = 0,$$

with solution

$$c(\boldsymbol{X}(\boldsymbol{\xi}, t), t) = c(\boldsymbol{\xi}, 0).$$

We need to introduce the probability density function (pdf) $f_c(\boldsymbol{x}, t|\boldsymbol{\xi})$, which givens the probability density that, starting from $\boldsymbol{\xi}$ at $t = 0$, a particle reach $\boldsymbol{x}$ at time t. The expected value of the concentration in $(\boldsymbol{x}, t)$ is

$$\overline{c}(\boldsymbol{x}, t) = \int_{\boldsymbol{\xi}\in\mathbb{R}^3} c(\boldsymbol{\xi}, 0) f_c(\boldsymbol{x}, t|\boldsymbol{\xi})\mathrm{d}^3\boldsymbol{\xi}.$$

In particular, if all mass M of the scalar is concentrated at $\boldsymbol{\xi} = 0$,

$$\begin{aligned} c(\boldsymbol{\xi}, 0) &= \frac{M}{A}\delta(\boldsymbol{\xi}); \\ \overline{c}(\boldsymbol{x}, t) &= \int_{\boldsymbol{\xi}\in\mathbb{R}^3} \frac{M}{A}\delta(\boldsymbol{\xi}) f_c(\boldsymbol{x}, t|\boldsymbol{\xi}) \mathrm{d}^3\boldsymbol{\xi} \\ &= \frac{M}{A} f_c(\boldsymbol{x}, t|0). \end{aligned}$$

In one dimension, we just saw (8.1). Let us interpret (8.1) with the help of the Central Limit Theorem for an integral (Tennekes and Lumley, 1972, Sec. 6.5). We will take $Z(t)$ to be a random variable produced by the "sum" of a large number of random variables $W(t')\,\mathrm{d}t'$: the Central Limit Theorem predicts that $Z(t)$ is normally distributed. Since we know that its mean is $\overline{Z(t)} = 0$ (*c.f.* (8.1)) and the standard deviation can be obtained from (8.20)–(8.21), we just use the large-time limit for Z^{rms} and obtain

$$Z^{\mathrm{rms}} = \sigma_Z = \sigma_w\sqrt{2\mathscr{T}_L t}. \tag{8.22}$$

Then, we immediately find that

$$\overline{c}(z, t) = \frac{M}{A\sqrt{2\pi}\sigma_Z} \exp\left[-\frac{z^2}{2\sigma_Z^2}\right]. \tag{8.23}$$

This can be readily generalized to three dimensions:

$$\overline{c}(x, y, z, t) = \frac{M}{(2\pi)^{3/2}\sigma_X\sigma_Y\sigma_Z} \exp\left[-\frac{x^2}{2\sigma_X^2}\right] \exp\left[-\frac{y^2}{2\sigma_Y^2}\right] \exp\left[-\frac{z^2}{2\sigma_Z^2}\right]. \tag{8.24}$$

8.5 – The eulerian concentration field

8.5.1 – One-dimensional solution of the diffusion equation

The same problem can be approached from the eulerian point of view, as the solution to the *diffusion equation*

$$\frac{\partial\overline{c}}{\partial t} = K_{zz}\frac{\partial^2\overline{c}}{\partial z^2}; \qquad c(z, 0) = \frac{M}{A}\delta(z); \qquad \lim_{z\to\pm\infty}\overline{c}(z, t) = 0, \tag{8.25}$$

which is (Dias, 2017, Example 15.6)

$$\overline{c}(z, t) = \frac{M}{A\sqrt{4K_{zz}\pi t}} \exp\left[-\frac{z^2}{4K_{zz}t}\right]. \tag{8.26}$$

Note that formally it is the same as the lagrangian solution! By equating (8.23) and (8.26), we immediately obtain

$$2\sigma_Z^2 = 4K_{zz}t, \tag{8.27}$$

$$4\overline{W^2}\,\mathscr{T}_L t = 4K_{zz}t \tag{8.28}$$

$$K_{zz} = \overline{W^2}\,\mathscr{T}_L \;\blacksquare \tag{8.29}$$

8.5.2 – Two- and three-dimensional solutions of the diffusion equation

The generalization of (8.25) to 3 dimensions is

$$\frac{\partial \overline{c}}{\partial t} = K_{xx}\frac{\partial^2 \overline{c}}{\partial x^2} + K_{yy}\frac{\partial^2 \overline{c}}{\partial y^2} + K_{zz}\frac{\partial^2 \overline{c}}{\partial z^2}; \tag{8.30}$$

$$c(z,0) = M\delta(x)\delta(y)\delta(z); \tag{8.31}$$

$$\lim_{x,y,z\to\pm\infty} \overline{c}(x,y,z,t) = 0, \tag{8.32}$$

Let us try a solution by means of separation of variables, of the type

$$c(x,y,z,t) = X(x,t)Y(y,t)Z(z,t); \tag{8.33}$$

substitution in (8.30) produces

$$YZ\frac{\partial X}{\partial t} + XZ\frac{\partial Y}{\partial t} + XY\frac{\partial Z}{\partial t} = YZK_{xx}\frac{\partial^2 X}{\partial x^2} + XZK_{yy}\frac{\partial^2 Y}{\partial y^2} + XYK_{zz}\frac{\partial^2 Z}{\partial z^2};$$

$$X(x,0)Y(y,0)Z(z,0) = M\delta(x)\delta(y)\delta(z),$$

$$X(\pm\infty,t)Y(\pm\infty,t)Z(\pm\infty,t) = 0.$$

This immediately yields 3 separate problems:

$$\frac{\partial X}{\partial t} = K_{xx}\frac{\partial^2 X}{\partial x^2}; \qquad X(x,0) = M^{1/3}\delta(x); \qquad X(\pm\infty) = 0; \tag{8.34}$$

$$\frac{\partial Y}{\partial t} = K_{yy}\frac{\partial^2 Y}{\partial y^2}; \qquad Y(y,0) = M^{1/3}\delta(y); \qquad Y(\pm\infty) = 0; \tag{8.35}$$

$$\frac{\partial Z}{\partial t} = K_{zz}\frac{\partial^2 Z}{\partial z^2}; \qquad Z(z,0) = M^{1/3}\delta(z); \qquad Z(\pm\infty) = 0. \tag{8.36}$$

Note that each one of (8.34)–(8.62) is the same as (8.25); therefore,

$$\begin{aligned} c(x,y,z,t) &= \frac{M^{1/3}}{\sqrt{4K_{xx}\pi t}}\exp\left[-\frac{x^2}{4K_{xx}t}\right] \\ &\times \frac{M^{1/3}}{\sqrt{4K_{yy}\pi t}}\exp\left[-\frac{y^2}{4K_{yy}t}\right] \\ &\times \frac{M^{1/3}}{\sqrt{4K_{zz}\pi t}}\exp\left[-\frac{z^2}{4K_{zz}t}\right] \\ &= \frac{M}{8(\pi t)^{3/2}(K_{xx}K_{yy}K_{zz})^{1/2}}\exp\left[-\frac{x^2}{4K_{xx}t} - \frac{y^2}{4K_{yy}t} - \frac{z^2}{4K_z t}\right]. \end{aligned} \tag{8.37}$$

8.6 – The advection-diffusion case

Let us now modify the diffusion equation and add an advection term. In most cases, it is enough to add advection in the x-direction, *and rotate the mean wind into the x axis*. The equation is

$$\frac{\partial \overline{c}}{\partial t} + \overline{u}\frac{\partial \overline{c}}{\partial x} = K_{xx}\frac{\partial^2 \overline{c}}{\partial x^2},$$

$$\overline{c}(x,0) = \frac{M}{A}\delta(x),$$

where $[\![A]\!] = \mathrm{YZ}$. Podemos tentar "adivinhar a solução" argumentando que, se $\overline{u}$ for constante, no sistema de coordenadas $x' \times t$ com It turns out that we can return to a purely diffusive problem by means of the change of variables

$$\begin{aligned} x' &= x - \overline{u}t, \\ t' &= t. \end{aligned}$$

In the new coordinates, the solution will be

$$\chi(x', t') = \overline{c}(x, t) = \overline{c}(x' + ut', t'). \tag{8.38}$$

Then,

$$\begin{aligned} \frac{\partial \chi}{\partial t'} &= \frac{\partial \overline{c}}{\partial t}\frac{\partial t}{\partial t'} + \frac{\partial \overline{c}}{\partial x}\frac{\partial x}{\partial t'}, \\ &= \frac{\partial \overline{c}}{\partial t} + \overline{u}\frac{\partial \overline{c}}{\partial x}; \\ \frac{\partial \chi}{\partial x'} &= \frac{\partial \overline{c}}{\partial x}\frac{\partial x}{\partial x'} = \frac{\partial \overline{c}}{\partial x}; \\ \frac{\partial^2 \chi}{\partial x'^2} &= \frac{\partial}{\partial x}\left[\frac{\partial \chi}{\partial x'}\right]\frac{\partial x}{\partial x'} = \frac{\partial}{\partial x}\left[\frac{\partial \overline{c}}{\partial x}\right]\frac{\partial x}{\partial x'} = \frac{\partial^2 \overline{c}}{\partial x^2}. \end{aligned}$$

This brings us back to the diffusion equation

$$\begin{aligned} \frac{\partial \overline{\chi}}{\partial t} &= K_{xx}\frac{\partial^2 \overline{\chi}}{\partial x'^2}, \\ \overline{\chi}(x', 0) &= \overline{c}(x, 0) = \frac{M}{A}\delta(x') \end{aligned}$$

with solution

$$\begin{aligned} \overline{\chi}(x', t') &= \frac{M}{A\sqrt{4K_{xx}\pi t'}}\exp\left[-\frac{(x')^2}{4K_{xx}t'}\right]; \Rightarrow \\ \overline{c}(x, t) &= \frac{M}{A\sqrt{4K_{xx}\pi t}}\exp\left[-\frac{(x - \overline{u}t)^2}{4K_{xx}t}\right]. \end{aligned}$$

Can we solve

$$\frac{\partial c}{\partial t} + u\frac{\partial c}{\partial x} = K_{xx}\frac{\partial^2 c}{\partial x^2} + K_{yy}\frac{\partial^2 c}{\partial y^2} + K_{zz}\frac{\partial^2 c}{\partial z^2}, \tag{8.39}$$

$$c(x, y, z, 0) = M\delta(x)\delta(y)\delta(z)? \tag{8.40}$$

Obviously we can. This time the change of variables is

$$x' = x - ut, \tag{8.41}$$

$$y' = y, \tag{8.42}$$

$$z' = z, \tag{8.43}$$

$$t' = t. \tag{8.44}$$

Put, as before,

$$\chi(x', y', z', t') = c(x, y, z, t) = c(x' + ut', y', z', t').$$

Then,

$$\frac{\partial \chi}{\partial t'} = \frac{\partial c}{\partial t}\frac{\partial t}{\partial t'} + \frac{\partial c}{\partial x}\frac{\partial x}{\partial t'} = \frac{\partial c}{\partial t} + u\frac{\partial c}{\partial x}, \tag{8.45}$$

$$\frac{\partial^2 \chi}{\partial x'^2} = \frac{\partial^2 c}{\partial x^2}, \tag{8.46}$$

$$\frac{\partial^2 \chi}{\partial y'^2} = \frac{\partial^2 c}{\partial y^2}, \tag{8.47}$$

$$\frac{\partial^2 \chi}{\partial z'^2} = \frac{\partial^2 c}{\partial z^2}. \tag{8.48}$$

Substituting back, we obtain the purely diffusive equation

$$\frac{\partial \chi}{\partial t} = K_{xx}\frac{\partial^2 \chi}{\partial x^2} + K_{yy}\frac{\partial^2 \chi}{\partial y^2} + K_{zz}\frac{\partial^2 \chi}{\partial z^2}, \tag{8.49}$$

$$\chi(x', y', z', 0) = c(x, z, z, 0) = M\delta(x')\delta(y')\delta(z'). \tag{8.50}$$

On account of (8.37), the solution is

$$c(x, y, z, t) = \frac{M}{8(\pi t)^{3/2}(K_{xx}K_{yy}K_{zz})^{1/2}} \exp\left[-\frac{(x-ut)^2}{4K_{xx}t} - \frac{y^2}{4K_{yy}t} - \frac{z^2}{4K_z t}\right]. \tag{8.51}$$

8.6.1 – Steady-state diffusion problems

Let us build a series of solutions to atmospheric dispersion problems based on the general ideas introduced in the previous sections Our first adaptation will be the *steady* one-dimensional problem

$$\overline{u}\frac{\partial \overline{c}}{\partial x} = K_{zz}\frac{\partial^2 \overline{c}}{\partial z^2}. \tag{8.52}$$

Formally, this is a diffusion equation completely similar to (8.25), but with t replaced by $x/\overline{u}$. Our initial condition now needs to be specified at $x = 0$, and modified to the right physical dimensions. It will be, accordingly, (Kumar and Sharan, 2010, eq. (2.5))

$$\overline{c}(x = 0, z) = \frac{q}{L\overline{u}}\delta(z),$$

with L indicating a length scale in the y direction: $[\![L]\!] = \mathsf{Y}$. The solution for a continuous injection of pollutant mass q ($[\![q]\!] = \mathsf{M}_p\mathsf{T}^{-1}$) is recovered from direct substitution:

$$\begin{aligned}\overline{c}(x, z) &= \frac{q}{L\overline{u}\sqrt{4\pi K_{zz}(x/\overline{u})}} \exp\left[-\frac{\overline{u}}{x}\left(\frac{z^2}{4K_{zz}}\right)\right] \\ &= \frac{q}{L\sqrt{4\pi K_{zz}\overline{u}x}} \exp\left[-\frac{\overline{u}}{x}\left(\frac{z^2}{4K_{zz}}\right)\right].\end{aligned} \tag{8.53}$$

This is a very useful expression for dispersion studies, which are usually made by analyzing 1-hour periods each of which is assumed to be a steady-state problem. Let us now extend this to y and z, in the form

$$\overline{u}\frac{\partial \overline{c}}{\partial x} = K_{yy}\frac{\partial^2 \overline{c}}{\partial y^2} + K_{zz}\frac{\partial^2 \overline{c}}{\partial z^2}, \tag{8.54}$$

$$\overline{c}(x = 0, y, z) = \frac{q}{\overline{u}}\delta(y)\delta(z) \tag{8.55}$$

As before, we try *separation of variables*:

$$\overline{c}(x,y,z) = Y(x,y)Z(x,z), \tag{8.56}$$

which produces:

$$\overline{u}\frac{\partial \overline{c}}{\partial x} = \overline{u}\left[Z\frac{\partial Y}{\partial x} + Y\frac{\partial Z}{\partial x}\right]; \tag{8.57}$$

$$K_{yy}\frac{\partial^2 \overline{c}}{\partial y^2} = ZK_{yy}\frac{\partial^2 Y}{\partial y^2}; \tag{8.58}$$

$$K_{zz}\frac{\partial^2 \overline{c}}{\partial z^2} = YK_{zz}\frac{\partial^2 Y}{\partial y^2}. \tag{8.59}$$

Grouped together, these equations are

$$\overline{u}\left[Z\frac{\partial Y}{\partial x} + Y\frac{\partial Z}{\partial x}\right] = ZK_{yy}\frac{\partial^2 Y}{\partial y^2} + YK_{zz}\frac{\partial^2 Y}{\partial y^2}, \tag{8.60}$$

$$Y(0,y)Z(0,z) = \left[\frac{q}{\overline{u}}\right]^{1/2}\delta(y)\left[\frac{q}{\overline{u}}\right]^{1/2}\delta(z) \tag{8.61}$$

This can quite obviously be dismembered into a pair of problems:

$$\overline{u}\frac{\partial Y}{\partial x} = K_{yy}\frac{\partial^2 Y}{\partial y^2}; \qquad Y(y,0) = \left[\frac{q}{\overline{u}}\right]^{1/2}\delta(y); \qquad Y(\pm\infty) = 0; \tag{8.62}$$

$$\overline{u}\frac{\partial Z}{\partial x} = K_{zz}\frac{\partial^2 Z}{\partial z^2}; \qquad Z(z,0) = \left[\frac{q}{\overline{u}}\right]^{1/2}\delta(z); \qquad Z(\pm\infty) = 0. \tag{8.63}$$

so that now

$$\begin{aligned} c(x,y,z) &= Y(x,y)Z(x,z) \\ &= \left[\frac{q}{\overline{u}}\right]^{1/2}\frac{1}{\sqrt{4\pi K_{yy}(x/\overline{u})}}\exp\left[-\frac{\overline{u}}{x}\left(\frac{y^2}{4K_{yy}}\right)\right] \\ &\times\left[\frac{q}{\overline{u}}\right]^{1/2}\frac{1}{\sqrt{4\pi K_{zz}(x/\overline{u})}}\exp\left[-\frac{\overline{u}}{x}\left(\frac{z^2}{4K_{zz}}\right)\right] \\ &= \frac{q}{4\pi x\sqrt{K_{yy}K_{zz}}}\exp\left[-\frac{\overline{u}}{4x}\left(\frac{y^2}{K_{yy}} + \frac{z^2}{K_{zz}}\right)\right]. \end{aligned} \tag{8.64}$$

9

The last lecture

Remember Richardson's number!

$$\mathrm{Ri} = \frac{g}{\overline{\theta}} \frac{\mathrm{d}\overline{\theta}/\mathrm{d}z}{(\mathrm{d}\overline{u}/\mathrm{d}z)^2}.$$

and Pasquill's stability classes:

$\overline{u}$ (10 m)	Solar irradiance			Cloud cover	
$\mathrm{m\,s^{-1}}$	$> 700\,\mathrm{W\,m^{-2}}$	$350 - 700\,\mathrm{W\,m^{-2}}$	$< 350\mathrm{W\,m^{-2}}$	$\geq 4/8$	$< 3/8$
< 2	A	A-B	B		
$2 - 3$	A-B	B	C	E	F
$3 - 5$	B	B-C	C	D	E
$5 - 6$	C	C-D	D	D	D
> 6	C	D	D	D	D

Stability classes have been empirically related to Obukhov's length:

$$\frac{1}{L_O} = a + b \log z_0,$$

and

Condição	Classe de Pasquill	a	b
Muito instável	A	−0.096	0.029
Moderadamente instável	B	−0.037	0.029
Levemente instável	C	−0.002	0.018
Neutra	D	0	0
Levemente estável	E	+0.004	−0.018
Moderadamente estável	F	+0.035	−0.036

The standard deviations σ_Z and σ_Y can also be "recovered" empirically from stability classes, *viz.*

$$\sigma = \exp\left[I + J(\ln x) + K(\ln x)^2\right]$$

Classe	para obter σ_z			para obter σ_y		
	I	J	K	I	J	K
A	6,035	2,1097	0,2770	5,357	0,8828	-0,0076
B	4,694	1,0629	0,0136	5,058	0,9024	-0,0096
C	4,110	0,9201	-0,0020	4,651	0,9181	-0,0076
D	3,414	0,7371	-0,0316	4,230	0,9222	-0,0087
E	3,057	0,6794	-0,0450	3,922	0,9222	-0,0064
F	2,621	0,6564	-0,0540	3,533	0,9191	-0,0070

9.1 – Exemplo

Calcule a concentração dos poluentes num receptor localizado ao nível do solo, no eixo da pluma de dispersão a uma distância $x = 1500$ m da chaminé.

A tabela a seguir lista dados meteorológicos medidos a cada 3 horas. Os valores representam médias horárias.

tempo (h)	direção	u(m s^{-1})	T_a(K)	R_s(W m^{-2})
3	0.0	1.8	291.2	0
6	0.0	0.9	291.3	0
9	0.0	1.3	291.7	134
12	0.0	2.7	294.0	405
15	22.5	2.2	296.6	210
18	0.0	2.7	293.3	2
21	0.0	2.2	292.3	0
24	22.5	0.9	292.0	0

Dados de emissão:

temperatura de saída do gás	400 K
velocidade de saída do gás	6.0 m s^{-1}
diâmetro da chaminé	2.0 m
altura da chaminé acima do solo	50.0 m
altura do anemômetro	10.0 m
tipo de terreno	rural

Fluxos de poluentes na chaminé:

poluente	emissão (g s^{-1})
MP	10.69
NOx	7.54
SOx	1.07

Agora calcula-se a classe de estabilidade de Pasquill para cada período de uma hora de medição:

Classes de estabilidade para cada período de medição:

tempo (h)	R_s(W m^{-2})	u(10 m)(m s^{-1})	classe
3	0	1.8	E
6	0	0.9	E
9	134	1.3	B
12	405	2.7	B
15	210	2.2	C
18	2	2.7	C
21	0	2.2	E
24	0	0.9	E

Parâmetro de estabilidade de Briggs:

$$s = \left(\frac{g}{T_a}\right)\frac{d\theta}{dz},$$

onde:

s parâmetro de estabilidade (s^{-2})

g $9,807\ \mathrm{m\,s}^{-2}$

T_a temperatura ambiente do ar

$d\theta/dz$ gradiente vertical de temperatura potencial

Relação entre classes de estabilidade e estratificação da temperatura potencial

classe	$d\theta/dz$($\mathrm{K\,m}^{-1}$)
A	< -0.009
B	-0.008
C	-0.006
D	0.000
E	0.015
F	> 0.025

Com as classes de estabilidade obtidas acima, nós encontramos os seguintes valores para $d\theta/dz$ e s:

tempo (h)	classe	$d\theta/dz$($\mathrm{K\,m}^{-1}$)	temperatura (K)	s(s^{-2})
3	E	0.015	291.2	0.000505
6	E	0.015	291.3	0.00505
9	B	-0.008	291.7	-0.000269
12	B	-0.008	294.0	-0.000267
15	C	-0.006	296.6	-0.000198
18	C	-0.006	293.3	-0.000201
21	E	0.015	292.3	0.000503
24	E	0.015	292.0	0.000504

Fator de flutuação de Briggs

$$F = g v_s r^2 \frac{T_s - T_a}{T_s}$$

onde:

F fator de flutuação de Briggs ($\mathrm{m}^4\,\mathrm{s}^{-3}$)

g $9,807\ \mathrm{m\,s}^{-2}$

v_s velocidade de saída do gás ($\mathrm{m\,s}^{-1}$)

T_a temperatura do ar ambiente (K)

T_s temperatura de saída do gás (K)

r raio da chaminé (m)

Distância da chaminé até o ponto máximo de elevação da pluma:

$$x_f = 119F^{0.40} \quad \text{para} \quad F \geq 55\mathrm{m}^4\mathrm{s}^{-3}$$

e

$$x_f = 49F^{0.625} \quad \text{para} \quad F < 55\mathrm{m}^4\mathrm{s}^{-3}$$

tempo (h)	temperatura (K)	$F(\ m^4s^{-3})$	$x_f(m)$
3	291,2	16,01	277,24
6	291,3	15,99	277,08
9	291,7	15,93	276,44
12	294,0	15,59	272,76
15	296,6	15,21	268,56
18	293,3	15,70	273,88
21	292,3	15,84	275,49
24	292,0	15,89	275,96

Relação entre velocidade do vento e altura:

$$u(z) = u_a\,(z/z_a)^n$$

onde:

$u(z)$ velocidade do vento na altura z

u_a velocidade do vento a altura do anemômetro z_a

n expoente em função da classe de estabilidade

Expoente de conversão da velocidade do vento

classe	n
A	0,10
B	0,15
C	0,20
D	0,25
E	0,25
F	0,30

Equações de Briggs para a altura de curvatura da pluma
Classes de estabilidade de Pasquill A, B, C, D:

$$\Delta h = 1.6F^{1/3}x^{2/3}u^{-1}, \quad \text{para} \quad x < x_f$$

e

$$\Delta h = 1.6F^{1/3}x_f^{2/3}u^{-1}, \quad \text{para} \quad x \geq x_f$$

Classes de estabilidade de Pasquill E, F:
Quando $1.84us^{-1/2} \geq x_f \implies$

$$\Delta h = 1.6F^{1/3}x^{2/3}u^{-1}, \quad \text{para} \quad x < x_f$$

e

$$\Delta h_{\max} = 1.6F^{1/3}x_f^{2/3}u^{-1}, \quad \text{para} \quad x \geq x_f$$

Quando $1.84us^{-1/2} < x_f \implies$

$$\Delta h = 1.6F^{1/3}x^{2/3}u^{-1}, \quad \text{para} \quad x < 1.84us^{-1/2}$$

e

$$\Delta h_{\max} = 2.4\,(F/us)^{1/3}, \quad \text{para} \quad x \geq 1.84us^{-1/2}$$

Altura efetiva de emissão:

$$H_e = h_s + \Delta h$$

Onde:

h_s altura da chaminé

Δh altura de curvatura da pluma

tempo (h)	classe	u(10 m)	n	u(50 m)	$1.84us^{-1/2}$(m)	Δh(m)	H_e(m)
3	E	1,8	0,25	2,69	220,35	54,62	104,62
6	E	0,9	0,25	1,35	110,39	68,70	118,70
9	B	1,3	0,15	1,65	—	103,54	153,54
12	B	2,7	0,15	3,44	—	48,87	98,87
15	C	2,2	0,20	3,04	—	54,28	104,28
18	C	2,7	0,20	3,73	—	45,30	95,30
21	E	2,2	0,25	3,29	269,83	50,96	100,96
24	E	0,9	0,25	1,35	110,33	68,60	118,60

Desvios-padrão:

$$\sigma = \exp\left[I + J(\ln x) + K(\ln x)^2\right]$$

onde:

σ coeficiente de dispersão rural (m)

x distância do receptor (km)

Constantes de McMullen para obtenção dos coeficientes de dispersão rural

Classe	para obter σ_z			para obter σ_y		
	I	J	K	I	J	K
A	6,035	2,1097	0,2770	5,357	0,8828	-0,0076
B	4,694	1,0629	0,0136	5,058	0,9024	-0,0096
C	4,110	0,9201	-0,0020	4,651	0,9181	-0,0076
D	3,414	0,7371	-0,0316	4,230	0,9222	-0,0087
E	3,057	0,6794	-0,0450	3,922	0,9222	-0,0064
F	2,621	0,6564	-0,0540	3,533	0,9191	-0,0070

tempo (h)	classe	H_e(m)	$u(H_e)$(m s^{-1})	σ_z(m)	σ_y(m)
3	E	104,62	3,24	27,80	73,32
6	E	118,70	1,67	27,80	73,32
9	B	153,54	1,96	168,55	226,40
12	B	98,87	3,81	168,55	226,40
15	C	104,28	3,52	88,48	151,72
18	C	95,30	4,24	88,48	151,72
21	E	100,96	3,92	27,80	73,32
24	E	118,60	1,67	27,80	73,32

Concentração das emissões da chaminé usando a equação de dispersão gaussiana generalizada; a dependência com x entra via σ_z e σ_y:

$$C(x,y,z) = \frac{Q}{(2\pi u \sigma_z \sigma_y)} \exp\left(-\frac{y^2}{2\sigma_y^2}\right)\left[\exp\left(-\frac{(z-H_e)^2}{2\sigma_z^2}\right) + \exp\left(-\frac{(z+H_e)^2}{2\sigma_z^2}\right)\right]$$

onde:

C concentração das emissões (μgm^{-3}) localizada

Q taxa de emissão da chaminé (μgs^{-1})

u velocidade do vento (m s^{-1})

σ_z desvio-padrão vertical (m)

σ_y desvio-padrão transversal (m)

H_e altura efetiva de emissão (m)

tempo (h)	concentrações (μgm^{-3})		
	MP	NOx	SOx
3	0.4	0.3	0.0
6	0.1	0.1	0.0
9	30.1	21.2	3.0
12	19.7	13.9	2.0
15	36.0	25.4	3.6
18	33.5	23.6	3.4
21	0.6	0.4	0.1
24	0.1	0.1	0.0

9.2 – Modernamente!

Os modelos de pluma gaussiana têm sido substituídos por modelos mais detalhados, que são capazes de levar em conta a evolução horária dos parâmetros meteorológicos, a topografia do terreno, etc..

Nos EUA, duas gerações desse tipo de modelo foram o ISC3 e, atualmente, o AERMOD. Ver:
https://www.epa.gov/scram/air-quality-dispersion-modeling-preferred-and-recommended-models

Uma das partes mais legais do AERMOD é a sua capacidade de acompanhar terreno.

Bibliography

Adkins, C. J. (1983). *Equilibrium thermodynamics*. New York: Cambridge University Press.

Alduchov, O. A. and R. E. Eskridge (1996). Improved Magnus form approximation of saturation vapor pressure. *J Appl Meteorol 35*, 601–609.

Aubinet, M. (2008). Eddy covariance co_2 flux measurements in nocturnal conditions: an analysis of the problem. *Ecological Applications 18*(6), 1368–1378.

Bakan, S. (1978). Note on the eddy correlation method for co_2 flux measurements. *Boundary-Layer Meteorol 14*, 597–600.

Baldocchi, D. D. (2003). Assessing the eddy covariance technique for evaluating carbon dioxide exchange rates of ecosystems: past, present and future. *Glob Chang Biol 9*, 479–492.

Batchelor, G. K. (1967). *An introduction to fluid dynamics*. Cambridge: Cambridge University Press.

Baumgartner, A. (1969). Meteorological approach to the exchange of co2 between the atmosphere and vegetation, particularly forests stands. *Photosynthetica 3*, 127–149.

Bird, R. B., W. E. Stewart, and E. N. Lightfoot (1960). *Transport phenomena*. New York: John Wiley and Sons.

Brunt, D. (1932). Notes on radiation in the atmosphere, 1. *Q J Roy Meteorol Soc 58*, 389–420.

Brutsaert, W. (1975). On a derivable formula for long-wave radiation from clear skies. *Water Resour Res 11*, 742–744.

Brutsaert, W. (1982). *Evaporation into the atmosphere*. Dordrecht: D. Reidel. 309 pp.

Brutsaert, W. (1992, March). Stability correction functions for the mean wind speed and temperature in the unstable surface layer. *Geophys Res Lett 19*(5), 469–472.

Buck, A. L. (1976). The variable-path lyman-alpha hygrometer and its opening characteristics. *Bull Amer Meteorol Soc 57*, 1113–1118.

Businger, J. A., J. C. Wyngaard, Y. Izumi, and E. F. Bradley (1971). Flux-profile relationships in the atmospheric surface layer. *J Atmos Sci 28*, 181–189.

Butenhoff, C. L. and M. A. K. Khalil (2002). Correction for water vapor in the measurement of atmospheric trace gases. *Chemosphere 47*(8), 823–836.

Chambers, J. Q., E. S. Tribuzy, L. C. Toledo, B. F. Crispim, N. Higuchi, J. dos Santos, A. C. Araujo, B. Kruijt, A. D. Nobre, and S. E. T. Rumbore (2004). Respiration from a tropical forest ecosystem: Partitioning of sources and low carbon use efficiency. *Ecological Applications 14*, S72–S88.

Cheng, Y. and W. Brutsaert (2005). Flux-profile relationships for wind speed and temperature in the stable atmospheric boundary layer. *Boundary-Layer Meteorol 114*, 519–538.

Cheng, Y., M. Parlange, and W. Brutsaert (2005). Pathology of Monin-Obukhov similarity in the stable boundary layer. *J of Geophys Res 110*, D06101.

CHOI, K.-S. and J. L. LUMLEY (2001, Jun). The return to isotropy of homogeneous turbulence. *Journal of Fluid Mechanics 436*, 59–84.

COESA (1976). U.s. standard atmosphere, 1976. Technical report, U.S. Government Printing Office.

Culf, A. D., G. Fisch, Y. Malhi, and C. A. Nobre (1997). The influence of the atmospheric boundary layer on carbon dioxide concentrations over a tropical forest. *Agricultural and Forest Meteorology 85*, 149–158.

da Rocha, H. R., H. C. Freitas, R. Rosolem, R. I. N. Ju?rez, R. N. Tannus, M. A. Ligo, O. M. R. Cabral, and M. A. F. S. Dias (2002). Measurements of co_2 exchange over a woodland savanna (Cerrado Sensu stricto) in southeast brasil. *Biota Neotropica 2*(1), 1–11.

de Bruin, H., B. van den Hurk, and L. J. M. Kroon (1999). On the temperature-humidity correlation and similarity. *Boundary-Layer Meteorol 93*, 453–468.

Deanmead, O. T. (1969). Comparative micrometeorology of a wheat field and a forest of pinus radiata. *Agricultural Meteorology 6*, 357–371.

Desjardins, R. L. (1974). A technique to measure co2 exchange under field conditions. *International Journal of Biometeorology 18*(1), 76–83.

Desjardins, R. L. and E. R. Lemon (1974). Limitations of an eddy-correlation technique for the determination of the carbon dioxide and sensible heat fluxes. *Boundary-Layer Meteorology 5*(4), 475–488.

Dias, N. L. (1986). Estimativas climatológicas de evaporação em lagos. Master's thesis, COPPE/UFRJ.

Dias, N. L. (1994). *The structure of temperature and humidity turbulent fluctuations in the stable surface layer*. Ph. D. thesis, Cornell University, Ithaca, NY.

Dias, N. L. (2017). *An introduction to mathematical methods for engineering (in Portuguese)*. Curitiba: Author's edition. Available at https://nldias.github.io/pdf/matappa-1ed.pdf.

Dias, N. L. (2020). O efeito do aumento de CO_2 atmosférico sobre a constante de gás do ar seco. *Revista Brasileira de Meteorologia (submitted)*.

Dias, N. L. and W. Brutsaert (1996). Similarity of scalars under stable conditions. *Boundary-Layer Meteorol 80*, 355–373.

Dias, N. L., M. Chamecki, A. Kan, and C. M. P. Okawa (2004). A study of spectra, structure and correlation functions and their implication on the stationarity of surface-layer turbulence. *Boundary-Layer Meteorol 110*, 165–189.

Dias, N. L., B. L. Crivellaro, and M. Chamecki (2018). The Hurst phenomenon in error estimates related to atmospheric turbulence. *Boundary-Layer Meteorol 168*(3), 387–416.

Dias, N. L., H. F. Duarte, S. R. Maggiotto, and L. Grodzki (2007). An attenuated eddy covariance method for latent heat flux measurements. *Water Resour Res 43*, W04415.

Dias, N. L., J. Hong, M. Leclerc, Black, Z. Nesic, and P. Krishnan (2009). A simple method of estimating scalar fluxes over forests. *Boundary-Layer Meteorol 132*, 401–414.

Dilley, A. C. (1968). On the computer calculation of vapor pressure and specific humidity gradients from psychrometric data. *J Appl Meteorol 7*, 717–719.

Duarte, H. F., N. L. Dias, and S. R. Maggiotto (2006). Assessing daytime downward longwave radiation estimates for clear and cloudy skies in Southern Brazil. *Agric For Meteorol 139*, 171–181.

Finnigan, J. (1999). A comment on the paper by Lee (1998): "On micrometeorological observations of surface-air exchange over tall vegetation". *Agric For Meteorol 97*, 55–64.

Finnigan, J. J. (2009). Response to comment by Dr. A.S. Kowalski on "The storage term in eddy flux calculations". *Agric For Meteorol 149*, 725 – 729.

Finnigan, J. J., R. Clement, Y. Malhi, R. Leuning, and H. A. Cleugh (2003). A re-evaluation of long-term flux measurement techniques part i: averaging and coordinate rotation. *Boundary-Layer Meteorol 107*, 1–48.

Fischer, H. B., E. J. List, R. C. Y. Koh, J. Imberger, and N. H. Brooks (1979). *Mixing in Inland and Coastal Waters*. New York: Academic Press.

Fleagle, R. G. and J. A. Businger (1980). *An introduction to atmospheric physics*. Orlando: Academic Press.

Fox, R. W. and A. T. McDonald (1981). *Introdução à Mecânica dos Fluidos*. Rio de Janeiro: Guanabara Dois.

Galperin, B., S. Sukoriansky, and P. S. Anderson (2007). On the critical Richardson number in stably stratified turbulence. *Atmospheric Science Letters 8*(3), 65–69.

Garcia, C., P. Jackson, and M. Garcia (2006). Confidence intervals in the determination of turbulent parameters. *Exp Fluids 40*(4), 514–522.

Garratt, J. (1994). *The Atmospheric Boundary Layer*. Cambridge University Press, U.K. 316 pp.

Gluhovsky, A. and E. Agee (1994). A definitive approach to turbulence statistical studies in planetary boundary layers. *J Atmos Sci 51*(12), 1682–1690.

Goulden, M. L., J. W. Munger, S.-M. Fan, B. C. Daube, and S. C. Wofsy (2006). Measurements of carbon sequestration by long-term eddy covariance: methods and a critical evaluation of accuracy. *Global Change Biology 2*(3), 169–118.

Hauf, T., U. Finke, J. Neisser, G. Bull, and J.-G. Stangenberg (1996). A ground-based network for atmospheric pressure fluctuations. *J Atmos Oceanic Technol 13*, 1001–1023.

Heinesch, B., M. Yernaux, and M. Aubinet (2007). Some methodological questions concerning advection measurements: a case study. *Boundary-Layer Meteorol 122*, 457–478.

Hicks, B. B. (1981). An examination of turbulence statistics in the surface boundary layer. *Boundary-Layer Meteorol 21*, 389–402.

Hill, R. J. (1989). Implications of Monin-Obukhov similarity theory for scalar quantities. *J Atmos Sci 46*, 2236–2244.

Hinze, J. O. (1975). *Turbulence*. New York: McGraw-Hill Publishing Company.

Holton, J. R. (1992). *An introduction to dynamic meteorology*. Sand Diego: Academic Press.

Houghton, J. T. (1986). *The physics of atmospheres* (2nd ed.). Cambridge University Press.

Högström, U. (1988). Non-dimensional wind and temperature profiles in the atmospheric surface layer: a re-evaluation. *Boundary-Layer Meteorol 42*, 55–78.

Iribarne, J. V. and W. L. Godson (1981). *Atmospheric Thermodynamics* (2$^{\underline{\text{nd}}}$ed.). Dordrecht: D. Reidel.

Jacobs, J. D. (1978). Radiation climate of broughton island. In R. G. Barry and J. D. Jacobs (Eds.), *Energy Budget Studies in Relation to Fast-ice Breakup Processes in Davis Strait.*, Number Occas. Paper No 26, pp. 105–120. Boulder, CO: Inst. of Arctic and Alp. Res, University of Colorado.

Jones, E. P. and S. D. Smith (1978). The air density correction to eddy flux measurements. *Boundary-Layer Meteorol 15*, 357–360.

Kader, B. A. and A. M. Yaglom (1990). Mean fields and fluctuation moments in unstably stratified turbulent boundary layers. *J Fluid Mech 212*, 637–662.

Kondo, J., O. Kanechica, and N. Yasuda (1978). Heat and momentum transfers under strong stability in the atmospheric surface layer. *J Atmos Sci 35*, 1012–1021.

Kumar, P. and M. Sharan (2010). An analytical model for dispersion of pollutants from a continuous source in the atmospheric boundary layer. *Proceedings of the Royal Society A 466*, 383–406.

Kundu, P. K. (1990). *Fluid Mechanics*. San Diego: Academic Press.

Kustas, W. P., J. H. Blanford, D. I. Stannard, C. S. T. Daughtry, W. D. Nichols, and M. A. Weltz (1994). Local energy flux estimates for unstable conditions using variance data in semiarid rangelands. *Water Resour Res 30*(5), 1351–1361.

Landau, L. D. and E. M. Lifshitz (1959). *Fluid Mechanics*. Oxford: Pergamon Press.

Leclerc, M. and G. Thurtell (1990). Footprint prediction of scalar fluxes using a markovian analysis. *Boundary-Layer Meteorol 52*, 247–258.

Lee, X. (1998). On micrometeorological observations of surface-air exchange over tall vegetation. *Agric For Meteorol 91*, 39–49.

Lee, X. and W. J. Massman (2011). A perspective on thirty years of the Webb, Pearman and Leuning density corrections. *Boundary-Layer Meteorol 139*, 37 – 59.

Leuning, R., O. T. Denmead, A. R. G. Lang, and E. Ohtaki (1982). Effects of heat and water vapor transport on eddy-covariance measurement of co2 fluxes. *Boundary-Layer Meteorol 23*, 209–222.

Leuning, R., S. Zegelin, K. Jones, H. Keith, and H. D. (2008). Measurement of horizontal and vertical advection of CO_2 within a forest canopy. *Agric For Meteorol 148*, 1777–1797.

Linsley, R. K., M. A. Kohler, and J. L. H. Paulhus (1975). *Hydrology for Engineers*. New York: McGraw-Hill.

Lumley, J. L. and G. R. Newman (1977, Aug). The return to isotropy of homogeneous turbulence. *Journal of Fluid Mechanics 82*(01), 161.

Lumley, J. L. and H. A. Panofksy (1964). *The structure of atmospheric turbulence*. New York: Interscience. 239 pp.

Massman, W. J. and X. Lee (2002). Eddy covariance flux corrections and uncertainties in long-term studies of carbon and energy exchanges. *Agric For Meteorol 113*, 121–144.

McNaughton, K. G. and J. Laubach (1998). Unsteadiness as a cause of non-equality of eddy diffusivities for heat and vapour at the base of an advective inversion. *Boundary-Layer Meteorol 88*(3), 479–504.

Miller, S. D., M. L. Gouden, M. C. Menton, and H. R. da Rocha (2004). Biometric and micrometeorological measurements of tropical forest carbon balance. *Ecological Applications 14(4)*, S114–S126.

Moncrieff, J. B., J. M. Massheder, H. de Bruin, J. Elbers, T. Friborg, B. Heusinkveld, P. Kabat, S. Scott, H. Soegaard, and A. Verhoef (1997). A system to measure surface fluxes of momentum, sensible heat, water vapour and carbon dioxide. *J of Hydrology 188–189*, 563–588.

Monin, A. S. and A. M. Yaglom (1971). *Statistical fluid mechanics: Mechanics of turbulence*, Volume 1. Cambridge, Massachusetts: MIT Press.

Murray, F. W. (1966). On the computation of saturation vapor pressure. *J Appl Meteorol 6*, 203–204.

NIST (2020). Nist chemistry web book, srd69. Available at https://webbook.nist.gov/chemistry/mw-ser/. Retrieved in 2020-04-10T09:05:36.

Obukhov, A. M. (1946 1971). Turbulence in an atmosphere with non-uniform temperature. *Boundary-Layer Meteorol 2*, 7–29.

Pahlow, M., M. B. Parlange, and F. Porté-Agel (2001). On Monin-Obukhov similarity in the stable atmospheric boundary layer. *Boundary-Layer Meteorol 99*, 225–248.

Pope, S. B. (2000). *Turbulent Flows*. Cambridge: Cambridge University Press.

Reynolds, O. (1895). On the dynamical theory of incompressible viscous fluids and the determination of the criterion. *Philos. Trans. R. Soc. Lond. A 186*, 123–164.

Rotta, J. (1951a). Statistische theorie nichthomogener turbulenz, 1. *Zeitschrift für Physik 129*, 547–572.

Rotta, J. (1951b). Statistische theorie nichthomogener turbulenz, 2. *Zeitschrift für Physik 131*, 51–77.

Ruelle, D. (1994, July). Where can one hope to profitably apply the ideas of chaos? *Physics Today 47*(7), 24–30.

Sakai, R. K., D. R. Fitzjarrald, and K. E. Moore (2001). Importance of low-frequency contributions to eddy fluxes observed over rough surfaces. *J Appl Meteorol 40*, 2178–2192.

Salesky, S. T. and M. Chamecki (2012). Random errors in turbulence measurements in the atmospheric surface layer: Implications for Monin-Obukhov similarity theory. *J Atmos Sci 69*, 3700–3714.

Salesky, S. T., M. Chamecki, and N. L. Dias (2012). Estimating the random error in eddy-covariance fluxes and other turbulence statistics: the filtering method. *Boundary-Layer Meteorol 144*, 113–135.

Schlyter, P. (2019). How to compute planetary positions. Internet: http://www.stjarnhimlen.se/comp/ppcomp.html. Retrieved in 2019-04-22T16:45:34.

Sellers, P. J., F. G. Hall, R. D. Kelly, A. Black, D. Baldocchi, J. Berry, M. Ryan, K. J. Ranson, P. M. Crill, D. P. Lettenmaier, H. Margolis, J. Cihlar, J. Newcomer, D. Fitzjarrald, P. G. Jarvis, S. T. Gower, D. Halliwell, D. Williams, B. Goodison, D. E. Wickland, and F. E. Guertin (1997). Boreas in 1997: Experiment overview, scientific results, and future directions. *Journal of geophysical research 102*, 28, 731 – 28, 769.

Simpson, I. J., G. C. Edwards, G. W. Thurtell, G. den Hartog, H. H. Neumann, and R. M. Staebler (1997). Micrometeorological measurements of methane and nitrous oxide exchange above a boreal aspen forest. *Journal of geophysical research 102*, 29,331–29,341.

Smith, S. D. and E. P. Jones (1979). Dry-air boundary conditions for corrections of eddy flux measurements. *Boundary-Layer Meteorol 17*, 375–379.

Stull, R. (1988). *An Introduction to Boundary-Layer Meteorology*. Dordrecht: Kluwer.

Stull, R. (1995). *Meteorology today for scientists and engineers*. Minneapolis/St.Paul: West Publishing Company.

Sun, X.-M., Z.-L. Zhu, X. F. Wen, G.-F. Yuan, and G.-R. Yu (2006). The impact of averaging period on eddy fluxes observed at chinaflux sites. *Agricultural and Forest Meteorology 137*, 188–193.

Swinbank, W. C. (1951). Measurement of vertical transfer of heat and water vapor by eddies in the lower atmosphere. *J Meteorol 8*, 135–145.

Taylor, G. I. (1921). Diffusion by continuous movements. *Proceedings of the London Mathematical Society 20*(2), 196–211.

Tennekes, H. and J. L. Lumley (1972). *A first course in turbulence*. Cambridge, Massachusetts: The MIT Press.

Tillman, J. E. (1972). The indirect determination of stability, heat and momentum fluxes in the atmospheric boundary layer from simple scalar variables during dry unstable conditions. *J Appl Meteorol 11*, 783–792.

Twine, T. E., W. P. Kustas, J. M. Norman, D. R. Cook, P. R. Houser, T. P. Meyers, J. H. Prueger, P. J. Starks, and M. L. Wesely (2000). Correcting eddy-covariance flux underestimates over a grassland. *Agric For Meteorol 103*, 274–300.

United States Naval Observatory (2019). Earth's seasons and apsides: Equinoxes, solstices, perihelion, and aphelion. https://aa.usno.navy.mil/data/docs/EarthSeasons.php. Retrieved 2019-04-24T09:58:08.

van Flandern, T. C. and K. F. Pulkkinen (1979, November). Low-precision formulae for planetary positions. *Astrophys J SupplS 41*, 391–411.

Wallace, J. M. and P. V. Hobbs (2006). *Atmospheric Science: an introductory survey* (2nd ed.). Amsterdam: Elsevier.

Webb, E. K. and G. I. Pearman (1977). Correction of co_2 transfer measurements for the effect of water vapor transfer. In *Second Australian Conference on Heat and Mass Transfer*, The University of Sydney, Australia, pp. 469–476.

Webb, E. K., G. I. Pearman, and R. Leuning (1980). Correction of flux measurements for density effects due to heat and water vapor transfer. *Q J Roy Meteorol Soc 106*, 85–100.

Wesely, M. L. (1988). Use of variance techniques to measure dry air-surface exchange rates. *Boundary-Layer Meteorol 44*, 13–31.

Wikipedia (2019). Okta. https://en.wikipedia.org/wiki/Okta. Retrived in 2019-05-22T10:40:15.

Wikipedia (2020). Atmosphere of earth. Available at https://en.wikipedia.org/wiki/Atmosphere_of_Earth. Retrieved in 2020-04-08T11:25:15.

Wilczak, J. M., S. P. Oncley, and S. A. Stage (2001). Sonic anemometer tilt correction algorithms. *Boundary-Layer Meteorol 99*, 127–150.

Wyngaard, J. C. (1973). On surface-layer turbulence. In D. A. Haugen (Ed.), *Workshop on micrometeorology*, pp. 101–149. Boston: American Meteorological Society.

Wyngaard, J. C. (1981). Boundary-layer modeling. In F. T. M. Niewstadt and H. van Dop (Eds.), *Atmospheric turbulence and air pollution modelling*, Chapter 3, pp. 69–106. Dordrecht: D. Reidel Publishing Company.

Wyngaard, J. C. (2010). *Turbulence in the atmosphere*. Cambridge.

Wyngaard, J. C., O. R. Coté, and Y. Izumi (1971). Local free convection, similarity, and the budgets of shear stress and heat flux. *J Atmos Sci 28*, 1171–1182.

Yaglom, A. M. (1987). *Correlation theory of stationary and related random functions I: Basic results*. New York: Springer-Verlag. 526 pp.

Yu, G.-R., X. F. Wen, X.-M. Sun, B. D. Tanner, X. Lee, and J.-Y. Chen (2006). Overview of ChinaFLUX and evaluation of its eddy covariance measurement. *Agricultural and Forest Meteorology 137*, 125–137.

Zilitinkevich, S. (1994). A generalized scaling for convective shear flows. *Boundary-Layer Meteorol 70*, 51–78.

Zilitinkevich, S. S., T. Elperin, N. Kleeorin, and I. Rogachevskii (2007). Energy- and flux-budget (EFB) turbulence closure model for stably stratified flows. part i: steady-state, homogeneous regimes. *Boundary-Layer Meteorol 125*, 167–191.

10

A camada de mistura

10.1 – A espiral de Ekman

A notação deste documento está, neste momento, uma grande bagunça. Mas isto é incontornável por enquanto. Vamos começar com uma rápida revisão das equações para uma camada-limite atmosférica na forma

$$\frac{\partial \overline{U}_i}{\partial t} + \overline{U}_k \frac{\partial \overline{U}_i}{\partial x_k} + \frac{\partial (\overline{u_i u_k})}{\partial x_k} = \frac{\overline{\delta \wp}}{\wp_s} g_i - \frac{1}{\wp_s} \frac{\partial \overline{\delta P}}{\partial x_i} + f_c \epsilon_{ik3} \overline{U}_k + \nu \frac{\partial^2 \overline{U}_i}{\partial x_k \partial x_k}. \quad (10.1)$$

Uma questão na qual não vou me aprofundar agora é até que ponto esta equação vale para *toda* a camada de mistura. As equações para o vento geostrófico são

$$\frac{1}{\wp_S} \frac{\partial \overline{\delta P}}{\partial x_i} = f_c \epsilon_{ik3} U_{Gk}, \quad (10.2)$$

de modo que a equação de *momentum* pode ser escrita com as componentes do vento geostrófico substituindo os gradientes horizontais de pressão:

$$\frac{\partial \overline{U}_i}{\partial t} + \overline{U}_k \frac{\partial \overline{U}_i}{\partial x_k} + \frac{\partial (\overline{u_i u_k})}{\partial x_k} = \frac{\overline{\delta \wp}}{\wp_s} g_i + f_c \epsilon_{ik3} \left(\overline{U}_k - U_{Gk} \right) + \nu \frac{\partial^2 \overline{U}_i}{\partial x_k \partial x_k}. \quad (10.3)$$

Para o caso estacionário e horizontalmente homogêneo, as equações tornam-se

$$\frac{\partial (\overline{uw})}{\partial z} = f_c (\overline{V} - V_G), \quad (10.4)$$

$$\frac{\partial (\overline{vw})}{\partial z} = -f_c (\overline{U} - U_G). \quad (10.5)$$

Use um modelo de fechamento muito simples, com uma difusividade turbulenta K:

$$\overline{uw} = -K \frac{\partial \overline{U}}{\partial z}, \quad (10.6)$$

$$\overline{vw} = -K \frac{\partial \overline{V}}{\partial z}. \quad (10.7)$$

Evidentemente, a única variável independente é z, e passaremos a utilizar derivadas ordinárias em lugar de derivadas parciais:

$$K \frac{d^2 \overline{U}}{dz^2} = f_c (V_G - \overline{V}), \quad (10.8)$$

$$K \frac{d^2 \overline{V}}{dz^2} = -f_c (U_G - \overline{U}). \quad (10.9)$$

Neste ponto, introduza as variáveis complexas

$$w \equiv \overline{U} + \mathrm{i}\overline{V}; \qquad w_G \equiv U_G + \mathrm{i}V_G; \tag{10.10}$$

o sistema de equações diferenciais ordinárias torna-se

$$\begin{aligned} K\frac{d^2w}{dz^2} &= K\left(\frac{d^2\overline{U}}{dz^2} + \mathrm{i}\frac{d^2\overline{V}}{dz^2}\right) \\ &= f_c(V_G - \overline{V}) - \mathrm{i}f_c(U_G - \overline{U}) \\ &= -\mathrm{i}f_c\left[(U_G + \mathrm{i}V_G) - (\overline{U} + \mathrm{i}\overline{V})\right] \\ &= -\mathrm{i}f_c\left[w_g - w\right]. \end{aligned} \tag{10.11}$$

O problema reduz-se, então, à solução da equação diferencial complexa

$$K\frac{d^2w}{dz^2} - \mathrm{i}f_c w = -\mathrm{i}f_c w_G. \tag{10.12}$$

As condições de contorno são

$$w(0) = 0, \tag{10.13}$$

$$\lim_{z\to\infty} w(z) = w_G. \tag{10.14}$$

Portanto, este é um problema de valor de contorno. Por inspeção, $w_p = w_G$ é uma solução particular; a equação característica é

$$\lambda^2 - \frac{\mathrm{i}f_c}{K} = 0, \tag{10.15}$$

com raízes

$$\lambda_{1,2} = \sqrt{\frac{\mathrm{i}f_c}{K}} = \sqrt{\frac{|f_c|}{K}}\sqrt{\mathrm{sinal}(f_c)\mathrm{i}}. \tag{10.16}$$

A solução agora deve depender do sinal de

$$f_c = 2\Omega \operatorname{sen}\varphi, \tag{10.17}$$

onde Ω é a velocidade angular da terra, e φ é a latitude. No Hemisfério Norte, $f_c > 0$, enquanto que no Hemisfério Sul, $f_c < 0$.

10.1.1 – Hemisfério Norte

Procura-se $\sqrt{\mathrm{i}}$:

$$w^2 = r^2 e^{2(\mathrm{i}\theta)} = e^{\mathrm{i}(\frac{\pi}{2}+2\pi)}, \tag{10.18}$$

$$r = 1, \tag{10.19}$$

$$\theta = \frac{\pi}{4} + \pi \tag{10.20}$$

Os dois valores possíveis para $\sqrt{\mathrm{i}}$ são

$$w_1 = \frac{\sqrt{2}}{2}(1 + \mathrm{i}), \tag{10.21}$$

$$w_2 = -\frac{\sqrt{2}}{2}(1 + \mathrm{i}). \tag{10.22}$$

A solução geral, portanto, é

$$w(z) = w_G + c_1 \exp\left(w_1\sqrt{\frac{f_c}{K}}z\right) + c_2 \exp\left(w_2\sqrt{\frac{f_c}{K}}z\right). \tag{10.23}$$

Para atender às condições de contorno (10.13)–(10.14), $c_1 = 0$ e $c_2 = -w_G$. A solução é

$$w(z) = w_G\left[1 - \exp\left(-(1+\mathrm{i})\sqrt{\frac{f_c}{2K}}\,z\right)\right], \tag{10.24}$$

$$= w_G\left[1 - \exp\left(-\sqrt{\frac{f_c}{2K}}\,z\right)\left(\cos\sqrt{\frac{f_c}{2K}}z - \mathrm{i}\,\mathrm{sen}\sqrt{\frac{f_c}{2K}}z\right)\right]. \tag{10.25}$$

Agora, se alinharmos o vetor vento geostrófico com o eixo x, ou seja, se $V_G = 0$, a solução para a velocidade média na camada-limite atmosférica é

$$\overline{U}(z) = U_G\left[1 - \exp\left(-\sqrt{\frac{f_c}{2K}}\,z\right)\cos\sqrt{\frac{f_c}{2K}}z\right], \tag{10.26}$$

$$\overline{V}(z) = U_G\left[\exp\left(-\sqrt{\frac{f_c}{2K}}\,z\right)\mathrm{sen}\sqrt{\frac{f_c}{2K}}z\right]. \tag{10.27}$$

10.1.2 – Hemisfério Sul

Procura-se $\sqrt{-\mathrm{i}}$:

$$w^2 = r^2 e^{2(\mathrm{i}\theta)} = e^{\mathrm{i}(-\frac{\pi}{2}+2\pi)}, \tag{10.28}$$

$$r = 1, \tag{10.29}$$

$$\theta = -\frac{\pi}{4} + \pi \tag{10.30}$$

Os dois valores possíveis para $\sqrt{\mathrm{i}}$ são

$$w_3 = \frac{\sqrt{2}}{2}(1 - \mathrm{i}), \tag{10.31}$$

$$w_4 = \frac{\sqrt{2}}{2}(-1 + \mathrm{i}). \tag{10.32}$$

A solução geral agora será

$$w(z) = w_G + c_3 \exp\left(w_3\sqrt{\frac{f_c}{K}}z\right) + c_4 \exp\left(w_4\sqrt{\frac{f_c}{K}}z\right). \tag{10.33}$$

Para atender às condições de contorno (10.13)–(10.14), $c_3 = 0$ e $c_4 = -w_G$. A solução é

$$w(z) = w_G\left[1 - \exp\left((-1+\mathrm{i})\sqrt{\frac{f_c}{2K}}\,z\right)\right], \tag{10.34}$$

$$= w_G\left[1 - \exp\left(-\sqrt{\frac{f_c}{2K}}\,z\right)\left(\cos\sqrt{\frac{f_c}{2K}}z + \mathrm{i}\,\mathrm{sen}\sqrt{\frac{f_c}{2K}}z\right)\right]. \tag{10.35}$$

Agora, se alinharmos o vetor vento geostrófico com o eixo x, ou seja, se $V_G = 0$, a solução para a velocidade média na camada-limite atmosférica é

$$\overline{U}(z) = U_G \left[1 - \exp\left(-\sqrt{\frac{f_c}{2K}}\, z \right) \cos \sqrt{\frac{f_c}{2K}} z \right], \tag{10.36}$$

$$\overline{V}(z) = -U_G \left[\exp\left(-\sqrt{\frac{f_c}{2K}}\, z \right) \operatorname{sen} \sqrt{\frac{f_c}{2K}} z \right]. \tag{10.37}$$

Note que a diferença entre a solução (10.26)–(10.27) obtida anteriormente para o Hemisfério Norte, e (10.36)–(10.37) obtida agora para o Hemisfério Sul, é que $\overline{V}$ muda de sinal, ou seja: o vetor velocidade do vento "gira" para a esquerda no Hemisfério Norte, e para a direita no Hemisfério Sul.

Neste modelo simplificado, é fácil calcular o ângulo total de giro da espiral:

$$\lim_{z \to 0} \frac{\overline{V}}{\overline{U}} = \pm 1, \tag{10.38}$$

onde o sinal de menos se aplica ao Hemisfério Sul. Portanto, o giro total é de $\pi/4$ radianos (45°).

10.2 – Similaridade de Rossby e *Asymptotic Matching*

(Extraído de H. Tennekes, "Similarity relations, scaling laws and spectral dynamics")

Suponha uma atmosfera neutra, $|L_O| = +\infty$ sobre uma superfície horizontalmente homogênea. Nela, o vetor velocidade horizontal do vento é

$$\overline{\boldsymbol{u}} = \overline{u}\, \boldsymbol{i} + \overline{v}\, \boldsymbol{j}, \tag{10.39}$$

de tal forma que no topo da camada-limite atmosférica:

$$|\overline{\boldsymbol{u}}| \to \sqrt{u_g^2 + v_g^2} \equiv G, \tag{10.40}$$

onde u_g e v_g são as componentes do vento geostrófico. As duas escalas de comprimento possíveis para o nosso problema são z_0 (a rugosidade da superfície para quantidade de movimento) e G/f, onde f é o parâmetro de Coriolis. Note que

$$\frac{G}{f} \sim L_p \quad \text{com} \quad \frac{\partial \overline{p}}{\partial x} \sim \frac{\Delta \overline{p}}{L_p}. \tag{10.41}$$

A razão entre estas duas escalas produz o *Número de Rossby de rugosidade*:

$$R_o = \frac{G}{f z_0}. \tag{10.42}$$

As equações médias de Reynolds para um problema homogêneo na horizontal e permanente são

$$f(\overline{v} - v_g) = \frac{\partial}{\partial z}(\overline{w'u'}), \tag{10.43}$$

$$f(u_g - \overline{u}) = \frac{\partial}{\partial z}(\overline{w'v'}) \tag{10.44}$$

Para tornar (10.43)–(10.44) adimensionais, divida por fu_*: nós vamos supor que dentro da CLA porém ainda suficientemente "longe" da superfície, os perfis de vento dependem do número adimensional zf/u_* de acordo com

$$\frac{\overline{v}-v_g}{u_*} = \frac{\partial(\overline{w'u'})}{\partial z f u_*} = F_y(\frac{zf}{u_*}), \tag{10.45}$$

$$\frac{\overline{u}-ug}{u_*} = -\frac{\partial(\overline{w'v'})}{\partial z f u_*} = F_x(\frac{zf}{u_*}) \tag{10.46}$$

Devido à eq. (10.40), no topo da CLA onde $z = z_i$ [1] devemos ter:

$$F_x(\frac{zf}{u_*}) = F_y(\frac{zf}{u_*}) = 0 \tag{10.47}$$

Ambas as funções adimensionais F_x e F_y devem possuir a mesma raiz, que denominaremos aqui e^A para facilitar a manipulação algébrica posterior; a constante A efetivamente *define* a espessura da CLA dinamicamente:

$$\frac{z_i f}{u_*} \equiv e^{-A} \Rightarrow z_i = \frac{e^{-A}u_*}{f} \tag{10.48}$$

Crítica: esta definição não funciona no equador, onde $f = 0$; na prática, aparentemente a similaridade de Rossby que estamos estudando não funciona muito bem em lugar nenhum, devido a diversos complicadores; mesmo assim, nós a estamos estudando aqui por seu interesse matemático.

Agora, sabemos que a adimensionalização proposta por (10.45)–(10.46) *não* vai funcionar à medida em que nos aproximarmos da superfície. Por exemplo, próximo de $z = 0$ a previsão de (10.45) é

$$-\frac{v_g}{u_*} = \frac{1}{fu_*}\frac{d\,\overline{w'u'}}{dz}; \tag{10.49}$$

mas $\overline{w'u'} = 0$ em $z = 0$; em alturas verticais próximas da rugosidade z_0 a contribuição viscosa para o fluxo de quantidade de movimento é significativa, e o termo de viscosidade teria que ser incluído nas equações de Reynolds para médias.

Uma alternativa, que nós já utilizamos quando estudamos os perfis de vento na sub-camada dinâmica, é tentar re-escrever as equações utilizando a rugosidade z_0; utilizando o número de Rossby de rugosidade, obtemos:

$$\frac{z_0 f}{G}\frac{G}{u_*}\frac{\overline{v}-v_g}{u_*} = \frac{d\,\overline{w'u'}/u_*^2}{dz/z_0} \tag{10.50}$$

$$\frac{z_0 f}{G}\frac{G}{u_*}\frac{\overline{u}-u_g}{u_*} = -\frac{d\,\overline{w'u'}/u_*^2}{dz/z_0} \tag{10.51}$$

Ora, o número de Rossby de rugosidade é necessariamente um número muito grande; quando $R_o \to \infty$, é razoável supor que

$$\left|\frac{G(\overline{v}-v_g)}{u_*^2}\right| < \infty \text{ e } \left|\frac{G(\overline{u}-u_g)}{u_*^2}\right| < \infty ;$$

[1] Note que apesar de eu estar usando o símbolo z_i, cuja origem é "altura de inversão", a definição da espessura da CLA utilizada aqui é *totalmente dinâmica*, e não tem nada a ver com a altura da inversão do perfil de temperatura potencial

já que u_* deve crescer com G, enquanto que $\overline{u} \sim G$ e $\overline{v} \sim G$ (no máximo). Portanto, quando $R_o \to \infty$, o lado esquerdo tende a zero, e consequentemente o lado direito também:

$$\lim_{R_o \to \infty} \frac{d\,\overline{w'u'}\,/u_*^2}{dz/z_0} = 0, \tag{10.52}$$

$$\lim_{R_o \to \infty} \frac{d\,\overline{w'v'}\,/u_*^2}{dz/z_0} = 0. \tag{10.53}$$

Então, ao orientarmos os eixos x e y de tal forma que em $z = 0$, $\overline{v} = 0$ e $\overline{w'v'} = 0$, obtemos:

$$\overline{w'u'} = u_*^2 = \text{cte} \tag{10.54}$$

$$\overline{w'v'} = 0 \tag{10.55}$$

Ambas as equações acima devem valer numa "camada superficial" dinamicamente definida por

$$1 \ll |z/z_0| < \infty.$$

Agora cabe fazer o *matching* propriamente dito. Nossos resultados até agora são:

1. Na "camada superficial":
$$\frac{u}{u_*} = g(z/z_0) \tag{10.56}$$
2. Na "camada-limite atmosférica":
$$\frac{\overline{u} - u_g}{u_*} = F_x\left(\frac{zf}{u_*}\right) \tag{10.57}$$
$$\frac{\overline{v} - v_g}{u_*} = F_y\left(\frac{zf}{u_*}\right) \tag{10.58}$$

O *matching* em si consiste em tentar "casar" estas equações quando $zf/u_* \to 0$ *e* $z/z_0 \to \infty$. Além disso, segundo Tennekes, eu *derivo* ambas as relações de similaridade, e faço o "casamento" para $\partial\overline{u}/\partial z$ e $\partial\overline{v}/\partial z$. Para $\overline{u}$:

$$\frac{\partial \overline{u}}{\partial z} = \frac{u_*}{z_0}\frac{\partial g}{\partial \xi}, \quad \text{onde} \quad \xi = \frac{z}{z_0} \tag{10.59}$$

$$\frac{\partial \overline{u}}{\partial z} = u_*\frac{\partial F_x}{\partial z} = f\frac{\partial F_x}{\partial \eta}, \quad \text{onde} \quad \eta = \frac{zf}{u_*} \tag{10.60}$$

Agora, quando $\xi \to \infty$ e $\eta \to 0$, devemos ter:

$$\frac{u_*}{z_0}\frac{\partial g}{\partial \xi} = f\frac{\partial F_x}{\partial \eta} \Rightarrow \tag{10.61}$$

$$\xi\frac{\partial g}{\partial \xi} = \eta\frac{\partial F_x}{\partial \eta} \tag{10.62}$$

Numa analogia com o método de separação de variáveis, cada um dos lados de (10.62) deve ser igual a uma constante *na região do casamento*:

$$\frac{z}{u_*}\frac{\partial \overline{u}}{\partial z} = \frac{1}{\kappa}, \tag{10.63}$$

onde a constante assintótica κ é a própria constante de von Kármán; integrando,

$$\frac{\kappa}{u_*}(\overline{u}_2 - \overline{u}_1) = \ln\frac{z_2}{z_1}. \tag{10.64}$$

Na camada superficial, escolho $\overline{u}_1 = 0$ em $z_1 = z_0$ e obtenho o bem-conhecido perfil logaritmico

$$\frac{u}{u_*} = \frac{1}{\kappa}\ln(\frac{z}{z_0}). \quad (z/z_0 \gg 1) \tag{10.65}$$

Se, por outro lado, eu tomar $\overline{u}_1$ como a velocidade dentro da CLA e $\overline{u}_2 = u_g$:

$$\frac{\kappa}{u_*}\left(u_g - \overline{u}\right) = \ln\frac{z_i}{z}, \tag{10.66}$$

$$\frac{\kappa}{u_*}\left(\overline{u} - u_g\right) = \ln\frac{zf}{u_*}\frac{u_*}{z_i f}. \tag{10.67}$$

usando (10.48):

$$\frac{\kappa}{u_*}\left(\overline{u} - u_g\right) = \ln\frac{zf}{u_*} + A \tag{10.68}$$

isto é:

$$\frac{\overline{u} - u_g}{u_*} = \frac{1}{\kappa}\left(\ln\left(\frac{zf}{u_*}\right) + A\right) \quad (zf/u_* \ll 1) \tag{10.69}$$

Eliminando-se agora $\overline{u}$ entre (10.65) e (10.68), obtém-se uma *relação de arrasto*,

$$\frac{u_g}{u_*} = \frac{1}{\kappa}\left(\ln\frac{u_*}{fz_0} - A\right) \tag{10.70}$$

Para $\overline{v}$, em $1 \ll z/z_0 < \infty$,

$$\overline{v} = 0, \tag{10.71}$$

enquanto que em $1 \gg (zf)/u_* \to 0$:

$$\frac{-v_g}{u_*} = F_y(0) = \frac{B}{\kappa}, \tag{10.72}$$

onde a segunda igualdade é a *definição* da constante B de forma análoga a A. Combinando-se (10.70) e (10.72):

$$\frac{G}{u_*} = \frac{1}{\kappa}\left\{\left[\ln\left(\frac{u_*}{fz_0}\right) - A\right]^2 + B^2\right\}^{1/2}. \tag{10.73}$$